Ultimate load limit analysis of steel structures accounting for nonlinear behaviour of connections

Ismar Imamovic

Par **Ismar IMAMOVIC**

Ultimate load limit analysis of steel structures accounting for nonlinear behaviour of connections

Thèse présentée pour l'obtention du grade de Docteur de l'UTC

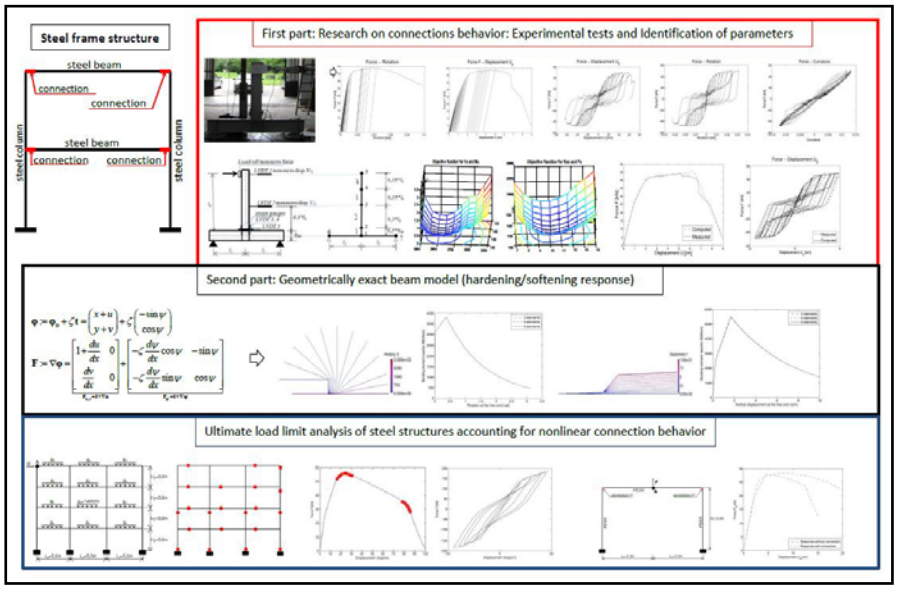

Soutenue le 22 septembre 2017
Spécialité : Mécanique Avancée : Unité de recherche en Mécanique - Laboratoire Roberval (UMR-7337)

D2373

Ultimate load limit analysis of steel structures accounting for nonlinear behaviour of connections

THÈSE DE DOCTORAT

Université de Technologie de Compièegne
(Champ disciplinaire: Mécanique Avancée)

par

Ismar IMAMOVIC

22 Septembre 2017

Composition du jury

Président du Jury:

Adnan IBRAHIMBEGOVIC, Professeur des Universités, UTC, France
Abdellatif OUASHINE, Professeur des Universités, UTC, France
Esad MESIC, Professeur des Universités, University of Sarajevo, Bosnia and Herzegovina
Mustafa HRASNICA, Professeur des Universités, University of Sarajevo, Bosnia and Herzegovina
Ivica KOZAR, Professeur des Universités, University of Rijeka, Croatia
Bostjan BRANK , Professeur des Universités, University of Ljubljana, Slovenia

Rapporteurs :

Ivica KOZAR, Professeur des Universités, University of Rijeka, Croatia

Bostjan BRANK, Professeur des Universités, University of Ljubljana, Slovenia

Invité:

Directeur de these:	Adnan IBRAHIMBEGOVIC, Professeur des Universités, UTC, France
Co- Directeur de these:	Esad MESIC, Professeur des Universités, University of Sarajevo, Bosnia and Herzegovina

‘‘Just work hard and do your best, and everything else will follow."

Author Unknown

To my family

Acknowledgments

This thesis was supported by Faculty of Civil Engineering of the University of Sarajevo and French Ministry of Foreign Affairs through a scholarship given by French Embassy in Sarajevo. This support is gratefully acknowledged.

I would like to thank in particular those who contributed to this thesis:

- My “French” supervisor, Prof. Adnan Ibrahimbegovic, who generously accepted me and who offered me his huge scientific knowledge, which helped me to develop and finish my thesis. He was always available for me during this process. Professor Ibrahimbegovic helped me in many situations, when I applied for the scholarship when I was arranging my accommodation in France, etc. On this occasion, I would also like to thank him and his wife Dzenita on wonderful dinners and friendly atmosphere in their home.

- My “Bosnian” supervisor, Prof. Esad Mesic, who offered me his knowledge and who supported me not only during my works on the thesis but throughout my academic career. His door has always been opened for me.

- Professor CatherineVayssade, who led me in the field of identification procedures. Her door was always opened for me and my questions, which were sometimes trivial.

- Reviewers of this thesis and also members of the evaluation committee of the thesis, Prof. Ivica Kozar, Prof. Bostjan Brank, Prof. Abdellatif Ouashine, and Prof. Mustafa Hrasnica, for their participation and useful comments and remarks.

- Management of Faculty of Civil Engineering of University Sarajevo, led by the dean Mustafa Hrasnica, on their great support. Among many things, I am very thankful for the paid absences from my work, and for the financial support of the experimental part of my research.

- The last but not the least, I thank my wife Adna, who was raising our son during my stay in France, and my parents and sister for their continuous support.

Ultimate load limit analysis of steel structures accounting for nonlinear behavior of connections

Abstract

This thesis deals with the ultimate load limit analysis of steel frame structures. The steel frame structure has a very ductile response and a large potential to dissipate energy, which is crucial in the case of earthquakes. The ductility in the response of the structure comes from the behavior of the material itself and the behavior of the semi-rigid structural connections. The semi-rigid connections between beams and columns can significantly influence the response of the structure, sometimes up to 30%. In this thesis, we propose a methodology for modeling steel frame structures with included connection behavior. The idea is to model the behavior of the structural connections by the beam elements positioned in the corners of the steel frame structure. Other members of the steel frame structure, steel beams, and columns, will be modeled with nonlinear beam elements.

This research consists of two parts. The first part deals with the behavior of the structural steel connections. In the second part, we present the development of the nonlinear beam element capable of representing the ductile behavior of steel structural elements, beams and columns.

In the first part of the thesis, we define constitutive parameters identification procedure for the coupled plasticity-damage model with eighteen unknowns. This constitutive model is very robust and capable of representing a wide range of problems. The identification procedure was used in the preparation of experimental tests for three different types of structural steel connections. The experimental tests have been performed for two load cases. In the first, the load was applied in one direction with both the loading and unloading cycles. From the experimental measurements, we have concluded that the response of the experimental structure can be represented by the plasticity model only because no significant change in the elastic response throughout the loading program was observed. Therefore, we have chosen an elastoplastic geometrically exact beam to describe connection behavior. The hardening response of the beam is governed by bilinear law, and the softening response is governed by nonlinear exponential law. The identification of the parameters has been successfully done with fifteen unknown parameters identified.

The two types of the experimental structures were also exposed to the cyclic loading. Measured experimental data shows complex connection behavior that cannot be described by the plasticity model alone. Namely, after changing load direction stiffness of the connection decreases. This suggests that the damage model should be incorporated in the constitutive law for the connections behavior as well. Therefore, we propose a new coupled plasticity-damage model capable of representing the loss in the stiffness of the connection with the changing of the load direction. At the end of this part, we also give the constitutive parameters identification for the proposed model.

The second part of the thesis deals with the theoretical formulation and numerical implementation of the elastoplastic geometrically exact beam. The hardening response of the beam includes interaction between stress resultant section forces (N, T and M), and the softening response of the beam, which is governed by the nonlinear law. This type of the beam element is capable of representing the ductile behavior of a steel frame structure, and it takes into account second order theory effects.

Performed numerical simulations show that the proposed geometrically nonlinear beam element is very robust and is able to provide a more precise limit load analysis of steel frame structures. By using proposed methodology for modeling steel structures, we are able to obtain the real distribution of section forces, including their redistribution caused by forming of the hinges and the connections behavior.

Ultime analyse de limite de charge des structures en acier représentant comportement non linéaire des connexions

Résumé

Cette thèse traite l'ultime analyse des structures de châssis en acier,qui s'utilise souvent comme la structure principale de support des batiments . La structure du cadre en acier est caracterisée par une réponse très ductile et un grand potentiel pour dissiper l'énergie, ce qui est crucial pour la resistance par rapport aux tremblements de terre. La ductilité dans la réponse de la structure est la cause du comportement du matériau lui-même et du comportement des connexions entre les elements de la structure. Les connexions entre les poutres et les poteaux peuvent influencer de manière significative la réponse de la structure du cadre en acier, parfois jusqu'à 30%.L'idée est de intégrer le comportement des connexions par les elements de poutres qui seront situés dans les coins du cadre et la modélisation du reste serra fait avec des elements de poutres non-linéaires qui décrirons le comportement des poutres en acier.

Cette recherche est composé de deux parties. La première partie est consacré au comportement des connexions structurelles,la deuxième partie présente le développement de l'élément fini du faisceau non linéaire capable de représenter le comportement ductile d'un élément de la structure en acier.

Dans la première partie de la thèse, nous définissons la procédure d'identification des paramètres constitutifs pour le modèle couplé de plasticité-dégâts avec dix-huit inconnus. Ce modèle constitutif est très robuste et capable de représenter une large gamme de problèmes. La procédure definis a été utilisée dans la préparation de tests expérimentaux pour trois types de connexions en acier structuré. Les tests expérimentaux ont été effectués pour deux cas de charge. Pour la première, la charge a été appliquée dans un sens avec les cycles de chargement et de déchargement. À partir des mesures expérimentales, nous avons conclu que le modèle de plasticité peut bien représentée le comportement de la connexion structurale. Paramètres constitutifs ont été déterminés à partir des résultats de l'expérimentation,on a utilisé une poutre géométriquement exacte avec la loi bilinéaires renforcement du materiale et la loi linéaire pour le ramollissement.

Également,on a effectué des essais expérimentaux de deux types de raccords en acier en cas de chargement cyclique.Les données mesurées montrent que le modèle de la plasticité n'est pas assez bon pour décrire le comportement de connexion pour ce type de charge. A savoir, en raison de changements du sense de l'apllication du chargement, les connexions montrent moins de rigidité, qui peut être décrite avec un modèle constitutif de dommages. Pour cette raison, nous avons développé un nouveau modèle plasticité-dommages qui est capable d'inclure le phénomène mentionné ci-dessus. A la fin de cette section est faite l'identification des paramètres constitutifs.

La deuxième partie de la thèse de doctorat est composé de formulations théoriques et la mise en oeuvre numérique des faisceaux géométriquement exacte . La réponse de durcissement de la poutre comprend l'interaction entre les forces de la section résultant du stress (N, T et M), et la réponse de ramollissement est definit par la loi non linéaire. Ce type d'élément fini de poutre est capable de décrire le comportement ductile des structures en acier et inclure les effets du second ordre, qui sont très importantes pour l'analyse ultime des structures de cadre en acier.

L'élément fini développé de poutre géométriquement exacte et les lois définies de liaison de comportement dans la construction en acier, offrant la possibilité d'une analyse de haute qualité des structures en acier.En utilisant les models de poutre proposé et la méthodologie de modélisation des structures de châssis en acier, il est possible de déterminer une distribution réaliste des forces de section transversale , y compris la redistribution due à la formation de rotules plastiques.

Konstitutivni zakon veze za analizu graničnih stanja čeličnih okvirnih konstrukcija

Sažetak

Ova doktorska disertacija se bavi graničnom analizom čeličnih okvirnih konstrukcija, koje se često koriste kao glavna nosiva konstrukcija objekata. Ove konstrukcije odlikuje veoma duktilan odgovor i veliki potencijal za disipaciju energije, što je krucijalno za seizmičku otpornost. Duktilnost ovih konstrukcija je posljedica karakteristika materijala (čelika) i popuštanja u vezama između elemenata konstrukcije. Naime, veze između greda i stubova imaju vežnu ulogu u ponašanju čelične okvirne konstrukcije, pa mogu promjeniti odgovor do 30% u odnosu na konstrukciju sa krutim vezama. Ideja je da se ponašanje veza uključi preko grednih elemenata koji bi se posatvili u uglove okvira a ostatak konstrukcije može biti modeliran nelinearnim grednim elementima, koji opisuju ponašanje ostalih elemenata čelične konstrukcije, greda i stubova.

Rad se praktično sastoji od dva dijela, prvi dio se bavi analizom ponašanja konstrukcijskih veza, a drugi razvojem konačnog elementa grede sposobnog da prezentira duktilno ponašanje elemenata konstrukcije.

Prvi dio se sastoji od definisanja procedure za identifikaciju konstitutivnih parametara modela, gdje koristimo povezani model plastičnost-oštećenje, koji sadrži 18 nepoznatih parametara. Ovaj model je jako robustan i sposoban da prestavi širok dijapazon fenomena. Uspješno definisana procedura identifikacije je iskorištena kao priprema za eksperimentalno ispitivanje tri karakteristična tipa čeličnih veza. Experimentalno ispitivanje je sprovedeno za dva različita tipa opterećenja. U prvom slučaju, opterećenje je aplicirano u jednom pravcu kao ciklusi opterećenja i rasterećenja. Eksperimentalno izmjereni rezultatia ukazuju, da model plastičnosti može kvalitetno opisati ponašanje veza. Konstitutivni parametri modela grede su uspješno određeni iz experimentalnih rezultata. U identifikaciji je korištena elasto-plastična geometrijski egzaktna greda sa bilinearnim zakonom ojačanja materijala i linearnim omekšanjem. Drugi tip opterećenja pri eksperimentalnom ispitivanju je ciklično opterećenje. Izvršeno eksperimentalno ispitivanje dva tipa čeličnih veza za ovaj tip opterećenja. Izmjereni podaci ukazuju da model plastičnosti nije dovoljno dobar da kvalitetno opiše ponašanje veza za ovaj tip opterećenja. Naime, usljed promjene pravaca djelovanja opterećenja, veze pokazuju smanjenu krutost, koja se može opisati sa konstitutivnim modelom oštećenja. Iz ovog razloga, razvijen je novi model povezane plastičnosti-oštećenja sposoban da uključi pomenuti fenomen. Na kraju ovog dijela je izvršena identifikacija konstitutivnih parametara.

Drugi dio doktorske disertacije se sastoji od teoretske formulacije i numeričke implementacije geometrijski egzaktne grede sa uključenom interakcijom između presječnih sila (M, N i T) u okviru ojačanja materijala, dok je omekšanje definisano nelinearnim zakonom. Ovaj tip grednog konačnog elementa je sposoban da opiše duktilno ponašanje čeličnih konstrukcija i uključi efekte teorije drugog reda, koji su vrlo važni za graničnu analizu čeličnih okvirnih konstrukcija.

Razvijeni konačni element geometrijski egzaktne grede i definisani zakoni ponašanja veza u čeličnim konstrukcija, pružaju mogućnost kvalitetne granične analize čeličnih okvirnih konstrukcije. Primjenom predloženih grednih modela i metodologije modeliranja čeličnih okvirnih konstrukcija moguće je odrediti realnu raspodjelu presječnih sila uključujući njihovu redistribuciju usljed formiranja plastičnih zglobova, kao i ponašanje popustljivih veza između elemenata konstrukcije.

Contents

List of Figures

List of Tables

List of Publications

Journals

[1] Imamovic I., Ibrahimbegovic A., Knopf-Lenoir C., Mesic E. (2015). Plasticity-damage model parameters identification for structural connections. Coupled Systems Mechanics, 4(4):337-364 .

[2] Imamovic I., Ibrahimbegovic A., Mesic E. (2017). Nonlinear kinematics Reissner's beam with combined hardening/softening elastoplasticity. Computers and Structures, 189: 12-20.

[3] Imamovic I., Ibrahimbegovic A., Mesic E. (2017). Experimental testing of structural steel connections and constitutive parameters identification. Engineering Structures (submitted)

Conferences and Workshops

[1] Imamovic I., Knopf-Lenoir C., Ayhan C., Ibrahimbegovic A. (2015). Identification of constitutive parameters for coupled plasticity-damage and softening models. The 2nd International conference on Multi-scale Computational Methods for Solids and Fluids - ECCOMAS 2015, Sarajevo, Bosnia and Herzegovina.

[2] Imamovic I., Ibrahimbegovic A., Mesic E. (2017). Geometrically exact beam with combined hardening/softening elastoplasticity. ECCOMAS MSF 2017 Thematic Conference, Ljubljana, Slovenia, September 2017 (accepted)

List of Symbols

Symbols	Interpretation	Equation
$\varepsilon, \varepsilon^e, \varepsilon^p, \varepsilon^d$	Total axial deformation, elastic part, plastic part and damage part	(2.1)
$\Psi, \Psi^e, \Psi^d, \Xi^p, \Xi^d$	Helmholtz free energy: total, elastic part, damage part, isotropic hardening (plasticity) part and isotropic hardening (damage) part	(2.2)
χ^e, χ^d	Elastic complementary energy and damage complementary energy	(2.2)
E, D, K^p, K^d	Young's modulus, Damage modulus, isotropic hardening modulus(plasticity) and isotropic hardening modulus (damage)	(2.2)
ξ^p, ξ^d	Internal hardening variables for plasticity and damage model	(2.2)
$\mathcal{D}, \mathcal{D}^p, \mathcal{D}^d$	Disipation, plastic part and damage part	(2.3)
q^p, q^d	Stress-like hardening internal variables for plasticity and damage model	(2.5)
ϕ^p, ϕ^d	Yield criterion for plasticity and damage model	(2.7)
γ^p, γ^d	Plastic and damage multipliers	(2.7)
C^{ep}, C^{ed}, C^{epd}	Elasto-plastic modulus, Elasto-damage modulus and Elasto-plastic-damage modulus	(2.11), (2.12)
$\tilde{G}$	Function which defines influence zone of the discontinuity	(2.13)
α	Localized jump	(2.13)
$\delta_{\bar{x}}$	Dirac delta function respect to $\bar{x}$	(2.13)
$\bar{\Psi}, \bar{\bar{\Psi}}$	Helmholtz free energy: regular strain energy and localized strain energy at the discontinuity	(2.14)
$\bar{\bar{\phi}}$	Yield softening criterion	(2.15)
t, σ_u	Traction force(at the discontinuity) and ultimate stress	(2.15)
$\bar{\bar{q}}, \bar{\bar{\xi}}, \bar{\bar{K}}^s$	Stress-like softening variable, internal softening variable and softening modulus	(2.15)
$\bar{\bar{\gamma}}$	Softening multiplier	(2.16)
$F_{Pi}^{com}, F_{Pi}^{\exp}$	Computed and measured forces at the load level (Pi)	(2.19)
$U_{Pi}^{com}, U_{Pi}^{\exp}$	Computed and measured displacements at the load level (Pi)	(2.19)
a, b, c	Constants - weights values	(2.19)
v, ψ	Vertical displacement and rotation	(3.1)
γ_s	Shear deformation	(3.1)
$M, V, q(x)$	Bending moment, Shear force and distributed load	(3.2)
G_s, A_v, I	Shear modulus, cross-section area (related to shear force) and moment of inertia	(3.4)
$\delta\mathbf{w}, \delta\boldsymbol{\varepsilon}$	Virtual displacement field and virtual deformation field	(3.7)
$\bar{\mathbf{u}}(x,t), \boldsymbol{\alpha}(t), H_{\bar{x}}(x)$	Vector of regular displacements, vector of localized jumps and Heaviside step function	(3.8)
$\kappa, \kappa^e, \kappa^p, \kappa^d$	Total curvature, elastic part, plastic part and damage part	(3.9)
$\bar{\xi}^p, \bar{\xi}^d, \bar{\xi}^s$	Internal hardening variables for: plasticity, damage and softening	(3.10)

$\bar{\phi}^p\left(M,\bar{q}^p\right), \bar{\phi}^d\left(M,\bar{q}^d\right)$	Yield criteria: plasticity and damage model	(3.12)
t_M, t_{Mu}	Bending traction and ultimate bending traction	(3.21)
$\bar{\bar{\phi}}\left(t_M,\bar{\bar{q}}^s\right)$	Softening yield criterion	(3.21)
α_ψ	Localized rotational jump	(3.24)
$\bar{\gamma}_s, \bar{\gamma}_s^e, \bar{\gamma}_s^p$	Total regular shear deformation, elastic part and plastic part of shear deformation	(3.25)
$\bar{\xi}_s^p, \bar{\bar{\xi}}_s^s$	Internal variables for hardening and softening	(3.26)
$V_y, \bar{q}_s^p$	Yield shear force and stress-like internal variable	(3.28)
t_V, t_{Vu}	Traction shear force and ultimate traction shear force	(3.32)
$\bar{\bar{\mathcal{D}}}^s, \alpha_v$	Localized plastic disipation and localized shear displacement	(3.33)
$N_1(x), N_2(x)$	Linear interpolation functions	(3.36)
$\mathbf{B}$	Set of first derivatives of interpolation functions	(3.37)
$J(d_p)$	Objective function in terms of unknown parameter d_p	(3.41)
$(\bullet)^{com}, (\bullet)^{\exp}$	Computed and experimntal measured value	(3.41)
$\Delta v_3^{\exp}, \Delta v_4^{\exp}$	Experimental measured relative displacements by LVDT 3 and LVDT 4	(3.45)
h, y	Height of the cross section and coordinate normal to the beam axis	(3.46)
$S_{j,b}$	Rotational stiffness of a joint/connection	(3.58)
$\boldsymbol{\varphi}, x, y$	Position vector and coordinates in global coordinate system	(4.1)
$\mathbf{F}, \mathbf{F}_{u,v}, \mathbf{F}_\psi$	Deformation gradient, displacemnts part and rotation part	(4.2)
$\mathbf{R}, \mathbf{U}$	Rotation and stretch tensors	(4.5)
$\mathbf{H}, \mathbf{I}$	Rotated strain measure tensor and identity tensor	(4.5)
$\hat{\mathbf{F}}, \mathbf{P}$	Deformation gradient variation and first Piola-Kirchoff stress tensor	(4.7)
$\hat{\mathbf{H}}, \mathbf{T}$	Rotated strain measure variation and Biot's stress tensor	(4.7)
$\bar{\phi}(\mathbf{T}, \bar{\mathbf{q}})$	Yield criterion in terms of Biot's stress tensor and hardening stress-like internal variables	(4.13)
$\bar{\mathbf{U}}^e, \bar{\mathbf{U}}^p$	Elastic part and plastic part of stretch tensor	(4.14)
Σ, Γ, K	Generalized strains in deformed configuration	(4.23)
$\hat{\mathbf{u}}, \hat{\mathbf{T}}, \hat{\mathbf{H}}$	Virtual displacements , virtual stress and virtual rotated strain measure	(4.29)
$\hat{\bar{\mathbf{H}}}, \hat{\bar{\bar{\mathbf{H}}}}$	Regular and irregular part of virtual rotated strain measure	(4.31)
$\hat{\mathbf{a}}, \hat{\mathbf{r}}, \hat{\boldsymbol{\Sigma}}$	Vector of virtual displacements , virtual stresses and virtual rotated strains in terms of stress-resultant forces	(4.32)
$\boldsymbol{\Lambda}$	Transformation matrix	(4.32)
$\psi^{\exp}$	Experimentally measured rotation of connection	(5.1)
K_i^h	Hardening moduli	(5.3)
S_j^{in}, S_j^p	Initial and platic stiffness of the conenction	(5.24)
$\Psi^{(+)}, \Psi^{(-)}$	Helmholtz free energy for positive and negative values of the bending moment	(6.1)

$\bar{\phi}_i^d(T_i, \bar{q}_i^d)$	Damage criterion	(6.2)
C_i^{ed}	Elasto-damage moduli for positive and negative values of bending moment	(6.11)
$\bar{\phi}_M^d(M, \bar{q}_M^d), M_f$	Damage criterion and yield damage bending moment	(6.19)

Chapter 1

Introduction

Contents

1.1. Motivation

The steel is one of the materials (next to concrete) most frequently used in the domain of Civil Engineering. The main interest of this research work is to master the ultimate behavior of the moment-resistant steel frame structures. The moment-resistant steel frames are frequently used as bearing structures in seismic regions. They have a very ductile response and a large potential to dissipate energy, which is crucial in the case of earthquakes. These characteristics result in the economical design of the structure and increase the resistance with respect to the seismic security. Structural connections between beams and columns play a crucial role in the response of a steel frame structure. They can significantly influence the response of the structure, sometimes up to 30% (Imamovic & Mesic, 2014).

The response of a moment-resistant frame structure depends on the connections behavior and steel structural elements behavior. Steel as a construction material has good mechanical properties, which result in smaller dimensions of the structural elements. Thin elements are sensitive to the local buckling and stability issues. On the other hand, steel is very ductile constructive material and thus is able to bear large deformations. Therefore, the large deformations should be combined with the nonlinear constitutive models of plasticity or damage when describing the behavior of a steel structural element. The nonlinear constitutive models should also be able to represent the forming of the hinges in the load-bearing structure which eventually leads to the development of the collapse mechanism. Development of the hinges depends on all stress resultant section forces. Because of that, all stress resultant section forces need to be combined in a yield criterion. The modern codes recommend certain rules about the reduction of plastic bending moment related to the value of axial force. These rules sometimes cause difficulties in practical applications. This work is focused on the development of the appropriate beam element, which can represent mentioned phenomena.

The study of connections behavior is very complex because every type of connections has a different response. In this work, we focus on three types of the structural connections: end plate connection with extended plate, end plate connection without extension and moment resistant connection with angle profiles. These connection types are frequently used in steel frame structures because they are very practical for the montage of the structure. The behavior of these connection types is very complex. Eurocode 3 (EC3, 2005) gives a procedure for the determination of load bearing capacity and stiffness, but only for bending moment. Shear force and axial force are neglected. Many experimental tests show that proposed procedure has its disadvantages. The main disadvantage is in the conservative prediction of the load-bearing capacity of the connection. Numerical analysis of the connection behavior can be performed with many nonlinear FEM commercial programs, using 3D solid finite elements. The refined nonlinear model can predict the behavior of a connection, but those computations are often too costly and not practical when modeling the response of the whole structure. For this reason, we propose the usage of the beam element as a better choice with respect to computational efficiency and reduced costs. The constitutive parameters of the beam element can be determined from experimental tests. The main novelty of the proposed beam element for representing the connection behavior is its ability to represent bending, axial and shearing inelastic response, which includes the softening part of the response, until the complete failure is reached.

Using proposed beam model capable of representing phenomena characteristic for steel member and beam elements in corners for representing connection behavior, we will be able to perform ultimate limit load analysis of a steel frame structure.

1.2. Overview

Many works about steel frame structures have been published. These works can be classified into two completely separated groups. The first group deals with connection behavior, while the second group develops FEM beam models. The research on the connection behavior has usually been focused on experimental tests or/and numerical simulations with refined FEM models, where authors often proposed analytical expressions for representing the connection behavior. On the other hand, many beam models that can be used for analysis of steel frame structures have been developed for a wide range of problems. However, appropriate numerical modeling of the connection behavior is still an issue. This section gives a short overview of the published works about beam models and connection behavior.

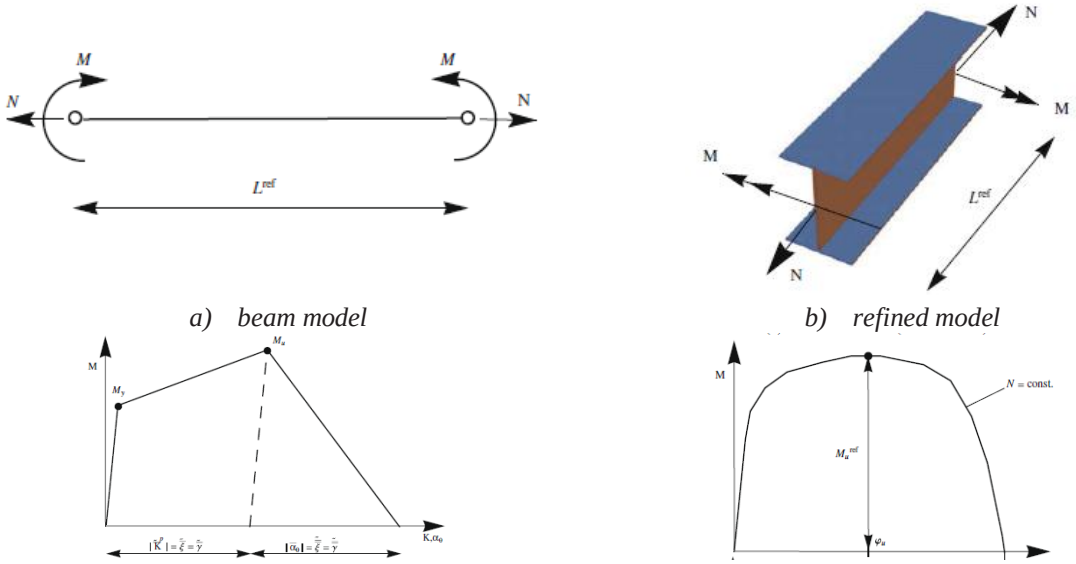

a) beam model *b) refined model*

c) Moment-curvature/rotation (beam model) *d) Moment-curvature/rotation (refined model)*

Figure 1.1 Evaluation of beam material parameters by using results of refined analysis (Dujc et al., 2010)

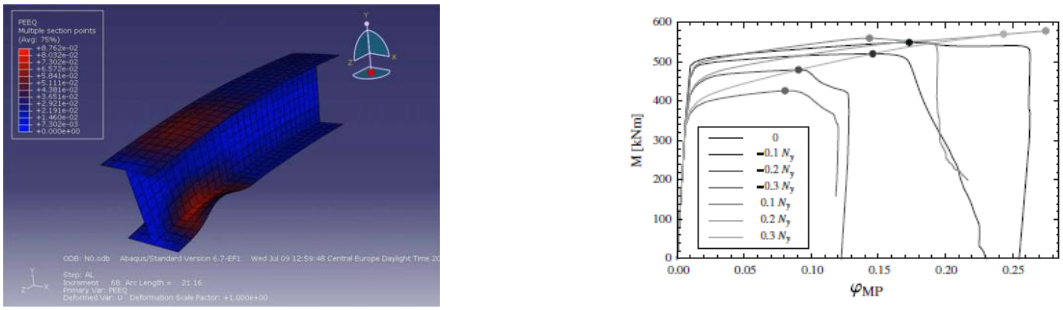

a) *The failure mode of the representative part of the frame member as computed by the shell model.* b) *Bending moment versus rotation curves for the end cross-section*

Figure 1.2 Refined model (Dujc et al., 2010)

Because of the good mechanical properties of the steel, cross-sectional dimensions of the structural members can be smaller compared to the dimensions of the same member made from different material e.g. concrete. However, because of the smaller dimensions, structural members made of steel are more sensitive on stability issues. In the paper (Dujc et al., 2010), authors proposed elastoplastic Euler-Bernoulli beam model with embedded discontinuity, with the hardening and the softening part of the response included in the constitutive law of the beam. The global buckling of

structural members is taken into account through *von Karman* strain measure, which is an appropriate choice for moderate rotations. The local buckling is computed separately, on the refined FEM model in nonlinear commercial computer program ABAQUS, see Figure 1.1. The numerical simulation has been performed using finite shell element with geometrical nonlinearity, while constitutive behavior is defined by the plasticity. In Figure 1.2 refined FEM model and numerically obtained response for I steel profile are shown. The obtained response of the steel beam in pure bending results in local buckling of the flange of the I-beam. Several numerical simulations have been presented, all showing the good performance of the proposed beam element.

In a structural steel design, we usually use compact cross-sections that are not susceptible to local buckling. The compact cross section beams are able to sustain large displacements and deformations. Geometrically exact beam finite element, capable of representing large displacements, has been presented in (Simo et al., 1984), where the constitutive model is defined as a viscoplasticity. The yield criterion is inspired by classic works (Neal, 1961; Drucker, 1956), where expression for interaction between section forces are explained and proposed. Several numerical simulations presented in the paper show good performance of the proposed beam model.

Incompatible mode method in the framework of the large displacement has been presented in (Ibrahimbegovic & Frey, 1993b), where authors presented theoretical formulation and numerical implementation of the proposed model. They showed, that a multiplicative decomposition of the deformation gradient into the regular and the enhanced part can be transformed to additive decomposition of the displacement gradient. In the large displacements framework, the multiplicative decomposition of the deformation gradient needs to be employed. This leads to the complex procedure of deriving the constitutive equations. The transformation from the multiplicative decomposition of the deformation gradient to the additive decomposition of the displacement gradient is crucial for embedded discontinuity method (EDFEM), where displacement gradient is decomposed into regular and irregular parts. In the recent work (Pirmanšek et al., 2017), authors presented theoretical formulation and numerical simulation of the geometrically exact beam, which includes the both, hardening and softening part of the response. Several numerical simulations applied to concrete structures show good performance of the proposed model. The work (Kozar et al., 2017) presents material model for load rate sensitivity, which researches application of load rate sensitive models to different types of the dynamic loading.

The influence of the connection behavior on the response of the steel frame can be included using beam model. Constitutive parameters of the beam model need to be identified from the connection response. The parameters identification of a nonlinear constitutive model can be very complex, sometimes impossible to determine. The parameters identification in general case is performed in two steps: i) defining an objective function based on experimental measurements; ii) minimizing this objective function in order to find values of constitutive parameters used in the model.

To ensure the success of the minimization process, the choice of the objective function is critical. In general case, the objective function can be defined as the gap between the measured and the computed values of the response (displacement, stress, deformation, reaction force, etc.). Minimization of the objective function can be formally written as minimization under constraint. The weak form of equilibrium equations acts as the corresponding constraint because the weak form of equilibrium equations has to be satisfied at every time step. The constrained minimization of the objective function can be transferred into unconstrained minimization by using Lagrange multiplier method (Ibrahimbegovic et al., 2004). This type of minimization of the objective function is very complex for several unknowns. In work (Kucerova et al., 2009), authors proposed a methodology for parameters identification of the constitutive plasticity model. The proposed

methodology splits identification procedure into three phases: elastic, hardening and softening, see Figure 1.3. It also proposes that measured data needs to include both local and global measurements. The local measurement depends on one constitutive parameter, whereas the global depends on all constitutive parameters. The proposed objective function is explained in details.

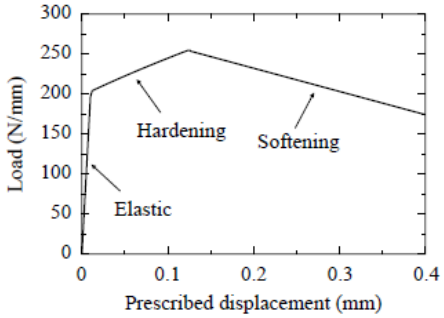

Figure 1.3 Identification phases (Kucerova et al., 2009)

Connection behavior is usually analyzed as an isolated problem. A group of authors (Faella et al., 2000) has performed detailed experimental and numerical research on the connection behavior. They have studied the end plate connection with two bolts per row and the application of the component method. The component method splits connection into components, where the weakest component defines load-bearing capacity, and all components define rotational stiffness, see Figure 1.4. Eurocode 3 procedure (EC3, 2005) is based on the component method. The research of the group of authors has been focused on the connection behavior under bending. The results of the research are the expressions for determining the load-bearing capacity and rotational spring stiffness of the end plate connection using the component method.

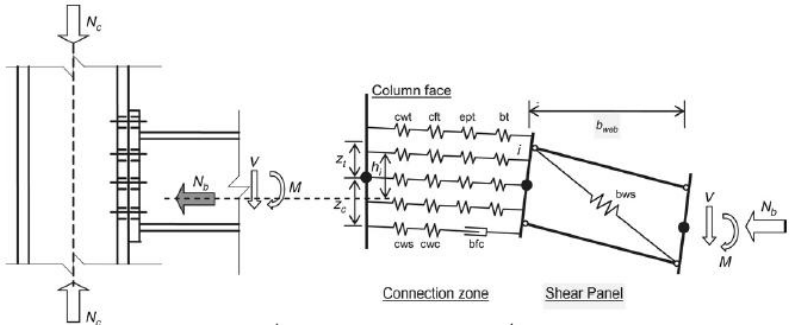

Figure 1.4 Component method
(EC3, 2005)

Many works about the experimental and numerical research on the connection behavior have been published. In this section, we list only a few of them (Hu et al., 2012; Latour et al., 2014; Ribeiro et al., 2015; Imamovic & Mesic, 2014). In these works, the experimental tests have been performed, and many phenomena in connection response under monotonic or cyclic or impact load have been explained. In most of the cases, authors proposed an analytical model for representing connection response where the connection behavior was modeled with several parallels or serially connected springs. The behavior of every spring was defined by the certain constitutive model, and the softening part of the response was usually neglected. These works did not provide a methodology for taking into account the behavior of the connections on the response of a steel frame structure.

1.3. Aims, scopes and methodology

The main scientific goal of this thesis is to more accurately perform ultimate load limit analysis of the steel frame structures. The proposed enhancement of the limit load analysis can be split into two parts. In the first, which deals with connections behavior, a methodology for taking into account the influence of the connections behavior on the global response of a steel frame structure is proposed. In the second part, the improved beam model capable of representing the behavior of the steel elements is presented. Combining these two parts, we are able to perform improved limit analysis of a steel frame structure. The hypothesis in the first part of the thesis is that beam model can be used to represent connection behavior. In the focus of the first part of the thesis is the identification of the constitutive parameters. The identification procedure for the very general case is developed, including an arrangement of the measuring equipment. This procedure is used as a preparation for the experimental testing which is part of this research. Using developed procedure, constitutive parameters can be identified from experimental measurements. The beam model with identified constitutive parameters is used to model connections in a steel frame structure by placing them at the corners of the frame.

In the second part, we present the improvements of the beam model in order to ensure the ability to represent the realistic behavior of the steel structural elements, beams and columns. These improvements include implementation of large displacements, second order theory effects, and interaction between the stress resultant section forces in the hardening part of the response. The softening part of the response is localized at the point.

The proposed methodology for the ultimate load limit analysis of a steel frame structure takes into account influence of connections behavior on the global response of the structure. It also provides real distribution of section forces and can be used to predict the collapse of a steel frame structure.

1.4. Outline

The outline of this thesis is as follow. In the second chapter, we present constitutive parameters identification procedure for the simplest 1D model of the truss bar with the constitutive behavior governed by coupled plasticity-damage model. In the third chapter, for a coupled plasticity-damage beam model of a structural connection, we present the constitutive parameters identification procedure containing eighteen unknown parameters. In the fourth chapter, we give a theoretical formulation and numerical implementation of the geometrically exact beam model with hardening and softening part of the response included in the constitutive law of the beam. In the hardening part of the response, interaction between stress resultant section forces is taken into account. The experimental tests of structural connections under monotonic load and identification of the unknown parameters are given in the fifth chapter. In this chapter, a modification of the beam model on the hardening response is presented. This modification relates to the use of bilinear hardening law with no interaction between stress resultant section forces. In the sixth chapter, experimental tests under cyclic loading and constitutive parameters identification procedure are given. Here, we also propose a further modification of the beam model. We propose the use of the coupled plasticity-damage model as an appropriate choice for the constitutive law of the beam under cyclic loading. The conclusion, which summarizes all the main findings of the thesis, and the suggestions for the future perspective of the study on this topic are given in the seventh chapter.

Chapter 2

Identification of constitutive parameters for the 1D model

Abstract :

In this chapter, we present a methodology for the constitutive parameters identification of the 1D coupled plasticity-damage model with eight unknowns. Both models, plasticity and damage, are able to represent a same response during the loading process. This implies that the constitutive parameters are dependent on each other, and that different combinations of parameters represent same response. The difference between models can be found in the unloading process. The focus of this chapter is the appropriate definition of the loading program and the objective function, that are able to overcome the dependency of parameters.

In the first part of this chapter, we present governing equations of the 1D coupled plasticity-damage model. The second part deals with the constitutive parameters identification procedure. The conclusions are stated in the last section of the chapter.

Contents of Chapter 2

2.1 Introduction

In this chapter, we present a methodology for the constitutive parameters identification of the 1D coupled plasticity-damage model with eight unknowns. Both models, plasticity and damage, are able to represent a same response during the loading process. This implies that the constitutive parameters are dependent and that different combinations of parameters represent same response. The difference between models can be found in the unloading process. The focus of this chapter is the definition of the loading program and the objective function, that are able to overcome dependency of parameters.

In the first part of this chapter, we present a theoretical formulation of the coupled plasticity-damage model. In the second part, we present detailed identification procedure. The identification procedure is split into three phases. In the first phase, we identify two parameters related to elasticity. The second phase is the most complex, where we analyze two possible cases in the identification of four constitutive parameters. In the third phase, we identify remaining two parameters of the softening model.

The objective function and loading program, the most important parts for the success of identification procedure, are defined for the 1D problem.

2.2 Theoretical formulation of coupled plasticity-damage model

In this section, we present main ingredients of the coupled plasticity-damage model in the framework of the thermodynamics. We show in particular that all these equations can be derived from three main ingredients: the additive decomposition of the total deformation, the strain energy, and yield/damage/softening criteria.

Deformation can be split additively into elastic part ε^e, plastic part ε^p and damage part ε^d, which can be written as:

$$\varepsilon = \varepsilon^e + \varepsilon^p + \varepsilon^d \tag{2.1}$$

Total strain energy with the contribution of both plasticity and damage is written as (Ibrahimbegovic et al., 2008):

$$\Psi(u, \sigma, \varepsilon^p, D, \xi^p, \xi^d) = \Psi^e(\varepsilon^e) + \Psi^d(\varepsilon^d, D) + \Xi^p(\xi^p) + \Xi^d(\xi^d) \tag{2.2}$$

where following represent:

$\Psi^e(\varepsilon^e) = \sigma\varepsilon^e - \chi^e(\sigma); \chi^e(\sigma) = \frac{1}{2}\sigma E^{-1}\sigma$ - elastic part of the strain energy

$\Psi^d(\varepsilon^d, D) = \sigma\varepsilon^d - \chi^d(\sigma, D); \chi^d(\sigma, D) = \frac{1}{2}\sigma D\sigma$ - damage part of the strain energy

$\Xi^p(\xi^p) = \frac{1}{2}\xi^p K^p \xi^p$ - isotropic hardening (plasticity) part of the strain energy

$\Xi^d(\xi^d) = \frac{1}{2}\xi^d K^d \xi^d$ - isotropic hardening (damage) part of the strain energy

In last expressions, used notation represents: ξ^p, ξ^d are internal hardening variables for plasticity and damage; K^p, K^d are hardening moduli for plasticity and damage; D, E are damage and

Young's modulus; σ is a stress; and χ denotes complementary energy. The total dissipation produced by this coupled plasticity-damage model must remain non-negative. By appealing to the second principle of thermodynamics, this can be written as:

$$0 \le \dot{\mathcal{D}} = \sigma\dot{\varepsilon} - \dot{\Psi} = \dot{\sigma}\left(\frac{\partial \chi^e}{\partial \sigma} - \varepsilon^e\right) + \dot{\sigma}\left(\frac{\partial \chi^d}{\partial \sigma} - \varepsilon^d\right) + \underbrace{\sigma\dot{\varepsilon}^p - \frac{\partial \Xi^p}{\partial \xi^p}\dot{\xi}^p}_{\dot{\mathcal{D}}^p} + \underbrace{\frac{\partial \chi^d}{\partial D}\dot{D} - \frac{\partial \Xi^d}{\partial \xi^d}\dot{\xi}^d}_{\dot{\mathcal{D}}^d} \tag{2.3}$$

In the last equation, we have two possible processes: elastic or plastic/damage. If we have an elastic process, then internal variables remain frozen in time: $\dot{\varepsilon}^p = 0$, $\dot{\xi}^p = 0$, $\dot{D} = 0$ and $\dot{\xi}^d = 0$, which implies that plastic and damage dissipations are equal to zero. For the elastic process we can obtain:

$$0 \le \dot{\mathcal{D}} = 0 \;\Rightarrow\; \varepsilon^e = \frac{\partial \chi^e}{\partial \sigma} = E^{-1}\sigma;\; \varepsilon^d = \frac{\partial \chi^d}{\partial \sigma} = D\sigma \tag{2.4}$$

Hardening stress variables q^p and q^d can be defined according to:

$$q^p = -\frac{\partial \Xi^p}{\partial \xi^p} = -K^p\xi^p; \quad q^d = -\frac{\partial \Xi^d}{\partial \xi^d} = -K^d\xi^d \tag{2.5}$$

By assuming the last results to remain valid for the inelastic process, we can write an equation for dissipation:

$$0 \le \dot{\mathcal{D}} = \underbrace{\sigma\dot{\varepsilon}^p - \frac{\partial \Xi^p}{\partial \xi^p}\dot{\xi}^p}_{\dot{\mathcal{D}}^p} + \underbrace{\frac{\partial \chi^d}{\partial D}\dot{D} - \frac{\partial \Xi^d}{\partial \xi^d}\dot{\xi}^d}_{\dot{\mathcal{D}}^d} \tag{2.6}$$

To determine the internal variables for plastic/damage process, we need to maximize dissipation. If we use Lagrange multiplier method for constrained minimization, we can write:

$$\min_{\phi^p(\sigma,q^p)=0,\phi^d(\sigma,q^d)=0}\left[-\mathcal{D}^p(\sigma,q^p) - \mathcal{D}^d(\sigma,q^d)\right] \Rightarrow \max_{\dot{\gamma}^p,\dot{\gamma}^d}\min_{\forall\sigma,q^p,q^d}\left[\mathcal{L}^p(\sigma,q^p) + \mathcal{L}^d(\sigma,q^d)\right]$$
$$\mathcal{L}^p(\sigma,q^p) = -\mathcal{D}^p(\sigma,q^p) + \dot{\gamma}^p\phi^p(\sigma,q^p); \quad \mathcal{L}^d(\sigma,q^d) = -\mathcal{D}^d(\sigma,q^d) + \dot{\gamma}^d\phi^d(\sigma,q^d) \tag{2.7}$$
$$\underbrace{\phi^p(\sigma,q^p) = |\sigma| - \left(\sigma_y - q^p\right)}_{\text{plastic criterion}} \qquad \underbrace{\phi^d(\sigma,q^d) = |\sigma| - \left(\sigma_f - q^d\right)}_{\text{damage criterion}}$$

Using Kuhn-Tucker optimality conditions, we can obtain the evolution equations of the internal variables:

$$\begin{aligned}
&0 = \frac{\partial \mathcal{L}^p}{\partial \sigma} = -\dot{\varepsilon}^p + \dot{\gamma}^p\frac{\partial \phi^p}{\partial \sigma} \Rightarrow \dot{\varepsilon}^p = \dot{\gamma}^p\frac{\partial \phi^p}{\partial \sigma};\\
&0 = \frac{\partial \mathcal{L}^p}{\partial q^p} = -\dot{\xi}^p + \dot{\gamma}^p\frac{\partial \phi^p}{\partial q^p} \Rightarrow \dot{\xi}^p = \dot{\gamma}^p\frac{\partial \phi^p}{\partial q^p}; \quad 0 = \frac{\partial \mathcal{L}^p}{\partial \dot{\gamma}^p} = \phi^p\\
&0 = \frac{\partial \mathcal{L}^d}{\partial \sigma} = -\dot{D}\sigma + \dot{\gamma}^d\frac{\partial \phi^d}{\partial \sigma} \Rightarrow \dot{D}\sigma = \dot{\gamma}^d\frac{\partial \phi^d}{\partial \sigma};\\
&0 = \frac{\partial \mathcal{L}^d}{\partial q^d} = -\dot{\xi}^d + \dot{\gamma}^d\frac{\partial \phi^d}{\partial q^p} \Rightarrow \dot{\xi}^d = \dot{\gamma}^d\frac{\partial \phi^d}{\partial q^d}; \quad 0 = \frac{\partial \mathcal{L}^p}{\partial \dot{\gamma}^d} = \phi^d
\end{aligned} \tag{2.8}$$

The value of plastic/damage multipliers can be computed from the consistency conditions on the stress state requiring that its evolution remains in agreement with the given yield criteria. This reduces to requirement that the time derivative of the yield functions remain equal to zero:

$$\dot{\phi}^p = 0 \;\Rightarrow\; \dot{\gamma}^p = \frac{\frac{\partial \phi^p}{\partial \sigma} E(\dot{\varepsilon} - \dot{\varepsilon}^d)}{\frac{\partial \phi^p}{\partial \sigma} E \frac{\partial \phi^p}{\partial \sigma} - \frac{\partial \phi^p}{\partial q^p} \frac{\partial q^p}{\partial \xi^p} \frac{\partial \phi^p}{\partial q^p}} \tag{2.9}$$

$$\dot{\phi}^d = 0 \;\Rightarrow\; \dot{\gamma}^d = \frac{\frac{\partial \phi^d}{\partial \sigma} D^{-1} \dot{\varepsilon}^d}{\frac{\partial \phi^d}{\partial \sigma} D^{-1} \frac{\partial \phi^d}{\partial \sigma} - \frac{\partial \phi^d}{\partial q^d} \frac{\partial q^d}{\partial \xi^d} \frac{\partial \phi^d}{\partial q^d}} \tag{2.10}$$

The values of plastic and damage multipliers can be exploited in order to obtain the stress rate constitutive equations:

$$C^{ep} = \frac{EK^p}{E + K^p}; \;\; C^{ed} = \frac{D^{-1}K^d}{D^{-1} + K^d} \tag{2.11}$$

Using condition that in both constitutive models stresses have the same value, we can obtain a stress rate constitutive equation for coupled damage/plasticity model:

$$C^{epd} = \frac{ED^{-1}K^pK^d}{ED^{-1}K^p + ED^{-1}K^d + EK^pK^d + D^{-1}K^pK^d} \tag{2.12}$$

2.2.1 Softening response

The presented plasticity-damage model can be further extended to the softening part of the response. The main differences are modifications in the strain field and the strain energy (including fracture energy):

$$\varepsilon = \underbrace{\frac{d\bar{u}}{dx} + \tilde{G}\alpha}_{\bar{\varepsilon}} + \underset{\bar{\bar{\varepsilon}}}{\delta_{\bar{x}}\alpha} \tag{2.13}$$

$$\Psi(\cdot) = \bar{\Psi}(\cdot) + \delta_{\bar{x}}\bar{\bar{\Psi}}(\bar{\bar{\xi}}) \tag{2.14}$$

In (2.13) $\bar{\varepsilon}$ presents the regular deformation part defined in (2.1) of the element, $\tilde{G}$ is a function which defines influence zone of the discontinuity, and $\bar{\bar{\varepsilon}} = \delta_{\bar{x}}\alpha$ is corresponding localized strain representation by Dirac function positioned at $\bar{x}$, whereas α is localized strain parameter. In (2.14) $\bar{\Psi}$ is defined as the strain energy, and $\bar{\bar{\Psi}}$ represents the localized strain energy at the discontinuity. The final modification relates to the softening criterion:

$$\bar{\bar{\phi}}(t, \bar{\bar{q}}) = |t| - (\sigma_u - \bar{\bar{q}}(\bar{\bar{\xi}})) \le 0 \tag{2.15}$$

where t is the traction at the discontinuity, $\bar{\bar{q}} = -\bar{\bar{K}}^s\bar{\bar{\xi}}$ is the softening stress variable.

If we use Lagrange multiplier method for a minimization with constraints, we can determine the maximum of dissipation and obtain internal variables for softening process:

$$\dot{\alpha} = \dot{\bar{\gamma}}; \quad \dot{\bar{\xi}} = \dot{\bar{\gamma}} \tag{2.16}$$

2.3 *Identification of the constitutive parameters*

We assume that experimental measures, such as tensile test, have been performed providing a set of points at the load-displacement curves. The coupled plasticity – damage model, presented before can be used for the identification of the constitutive parameters of the material. A least squares minimization problem is formulated in order to express that the actual constitutive parameters of the material minimize the gap between the values provided by measurements (displacements, strain or stresses values) and those obtained by the numerical simulation:

$$J(\mathbf{d}_{\mathrm{p}}) = \sum_{j \in J} n\left(\mathbf{u}_j^{com}(\mathbf{d}_{\mathrm{p}}) - \mathbf{u}_j^{\exp}\right)^2 \tag{2.17}$$

where $\mathbf{d_p}$ are the model parameters that we seek to identify or similar, $\mathbf{u}_i^{com}(\mathbf{d}_{\mathrm{p}})$ and $\mathbf{u}_i^{\exp}$ are, respectively, computed and experimentally measured values of displacements/stresses/strains and *n* is weighting factor. The coupled plasticity – damage model is complex for identification because both plasticity and damage can represent same behavior during the loading process. However, the difference can be found in the unloading process. For that reason, the objective function in the hardening phase needs to contain information from the unloading process.

The presented 1D coupled plasticity-damage model contains eight unknowns. The simultaneous identification of all unknowns is very complex. Because of that, we split identification process into three phases. The first phase contains two unknowns parameters of the elasticity: Young's modulus (E), and damage modulus (D) for the virgin material. These two parameters are practically one parameter if we employ the following relation:

$$D = \frac{1}{E} \tag{2.18}$$

The second phase deals with constitutive parameters related to the hardening. This phase is the most complex. Here we need to identify four parameters: N_y - yield axial force; K^p - hardening modulus (plasticity); N_f - damage yield axial force; and K^d - hardening modulus (damage model). In this phase, the identification process can be split into two possible cases: the hardening phase in both models begins for close values of axial forces $\left(N_y \approx N_f\right)$ and hardening phase does not begin for close values of axial forces $\left(N_y >> N_f \text{ or } N_y << N_f\right)$.

The first case imposes simultaneous identification of four parameters, whereas the second case allows the identification of parameters in a two-by-two manner. The last phase deals with the identification of two parameters related to the softening response: N_u - ultimate axial force; and K^s - softening modulus. The loading program contains cycles of loading and unloading, as shown in Figure 2.1.

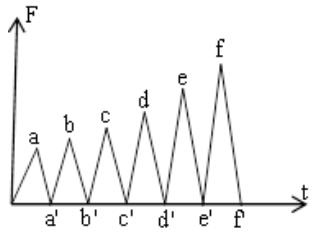

Figure 2.1 Loading program

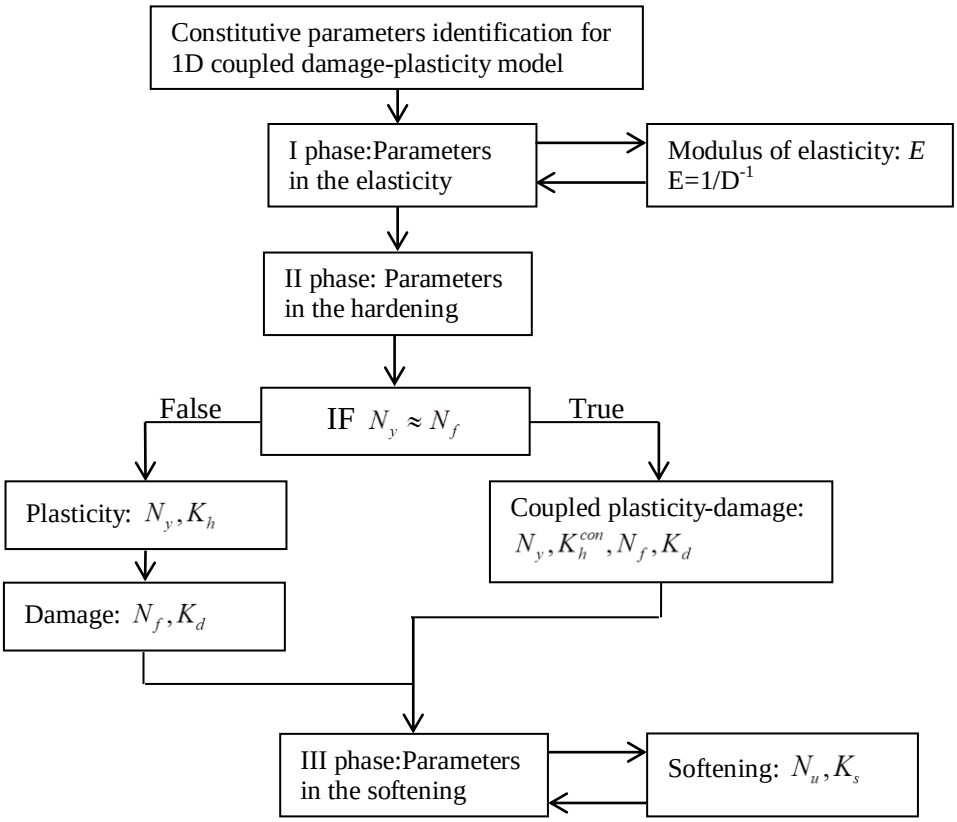

Figure 2.2 Flow chart of parameters identification

2.3.1 Application example

The tensile test is the simplest example for presenting the identification procedure of constitutive parameters. In our example we have chosen a simple model of truss bar with only one degree of freedom per node. The numerical simulation is taken as experimental measurements. The identification procedure is split in three phase (Figure 2.3.).

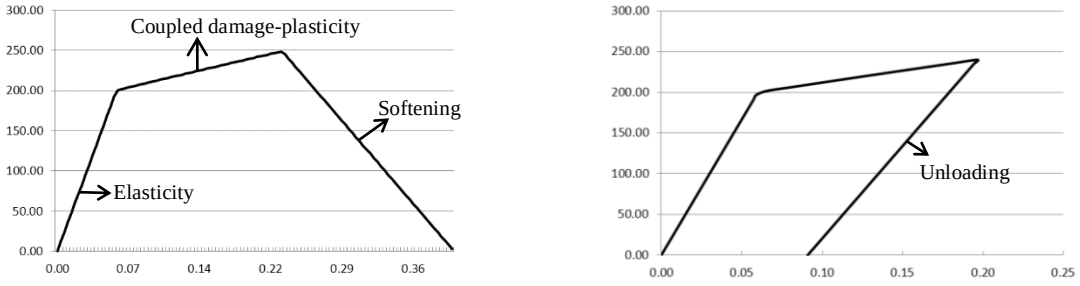

Figure 2.3 Response of the axial bar

The objective function appropriate for all identification phases can be written as:

$$J\left(\mathbf{d}_p\right)=\sum_{i=1}^{3}a\left(F_{Pi}^{com}-F_{Pi}^{\exp}\right)^2+\sum_{i=1}^{3}b\left(U_{Pi}^{com}-U_{Pi}^{\exp}\right)^2+\sum_{i=1}^{3}c\left(U_{Pi'}^{com}-U_{Pi'}^{\exp}\right)^2 \tag{2.19}$$

where: $F_{Pi}^{com},F_{Pi}^{\exp}$ are forces for different load level (*Pi*); $U_{Pi}^{com},U_{Pi}^{\exp}$ are displacements (*Pi*); $U_{Pi'}^{com},U_{Pi'}^{\exp}$ are residual displacements (unloaded points *Pi*); and a,b,c are constants.

The identification of the parameters is carried out with Matlab and research program FEAP. The first is used for the minimization of the objective function (2.19), and the second for the FEM computations.

2.3.1.1 First phase – constitutive parameters in elasticity

In the first phase, only one unknown parameter is to be identified. Three referent points at the response diagrams (Figure 2.4a) are proposed. The shape of the objective function is shown in the Figure 2.4b. We can see that the shape function is convex. Thus it has minimum and can be minimized.

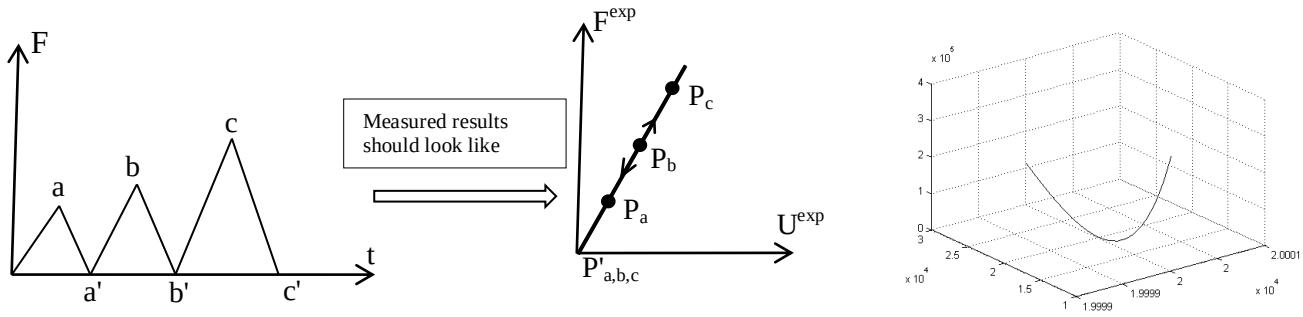

a) Loading program and measurements in the elasticity *b) Shape of the objective function*

Figure 2.4 Loading program and shape of the objective function (Elasticity)

2.3.1.2 Second phase – constitutive parameters in hardening

The first case is the most complex for the identification, and it cannot be split into two parts. The damage yield axial force and the yield axial force in plasticity model have close values (Figure 2.5), and we need to identify all four parameters simultaneously. The identification of four parameters is possible with the same objective function. The efficiency and the accuracy of the minimization process depend on the first guess values. If we have good starting values, we can obtain parameters

with acceptable values of errors. The shape of the objective function, which is in four dimensions, cannot be shown in the figure.

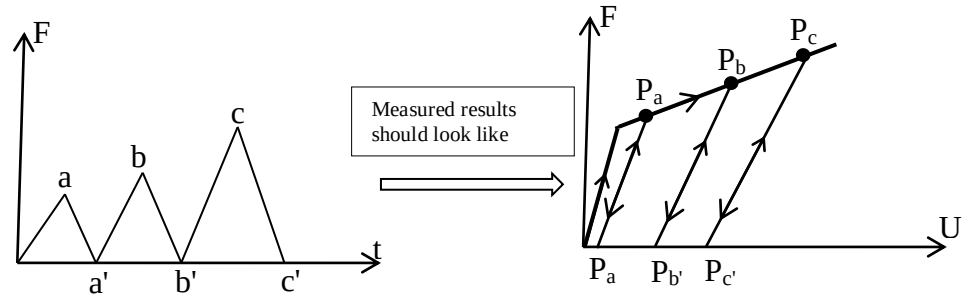

Figure 2.5 Loading program and results of measurements in the coupled plasticity-damage

The second case is simpler for identification because we can first identify parameters for the plasticity, and then parameters for the damage model. Consider having the case where minimum three cycles occur with typical plasticity type of the response (unloading lines parallel with first loading line). The measured values should look like those in diagram shown in Figure 2.6

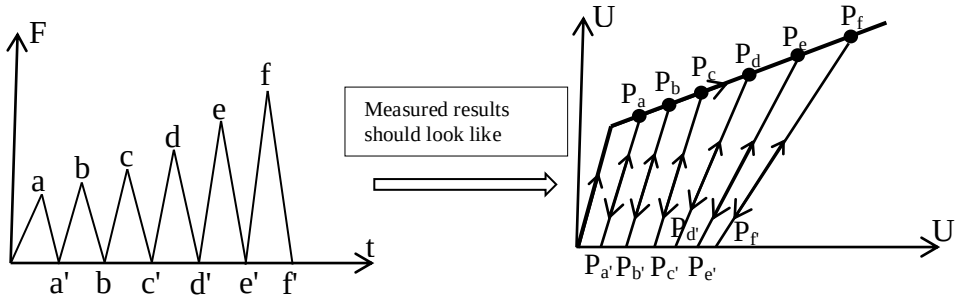

Figure 2.6 Loading program and results of measurements in the coupled plasticity-damage

The shapes of the objective function are shown in Figure 2.7. These shapes are convex, and both can easily be minimized.

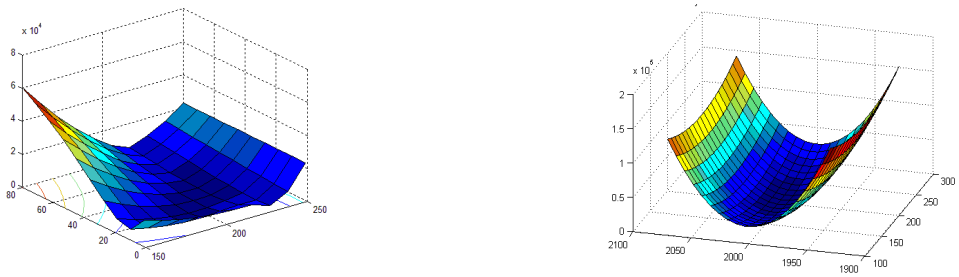

a) Plasticity: N_y, K^p *b) Damage:* N_f, K^d

Figure 2.7 Shapes of the objective function for parameters in the second phase

2.3.1.3 Third phase – constitutive parameters in softening

The identification of the constitutive parameters in the softening part of the response can be performed using the same objective function. In the third identification phase, we have two unknown parameters which are not dependent on each other. This independence ensures simplification in the loading program because cycles of loading and unloading are no longer

needed. By entering in the softening part of the response, we impose displacement at the end of the testing spacemen and constantly measure reactive force in the load cell, such as is shown in Figure 2.8.

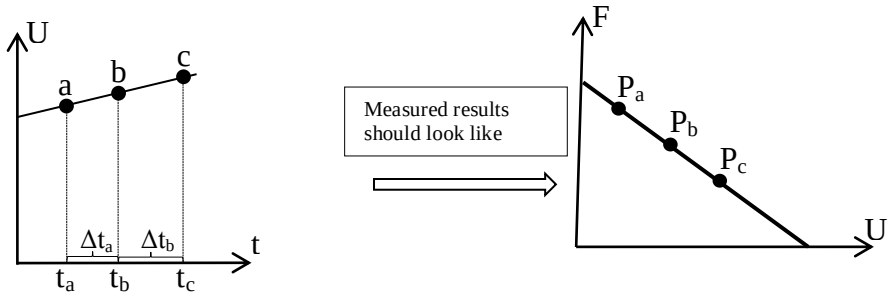

Figure 2.8 Loading program and expected results of measurements in the softening response

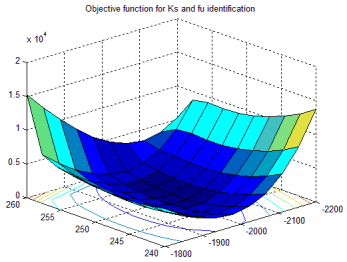

Figure 2.9 Shape of the objective function in the third phase for unknowns: N_u, K^s

By taking three pairs of measured values (force and displacement), we provide identification procedure of unknown parameters in the softening response. The shape of the objective function for unknown parameters is shown in Figure 2.9. The shape of the surface is convex. Thus it has a minimum.

2.4 *Concluding remarks*

In this chapter, we have proposed constitutive parameters identification procedure for the 1D truss bar. The constitutive model of the truss bar consists of coupled plasticity-damage in the hardening and the linear law in the softening. The most important conclusions can be stated as follows:

- Proposed methodology is able to identify all unknown parameters (eight) when these parameters are split into three phases: elasticity, hardening and softening.

- The focus of this chapter was in the constitutive models and the choice of the objective function. In this chapter, we have shown that by using loading program, which contains both loading and unloading cycles, we can identify all unknown constitutive parameters. These cycles are needed in order to make a difference in the responses obtained for plasticity and damage models. Both models can describe the same behavior in the loading regime, and only in unloading, we can see the difference between them.

Chapter 3

Plasticity-Damage Model Parameters Identification for Structural Connections

Abstract

In this chapter, we present a methodology for parameters identification of constitutive model which is able to present behavior of a connection between two members in a steel structure. Such a constitutive model for frame connections can be cast in the most general form of the Timoshenko beam, which can present three failure modes. The first failure mode pertains to the bending in connection, which is defined as coupled plasticity-damage model with nonlinear softening. The second failure mode is seeking to capture the shearing of connection, which is defined as plasticity with linear hardening and nonlinear softening. The third failure mode pertains to the axial force failure in the members. The theoretical formulation of this Timoshenko beam model and its finite element implementation are presented in the second section. The parameter identification procedure that will allow us to define eighteen unknown parameters is given in Section 3.3. The proposed methodology splits identification into three phases, with all details presented in Section 3.4 through three different examples. We also present the experimental results. The conclusions are stated in the last part of the chapter.

Contents of Chapter 3

3.1 Introduction

In this chapter, we present a methodology for constitutive parameters identification of the model capable of representing the behavior of a connection between two members in a structure. Connections have a significant influence on the nonlinear behavior of frame structures, especially those built from the steel and the timber. There are many types of connection, and practically each of them has something specific. Thus, the best choice of adequate model for describing these phenomena is a very challenging task.

The Timoshenko beam (Medic et al., 2013) provides the possibility for constructing the optimal model of this kind. There precisely, we use coupled plasticity-damage model (Ibrahimbegovic et al., 2008; Ayhan et al., 2013) with included softening part of the response (Ibrahimbegovic, 2009). Plasticity and damage models are defined with linear hardening while the softening response is defined as a nonlinear law. Transverse displacement or shearing of the connection is defined by plasticity model combined with hardening/softening response. The theoretical formulation of the link element which can describe this kind of the behavior for the bending and shearing is presented in the next section of the chapter.

Each structural element of the frame structure is modeled with the Euler-Bernoulli beam (Dujc et al., 2010). The constitutive law is defined as plasticity with linear hardening and nonlinear softening models. This type of beam model is adequate for slender elements where length l of the elements versus high h ratio l/h >10. Rather, the main focus of this research pertains to the identification of model parameters for the connection between two members of a structure.

The model parameters identification procedure can be split into three subsequent phases, following (Kucerova et al., 2009). In the first phase, we present identification of parameters governing the elasticity response, where we have three unknowns. The second phase deals with the identification of parameters for coupled plasticity-damage model. Two unknown parameters are active in Euler-Bernoulli beam and six parameters in the connection. Identification of connection behavior can be split into the shearing and the bending. In the bending case there are two possible scenarios. First when parameters for plasticity and damage models take very close values, and the second when the values of parameters are not as close so that we can identify two by two parameters.

The identification of these parameters in each phase is made using a combination of two computer programs: Matlab and FEAP (Taylor, 2008). FEAP is the finite element program which is used for FEM analysis task in the identification process. Matlab is used for computing the minimization of objective or cost function. Objective functions for different phases of identification are presented in the third section of this chapter.

The outline of the chapter is as follows. In the next section, we present the main ingredients of the proposed link element for representing the behavior of connection regarding the Timoshenko beam (Bui et al., 2014). In the third section, we describe the global identification problem of a connection. The fourth section presents a proposition for the experimental setup, the loading program and all phases of identification in three different examples. In the fifth section, we also compare examples of identification against real experimental results (Gang Shi, 2007; Mesic, 2003).

3.2 Theoretical formulation of the Timoshenko beam audits finite element implementation

In this section, we present theoretical formulations for the link element regarding the Timoshenko beam. The link element is a slight modification of the Timoshenko beam defined in (Bui et al., 2014; Nikolic & Ibrahimbegovic, 2015) with embedded discontinuity. The need for this modification can be found in physically admissible displacement/deformation of connections. Namely, for pure bending in the connection transverse displacement does not exist, practically only rotation exists. If we use Timoshenko or Euler-Bernoulli beam, this condition is not satisfied. The modification of the Timoshenko beam starts in (3.1), where we modify expression for the shear deformation. The Euler-Bernoulli beam with embedded discontinuity (Dujc et al., 2010) is used to represent bending behavior of members of the frame structure. The constitutive law is defined as plasticity with linear hardening for the continuous part, while the softening at the discontinuity is defined according to the nonlinear law.

3.2.1. Timoshenko modified beam element

The theoretical formulation of the link element - modified Timoshenko beam can be first defined regarding its strong form of equilibrium equation. Here, we present the main ingredients of these models.

3.2.1.1. Strong form of equilibrium equations

In Figure 3.1 we present different formulation of beam curvature measure in a given cross section.

It can be written:

$$\begin{aligned} &\frac{dv}{dx} = \psi && \text{- Euler-Bernoulli beam} \\ &\frac{dv}{dx} = \psi + \gamma && \text{- Timoshenko beam} \\ &\frac{dv}{dx} = \gamma && \text{- Link element - modified T. beam} \end{aligned} \tag{3.1}$$

where γ is shear deformation of the beam cross section.

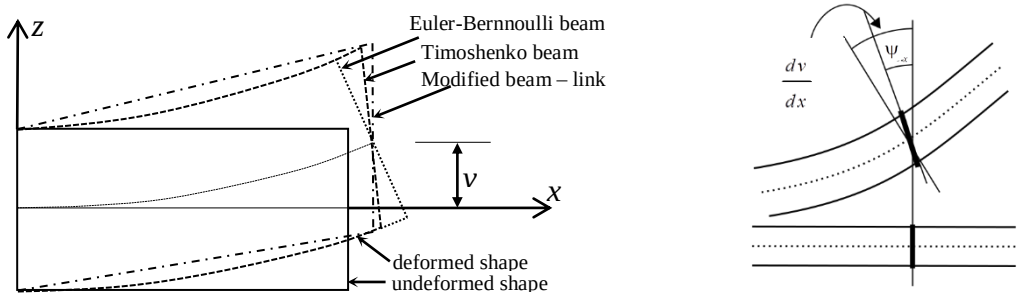

Figure 3.1 Deformation of beams

The equilibrium equations at the infinitesimal beam:

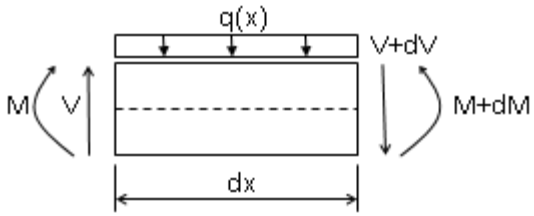

Figure *3.2 Equilibrium at the infinitesimal beam*

$$\left.\begin{aligned}\Sigma M_{right-side} &= M + dM - M - Vdx + \underbrace{q(x)dx\frac{dx}{2}}_{\approx 0 \text{ (small def.)}} = 0 \rightarrow V = \frac{dM}{dx} \\ \Sigma V &= V - V - dV - q(x)dx = 0 \rightarrow \frac{dV}{dx} = -q(x)\end{aligned}\right\} \rightarrow \frac{d^2M}{dx^2} = -q(x) \tag{3.2}$$

The relation between internal forces and deformations when restricted to linear elasticity:

$$M(x) = EI\frac{d\psi}{dx}; V(x) = GA_v\left(\frac{dv}{dx} - \psi\right) \text{ - Timoshenko beam} \tag{3.3}$$

$$M(x) = EI\frac{d\psi}{dx}; V(x) = GA_v\left(\frac{dv}{dx}\right) \text{ - Link element} \tag{3.4}$$

By using equations (3.1), (3.2), (3.3) and (3.4) we can obtain the strong form of the equilibrium equations:

Timoshenko beam:
$$\left.\begin{aligned}\frac{d^2}{dx^2}\left(EI\frac{d\psi}{dx}\right) &= -q(x) \\ \frac{dv}{dx} &= \psi - \frac{EI}{GA_v}\frac{d^2\psi}{dx^2}\end{aligned}\right\} \rightarrow EI\frac{d^4v}{dx^4} = q(x) - \frac{EI}{GA_v}\frac{d^2q}{dx^2} \tag{3.5}$$

Link element:
$$\left.\begin{aligned}\frac{d^2}{dx^2}\left(EI\frac{d\psi}{dx}\right) &= -q(x) \\ \frac{dv}{dx} &= \frac{EI}{GA_v}\frac{d^2\psi}{dx^2}\end{aligned}\right\} \rightarrow \frac{d^2v}{dx^2}GA_v = -q(x) \tag{3.6}$$

3.2.1.2. Weak form of equilibrium equations

The corresponding weak form of the equilibrium equation can be written in the standard form for both beam models (Bui et al., 2014):

$$G(\boldsymbol{\varepsilon}, \zeta^p, \zeta^d; \delta\mathbf{w}) = \int_0^l \boldsymbol{\sigma}^T \delta\boldsymbol{\varepsilon} dx - \underbrace{\int_0^l \mathbf{f}^T \delta\mathbf{w} dx - \mathbf{F}^T \delta\mathbf{w}}_{External\ \ force} = 0 \tag{3.7}$$

where $\boldsymbol{\sigma} = \left[M, T, N\right]^T$ is a vector of stress resultant forces, $\delta\boldsymbol{\varepsilon} = \left[\delta\kappa, \delta\gamma, \delta\varepsilon^N\right]$ is a vector of virtual deformations, $\mathbf{f} = \left[m, q, n\right]^T$ is a vector of the external distributed load, $\delta\mathbf{w} = \left[\delta\theta, \delta w, \delta u\right]$ is a generalized virtual displacement and $\mathbf{F} = \left[M^{ext}, T^{ext}, N^{ext}\right]^T$ is a vector of the external concentrated end forces.

The generalized displacements are split into regular part and jump point introducing the generalized displacement at the discontinuity:

$$\mathbf{u}(x,t)=\bar{\mathbf{u}}(x,t)+\boldsymbol{\alpha}(t)H_{\bar{x}}(x)=\begin{bmatrix}\bar{u}(x,t)\\ \bar{v}(x,t)\\ \bar{\psi}(x,t)\end{bmatrix}+\begin{bmatrix}\alpha_u(t)\\ \alpha_v(t)\\ \alpha_\psi(t)\end{bmatrix}H_{\bar{x}}(x);\ \ H_{\bar{x}}(x)=\begin{cases}1;\ \ x>\bar{x}\\ 0;\ \ x\le\bar{x}\end{cases} \tag{3.8}$$

where $\boldsymbol{\alpha}$ is a vector of generalized displacement jumps at the point $\bar{x}$, $H_{\bar{x}}(x)$ is the Heaviside function and $\bar{\mathbf{u}}(x,t)$ is a vector of regular displacements in the beam.

3.2.1.3. Constitutive equations for bending

In this section, we present constitutive models for bending strains, both the continuous part and the discontinuity. The continuous part is defined with coupled plasticity-damage model, with linear hardening and nonlinear softening. The main ingredients of the coupled plasticity - damage model (Ibrahimbegovic et al., 2008) are:

- Additive decomposition of the regular curvature field of the beam:

$$\bar{\kappa}=\bar{\kappa}^e+\bar{\kappa}^p+\bar{\kappa}^d \tag{3.9}$$

- Helmholtz free energy:

$$\bar{\Psi}\left(\bar{\kappa},\bar{\kappa}^d,D,\bar{\kappa}^p,\bar{\xi}^p,\bar{\xi}^d\right)=\underbrace{M\bar{\kappa}^e-\overbrace{\frac{1}{2}M\left(EI\right)^{-1}M}^{\bar{\chi}^e(M)}}_{\bar{\Psi}^e}+\underbrace{\frac{1}{2}\bar{\xi}^p\bar{K}_p\bar{\xi}^p}_{\bar{\Xi}^p}+\underbrace{M\bar{\kappa}^d-\overbrace{\frac{1}{2}MDI^{-1}M}^{\bar{\chi}^d(M,D)}}_{\bar{\Psi}^d}+\underbrace{\frac{1}{2}\bar{\xi}^d\bar{K}_d\bar{\xi}^d}_{\bar{\Xi}^d} \tag{3.10}$$

$$\bar{\bar{\Psi}}\left(\bar{\bar{\xi}}^s\right)=\underbrace{\frac{1}{2}\bar{\bar{\xi}}^s\bar{K}_s\bar{\bar{\xi}}^s}_{\bar{\bar{\Xi}}^s};\ \ \Psi(\cdot)=\bar{\Psi}(\cdot)+\bar{\bar{\Psi}}(\bar{\bar{\xi}}^s)\delta_{\bar{x}}$$

where E is the elasticity modulus, $\bar{\xi}^p,\bar{\xi}^d,\bar{\xi}^s$ are internal hardening variables for: plasticity, damage and softening, respectively, M is an bending moment in the integration point, $\bar{K}_d,\bar{K}_p$ are hardening moduli for the damage and the plasticity models, $\bar{K}_s$ is softening modulus, and I is moment of the inertia.

- The total dissipation produced by this coupled plasticity-damage model must remain non-negative. That can be written by appealing to the second principle of thermodynamics:

$$0\le\bar{\mathcal{D}}=\underbrace{\dot{\bar{M}}\left(\frac{\partial\bar{\chi}^e}{\partial M}-\bar{\kappa}^e\right)+\dot{M}\left(\frac{\partial\bar{\chi}^d}{\partial M}-\bar{\kappa}^d\right)}_{\bar{\mathcal{D}}^e=0}+\underbrace{M\dot{\bar{\kappa}}^p-\frac{\partial\bar{\Xi}^p}{\partial\bar{\xi}^p}\dot{\bar{\xi}}^p}_{\bar{\mathcal{D}}^p}+\underbrace{\frac{\partial\bar{\kappa}^d}{\partial\bar{D}}\dot{\bar{D}}I^{-1}-\frac{\partial\bar{\Xi}^d}{\partial\bar{\xi}^d}\dot{\bar{\xi}}^d}_{\bar{\mathcal{D}}^d} \tag{3.11}$$

where $\bar{\chi}$ is complementary energy, see (Ibrahimbegovic, 2009).

- Yield functions for plasticity and damage:

$$\begin{aligned}\bar{\phi}^p\left(M,\bar{q}^p\right) &= |M| - \left(M_y - \bar{q}^p\right) \le 0\\ \bar{\phi}^d\left(M,\bar{q}^d\right) &= |M| - \left(M_f - \bar{q}^d\right) \le 0\end{aligned} \tag{3.12}$$

where $M_y > 0$ denotes the yield stress, $M_f > 0$ denotes the damage stress at the beginning of the fracture process zone initiation.

- The principle of maximum plastic dissipation states that among all the variables $\left(M,\bar{q}^p\right)$ that satisfy the yield criterion $\bar{\phi}^p\left(M,\bar{q}^p\right)$ the ones we choose are those that maximize plastic dissipation. That can be written as a constrained minimization problem:

$$\min_{M,\bar{q}^p}\max_{\dot{\bar{\gamma}}^p}\left[\bar{L}^p(M,\bar{q}^p,\dot{\bar{\gamma}}^p) = -\bar{\mathcal{D}}^p(M,\bar{q}^p) + \dot{\bar{\gamma}}^p\bar{\phi}^p(M,\bar{q}^p)\right] \tag{3.13}$$

where the plastic multiplier $\dot{\bar{\gamma}}^p \ge 0$ plays the role of Lagrange multiplier. The corresponding Kuhn-Tucker optimality condition is a constraint for this minimization problem, that can provide the evolution equations for internal variables along with the loading/unloading conditions:

$$\begin{aligned}&\frac{\partial\bar{L}^p}{\partial M} = -\dot{\bar{\kappa}}^p + \dot{\bar{\gamma}}^p\frac{\partial\bar{\phi}}{\partial M} = 0 \Rightarrow \dot{\bar{\kappa}}^p = \dot{\bar{\gamma}}^p sign(M)\\ &\frac{\partial\bar{L}^p}{\partial\bar{q}} = -\dot{\bar{\xi}}^p + \dot{\bar{\gamma}}^p\frac{\partial\bar{\phi}}{\partial\bar{q}} = 0 \Rightarrow \dot{\bar{\xi}}^p = \dot{\bar{\gamma}}^p\\ &\dot{\bar{\gamma}}^p \ge 0,\ \ \bar{\phi}^p \le 0,\ \ \dot{\bar{\gamma}}^p\bar{\phi}^p = 0\end{aligned} \tag{3.14}$$

The correct value of plasticity multiplier $\dot{\bar{\gamma}}^p$ can be computed from the plastic consistency condition on stress state (bending moment):

$$\dot{\bar{\phi}}^p = 0 \ \Rightarrow\ \dot{\bar{\gamma}}^p = \frac{\frac{\partial\bar{\phi}^p}{\partial\sigma}EI(\dot{\bar{\kappa}} - \dot{\bar{\kappa}}^d)}{\frac{\partial\bar{\phi}^p}{\partial M}E\frac{\partial\bar{\phi}^p}{\partial M} - \frac{\partial\bar{\phi}^p}{\partial\bar{q}^p}\frac{\partial\bar{q}^p}{\partial\bar{\xi}^p}\frac{\partial\bar{\phi}^p}{\partial\bar{q}^p}} \tag{3.15}$$

- The principle of maximum damage dissipation states that among all the variables $(M,\bar{q}^d)$ that satisfy the yield criterion $\bar{\phi}^d\left(M,\bar{q}^d\right)$,we have to select those that maximize damage dissipation. That can be written as a constrained minimization problem:

$$\min_{M,\bar{q}^d}\max_{\dot{\bar{\gamma}}^d}\left[\bar{L}^d(M,\bar{q}^d,\dot{\bar{\gamma}}^d) = -\bar{\mathcal{D}}^d(M,\bar{q}^d) + \dot{\bar{\gamma}}^d\bar{\phi}^d(M,\bar{q}^d)\right] \tag{3.16}$$

where the damage multiplier $\dot{\bar{\gamma}}^d \ge 0$ plays the role of Lagrange multiplier. By appealing to the Kuhn-Tucker optimality conditions, from the last result, we can provide the evolution equations for internal variables along with the loading/unloading conditions:

$$\begin{aligned}&\frac{\partial\bar{L}^d}{\partial M} = -\dot{D}M + \dot{\bar{\gamma}}^d\frac{\partial\bar{\phi}^d}{\partial M} = 0 \Rightarrow \dot{D} = \dot{\bar{\gamma}}^d\frac{1}{M}sign(M)\\ &\frac{\partial\bar{L}^d}{\partial\bar{q}^d} = -\dot{\bar{\xi}}^d + \dot{\bar{\gamma}}^d\frac{\partial\bar{\phi}^d}{\partial\bar{q}^d} = 0 \Rightarrow \dot{\bar{\xi}}^d = \dot{\bar{\gamma}}^d\end{aligned} \tag{3.17}$$

The damage consistency conditions can finally provide the correct value for damage multiplier $\dot{\bar{\gamma}}^d$:

$$\dot{\bar{\gamma}}^d \geq 0,\ \ \bar{\phi}^d \leq 0,\ \ \dot{\bar{\gamma}}^d \bar{\phi}^d = 0 \tag{3.18}$$

$$0 < \dot{\bar{\gamma}}^d;\ \ \bar{\phi}^d = 0;\ \ \dot{\bar{\phi}}^d = 0 \ \Rightarrow\ \dot{\bar{\gamma}}^d = \frac{\dfrac{\partial \bar{\phi}^d}{\partial M} \bar{D}^{-1} \dot{\bar{\kappa}}^d}{\dfrac{\partial \bar{\phi}^d}{\partial M} \bar{D}^{-1} \dfrac{\partial \bar{\phi}^d}{\partial M} - \dfrac{\partial \bar{\phi}^d}{\partial \bar{q}^d} \dfrac{\partial \bar{q}^d}{\partial \bar{\xi}^d} \dfrac{\partial \bar{\phi}^d}{\partial \bar{q}^d}} \tag{3.19}$$

- By enforcing the condition that bending moment has the same value in both constitutive models, we can obtain a bending moment rate constitutive equation for coupled damage/plasticity model and define the corresponding elastoplastic-damage tangent modulus:

$$\dot{M} = C^{epd} \dot{\bar{\kappa}} = C^{ep} \left(\dot{\bar{\kappa}} - \dot{\bar{\kappa}}^d \right) = C^{ed} \dot{\bar{\kappa}}^d \Rightarrow C^{epd} = \frac{C^{ep} C^{ed}}{C^{ep} + C^{ed}} \tag{3.20}$$

The remaining model ingredients define the softening response. In particular, we have:

- Yield criterion for the plasticity at the discontinuity can be written as:

$$\bar{\bar{\phi}}(t_M, \bar{\bar{q}}^s) = |t_M| - \left(t_{M_u} - \bar{\bar{q}}^s \right) \leq 0 \tag{3.21}$$

where t_M is bending traction, t_{M_u} is ultimate bending traction and $\bar{\bar{q}}^s(\bar{\bar{\xi}}^s)$ is softening stress like variable at the discontinuity, which depends on internal softening variable $\bar{\bar{\xi}}^s$.

- The principle of maximum plastic dissipation at discontinuity states that among all admissible variables $(t_M, \bar{q}^s)$ that satisfy the yield criterion $\bar{\bar{\phi}}^s \left(t_M, \bar{\bar{q}}^s \right)$ the ones we choose are those that maximize softening dissipation. That can be written as a constrained minimization problem:

$$\min_{\sigma, \bar{\bar{q}}^p} \max_{\dot{\bar{\bar{\gamma}}}^p} \left[\bar{\bar{L}}^s (t_M, \bar{\bar{q}}^s, \dot{\bar{\bar{\gamma}}}^s) = -\bar{\bar{\mathcal{D}}}^s (t_M, \bar{\bar{q}}^s) + \dot{\bar{\bar{\gamma}}}^s \bar{\bar{\phi}}^s (t_M, \bar{\bar{q}}^s) \right] \tag{3.22}$$

where $\dot{\bar{\bar{\gamma}}}^s \geq 0$ plays the role of Lagrange multiplier, $\bar{\bar{\mathcal{D}}}^s = t_M \dot{\alpha}_\psi + \bar{\bar{q}}^s \dot{\bar{\bar{\xi}}}^s$ is a dissipation of the energy in the softening process. By using Kuhn-Tucker loading/unloading condition, the last result can provide the evolution equations for softening internal variables:

$$\begin{aligned}
&\frac{\partial \bar{\bar{L}}^s}{\partial t_M} = -\dot{\alpha}_\psi + \dot{\bar{\bar{\gamma}}}^s \frac{\partial \bar{\bar{\phi}}^s}{\partial t_M} = 0 \Rightarrow \dot{\alpha}_\psi = \dot{\bar{\bar{\gamma}}}^s sign(t_M) \\
&\frac{\partial \bar{\bar{L}}^s}{\partial \bar{\bar{q}}^s} = -\dot{\bar{\bar{\xi}}}^s + \dot{\bar{\bar{\gamma}}}^s \frac{\partial \bar{\bar{\phi}}^s}{\partial \bar{\bar{q}}^s} = 0 \Rightarrow \dot{\bar{\bar{\xi}}}^s = \dot{\bar{\bar{\gamma}}}^s \\
&\dot{\bar{\bar{\gamma}}}^s \geq 0,\ \ \bar{\bar{\phi}}^s \leq 0,\ \ \dot{\bar{\bar{\gamma}}}^s \bar{\bar{\phi}}^s = 0,\ \ \dot{\bar{\bar{\gamma}}}^s \dot{\bar{\bar{\phi}}}^s = 0
\end{aligned} \tag{3.23}$$

For softening process at the discontinuity and elasticity process in the regular part of the beam, we can write an expression for the final stress resultant value:

$$\dot{t}_M = -\int_L \tilde{G}^e (x, \bar{x}) \dot{M} \left(\dot{\kappa}^{(i)}, \dot{\alpha}_\psi \right) dx \tag{3.24}$$

3.2.1.4. Constitutive equations for the shear response

The constitutive law for the shear response of connection is defined as the plasticity with linear hardening and nonlinear softening. Main ingredients for such a plasticity model are:

- Additive decomposition of shear strain into elastic and plastic:

$$\bar{\gamma}_s = \bar{\gamma}_s^e + \bar{\gamma}_s^p \tag{3.25}$$

- Helmholtz free energy:

$$\begin{aligned} &\bar{\Psi}_s\left(\bar{\gamma}_s, \bar{\gamma}_s^e, \bar{\xi}_s^p\right) = \underbrace{\frac{1}{2}\bar{\gamma}_s^e G A_v \bar{\gamma}_s^e}_{\bar{\Psi}^e} + \underbrace{\frac{1}{2}\bar{\xi}_s^p \bar{K}_{s,p} \bar{\xi}_s^p}_{\bar{\Xi}^p}; \bar{\bar{\Psi}}_s\left(\bar{\bar{\xi}}_s^s\right) = \frac{1}{2}\bar{\bar{\xi}}_s^s \bar{\bar{K}}_{s,s} \bar{\bar{\xi}}_s^s \\ &\Psi\left(\bar{\gamma}_s, \bar{\gamma}_s^e, \bar{\xi}_s^p, \bar{\bar{\xi}}_s^s\right) = \bar{\Psi}_s\left(\bar{\gamma}_s, \bar{\gamma}_s^e, \bar{\xi}_s^p\right) + \bar{\bar{\Psi}}_s\left(\alpha_v, \bar{\bar{\xi}}_s^s\right)\delta_{\bar{x}}; \end{aligned} \tag{3.26}$$

where G is the shear modulus, A_v is shear area of the cross-section, $\bar{\xi}^p, \bar{\xi}^s$ are internal hardening and softening variables, $\bar{K}_{s,p}$ is the hardening modulus and $\bar{\bar{K}}_{s,s}$ is the softening modulus.

- The plastic dissipation produced by this model must remain non-negative. That can be written as:

$$0 \le \bar{\mathcal{D}}_s^p = V\dot{\bar{\gamma}}_s - \dot{\bar{\Psi}} = \underbrace{\left(V - \frac{\partial \bar{\Psi}^e}{\partial \bar{\gamma}_s^e}\right)}_{\bar{\mathcal{D}}_s^e = 0}\dot{\bar{\gamma}}_s^e + V\dot{\bar{\gamma}}_s^p - \frac{\partial \bar{\bar{\Xi}}^p}{\partial \bar{\xi}^p}\dot{\bar{\xi}}^p \tag{3.27}$$

- Yield functions for the shear response:

$$\bar{\phi}^p\left(V, q_s^p\right) = |V| - \left(V_y - \bar{q}_s^p\right) \le 0 \tag{3.28}$$

where $V_y > 0$ denotes the yield shear force.

- The principle of the maximum plastic dissipation which states that among all the variables $\left(V, \bar{q}_s^p\right)$ that satisfy the yield criteria $\bar{\phi}^p\left(V, \bar{q}_s^p\right)$ we ought to choose those that maximize the plastic dissipation. That can be written as a constrained minimization problem:

$$\min_{\sigma, \bar{q}^p} \max_{\dot{\bar{\gamma}}^p} \left[\bar{L}^p(V, \bar{q}_s^p, \dot{\bar{\gamma}}^p) = -\bar{\mathcal{D}}_s^p(V, \bar{q}_s^p) + \dot{\bar{\gamma}}^p \bar{\phi}^p(V, \bar{q}_s^p)\right] \tag{3.29}$$

where $\dot{\bar{\gamma}}^p$ plays the role of Lagrange multiplier. By using the Kuhn-Tucker optimality conditions, the last result can provide the evolution equations for internal variables along with the loading/unloading conditions:

$$\begin{aligned} &\frac{\partial \bar{L}^p}{\partial V} = -\dot{\bar{\gamma}}_s^p + \dot{\bar{\gamma}}^p \frac{\partial \bar{\phi}}{\partial V} = 0 \Rightarrow \dot{\bar{\gamma}}_s^p = \dot{\bar{\gamma}}^p sign(V) \\ &\frac{\partial \bar{L}^p}{\partial \bar{q}_s^p} = -\dot{\bar{\xi}}_s^p + \dot{\bar{\gamma}}^p \frac{\partial \bar{\phi}}{\partial \bar{q}_s^p} = 0 \Rightarrow \dot{\bar{\xi}}_s^p = \dot{\bar{\gamma}}^p \\ &\dot{\bar{\gamma}}^p \ge 0, \;\; \bar{\phi}^p \le 0, \;\; \dot{\bar{\gamma}}^p \bar{\phi}^p = 0 \end{aligned} \tag{3.30}$$

- The correct value of plastic multiplier can be computed from the consistency condition, which imposes the plastic admissibility of stress:

$$\dot{\bar{\phi}}^p = 0 \Rightarrow \dot{\bar{\gamma}}^p = \frac{\frac{\partial \bar{\phi}^p}{\partial V} G \dot{\bar{\gamma}}_s}{\frac{\partial \bar{\phi}^p}{\partial V} G \frac{\partial \bar{\phi}^p}{\partial V} - \frac{\partial \bar{\phi}^p}{\partial \bar{q}_s^p} \frac{\partial \bar{q}_s^p}{\partial \bar{\xi}^p} \frac{\partial \bar{\phi}^p}{\partial \bar{q}_s^p}} \tag{3.31}$$

The remaining model ingredients define the softening response:

- The yield criterion for plasticity at the discontinuity can then be written:

$$\bar{\bar{\phi}}^s\left(t_V, \bar{\bar{q}}_s^p\right) = |t_V| - \left(t_{V_y} - \bar{\bar{q}}_s^s\right) \leq 0 \tag{3.32}$$

  where t_V is the shearing traction, t_{V_y} is the yield shearing traction and $\bar{\bar{q}}_s^s\left(\bar{\bar{\xi}}^s\right)$ is the softening shear stress variable at the discontinuity $\bar{x}$.

- The principle of the maximum plastic dissipation at the discontinuity states that among all the variables $(t_v, \bar{\bar{q}}_s^s)$ that satisfy the yield criterion $\bar{\bar{\phi}}_s^s\left(t_V, \bar{\bar{q}}_s^s\right)$ we choose those that maximize the plastic dissipation. That can be written as a constrained minimization problem:

$$\min_{t_V, \bar{\bar{q}}_s^s} \max_{\dot{\bar{\bar{\gamma}}}^p} \left[\bar{\bar{L}}^s(t_V, \bar{\bar{q}}_s^s, \dot{\bar{\bar{\gamma}}}^s) = -\bar{\bar{\mathcal{D}}}_s^s(t_V, \bar{\bar{q}}_s^s) + \dot{\bar{\bar{\gamma}}}^s \bar{\bar{\phi}}_s^s(t_V, \bar{\bar{q}}_s^s) \right] \tag{3.33}$$

  where $\dot{\bar{\bar{\gamma}}}^s$ plays the role of Lagrange multiplier, $\bar{\bar{\mathcal{D}}}^s = t_V \dot{\alpha}_v + \bar{\bar{q}}_s^s \dot{\bar{\bar{\xi}}}^s$ is a dissipation of the energy in the softening process. By using the Kuhn-Tucker optimality conditions, the last result can provide the evolution equations for internal variables along with the loading/unloading conditions:

$$\begin{aligned}
&\frac{\partial \bar{\bar{L}}^s}{\partial t_V} = -\dot{\alpha}_v + \dot{\bar{\bar{\gamma}}}^s \frac{\partial \bar{\bar{\phi}}}{\partial t_V} = 0 \Rightarrow \dot{\alpha}_v = \dot{\bar{\bar{\gamma}}}^s sign(t_V) \\
&\frac{\partial \bar{\bar{L}}^s}{\partial \bar{\bar{q}}_s^s} = -\dot{\bar{\bar{\xi}}}^s + \dot{\bar{\bar{\gamma}}}^s \frac{\partial \bar{\bar{\phi}}}{\partial \bar{\bar{q}}_s^s} = 0 \Rightarrow \dot{\bar{\bar{\xi}}}^s = \dot{\bar{\bar{\gamma}}}^s \\
&\dot{\bar{\bar{\gamma}}}^s \geq 0, \ \bar{\bar{\phi}}^s \leq 0, \ \dot{\bar{\bar{\gamma}}}^s \bar{\bar{\phi}}^s = 0
\end{aligned} \tag{3.34}$$

3.2.1.5. Finite element implementation

The finite element formulation is practically the same as the formulation for the Timoshenko beam (Bui et al., 2014). In this section, we present only the difference between these two elements.

The finite element implementation of the model is based on the incompatible mode method (Ibrahimbegovic & Wilson, 1991). The use of such a technique ensures that the enrichment with a generalized displacement jump remains local, with no additional degrees of freedom required at the global level. We consider the standard two-node Timoshenko beam and modified beam finite element interpolations, with linear polynomials as shape functions:

$$N_1(x) = 1 - \left(x / L^e\right); N_2(x) = x / L^e \tag{3.35}$$

The standard interpolation of displacements at the continuous part can be written:

$$\begin{aligned} u^h(x) &= N_1(x)u_1 + N_2(x)u_2 \\ v^h(x) &= N_1(x)v_1 + N_2(x)v_2 \\ \psi^h(x) &= N_1(x)\psi_1 + N_2(x)\psi_2 \end{aligned} \tag{3.36}$$

where u_a , v_a , ψ_a are nodal values of generalized displacements and $N_a(x)$ is the interpolation function for node "a".

Thus, the corresponding interpolation of strain regular field for the modified Timoshenko beam can be written as:

$$\left.\begin{aligned} \varepsilon_N^h &= \frac{du^h}{dx} = B_1(x)u_1 + B_2(x)u_2 \\ \gamma^h &= \frac{dv^h}{dx} = B_1(x)v_1 + B_2(x)v_2 \\ \kappa^h &= \frac{d\psi^h}{dx} = B_1(x)\psi_1 + B_2(x)\psi_2 \end{aligned}\right\} \rightarrow \boldsymbol{\varepsilon}^h = \mathbf{Bd} \tag{3.37}$$

where:

$$\begin{aligned} \mathbf{B} &= \begin{bmatrix} B_1 & 0 & 0 & B_2 & 0 & 0 \\ 0 & B_1 & 0 & 0 & B_2 & 0 \\ 0 & 0 & B_1 & 0 & 0 & B_2 \end{bmatrix}; \; B_a = \frac{dN_a(x)}{dx} \\ \mathbf{d}^T &= \begin{bmatrix} u_1 & v_1 & \psi_1 & u_2 & v_2 & \psi_2 \end{bmatrix} \end{aligned} \tag{3.38}$$

We note that the choice we made herein is different from the standard interpolation of strain Timoshenko beam, recall that the latter can be written:

$$\left.\begin{aligned} \varepsilon_N^h &= \frac{du^h}{dx} = B_1(x)u_1 + B_2(x)u_2 \\ \gamma^h = \frac{dv^h}{dx} &= B_1(x)v_1 + B_2(x)v_2 - N_1(x)\psi_1 - N_2(x)\psi_2 \\ \kappa^h &= \frac{d\psi^h}{dx} = B_1(x)\psi_1 + B_2(x)\psi_2 \end{aligned}\right\} \rightarrow \boldsymbol{\varepsilon}^h = \mathbf{Bd} \tag{3.39}$$

where:

$$\begin{aligned} \mathbf{B} &= \begin{bmatrix} B_1 & 0 & 0 & B_2 & 0 & 0 \\ 0 & B_1 & -N_1 & 0 & B_2 & -N_2 \\ 0 & 0 & B_1 & 0 & 0 & B_2 \end{bmatrix} \\ \mathbf{d}^T &= \begin{bmatrix} u_1 & v_1 & \psi_1 & u_2 & v_2 & \psi_2 \end{bmatrix} \end{aligned} \tag{3.40}$$

This different interpolation of the strains we choose herein produces uncoupling between transverse displacement and bending moment. Details of the finite element formulation and the computational procedure were presented in (Bui et al., 2014).

3.3 Identification procedure for model parameters

In the case of connection testing, the global response of a specimen can be represented regarding a load-displacement *F-u* diagram. Any such curve can be related to three-phases of the connection response: elastic, hardening and softening part (Figure 3.3). Model for the hardening behavior of the connection is defined as the coupled plasticity-damage while the softening response is governed by the nonlinear law. For the most general case, in the elastic phase, we need to identify four parameters, whereas in the hardening phase eight and the softening phase another six parameters.

The identification in a general case is performed in two steps: i) definition of an objective function based on some experimental measurements; ii) minimization of this objective function in order to find values of constitutive parameters used in the model.

The choice of objective function is a crucial step in ensuring the success of the minimization. In a general case, the objective function can be defined as the gap between measured and computed response values (displacement, stress, deformation, reaction force, etc.):

$$J(\mathbf{d}_{\mathrm{p}}) = \sum_{j \in J} n\left(\mathbf{u}_j^{com}(\mathbf{d}_{\mathrm{p}}) - \mathbf{u}_j^{\exp}\right)^2 \tag{3.41}$$

where $\mathbf{d_p}$ are the model parameters that we seek to identify or similar, $\mathbf{u}_i^{com}(\mathbf{d}_{\mathrm{p}})$ and $\mathbf{u}_i^{\exp}$ are, respectively, computed and experimentally measured values of displacements/stresses/strains and *n* is a weighting factor. The coupled plasticity – damage model is complex for the identification because the both plasticity and damage can represent the same behavior during the loading process. However, we can find a difference in the unloading process. For that reason, the objective function in the hardening phase needs to contain information from the unloading process.

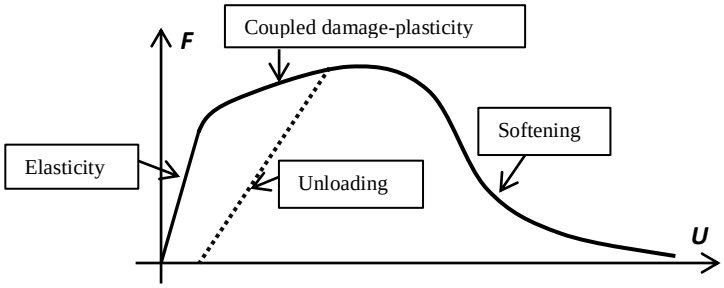

Figure 3.3 Curve force F – displacement U

The minimization of the objective function can formally be written as minimization under constraint:

$$\min_{G(\boldsymbol{\sigma};\delta w)=0} J(\mathbf{d}_{\mathrm{p}}) = \sum_{j \in J} n\left(\mathbf{u}_j^{com}(\mathbf{d}_{\mathrm{p}}) - \mathbf{u}_j^{\exp}\right)^2 \tag{3.42}$$

where the weak form of equilibrium equations $G(\boldsymbol{\sigma};\delta w) = 0$ is the corresponding constraint. Namely, the weak form of equilibrium equations has to be satisfied at every moment. The constrained minimization of the objective function can be transferred into an unconstrained minimization by using Lagrange multiplier method (Ibrahimbegovic et al., 2004):

$$\max_{\forall \lambda} \min_{G(\sigma;\mathbf{d}_p)=0} L(\sigma, \mathbf{d}_{\mathrm{p}}, \lambda) = J(\mathbf{d}_p) + G(\boldsymbol{\sigma};\lambda) \tag{3.43}$$

where λ are Lagrange multipliers inserted into the weak form of equilibrium equations instead of the virtual displacement. This type of minimization of the objective function is very complex for eighteen unknowns.

Such an unconstrained minimization of the objective function is split in several phases, in every phases number of unknowns decreases to maximal of four parameters.

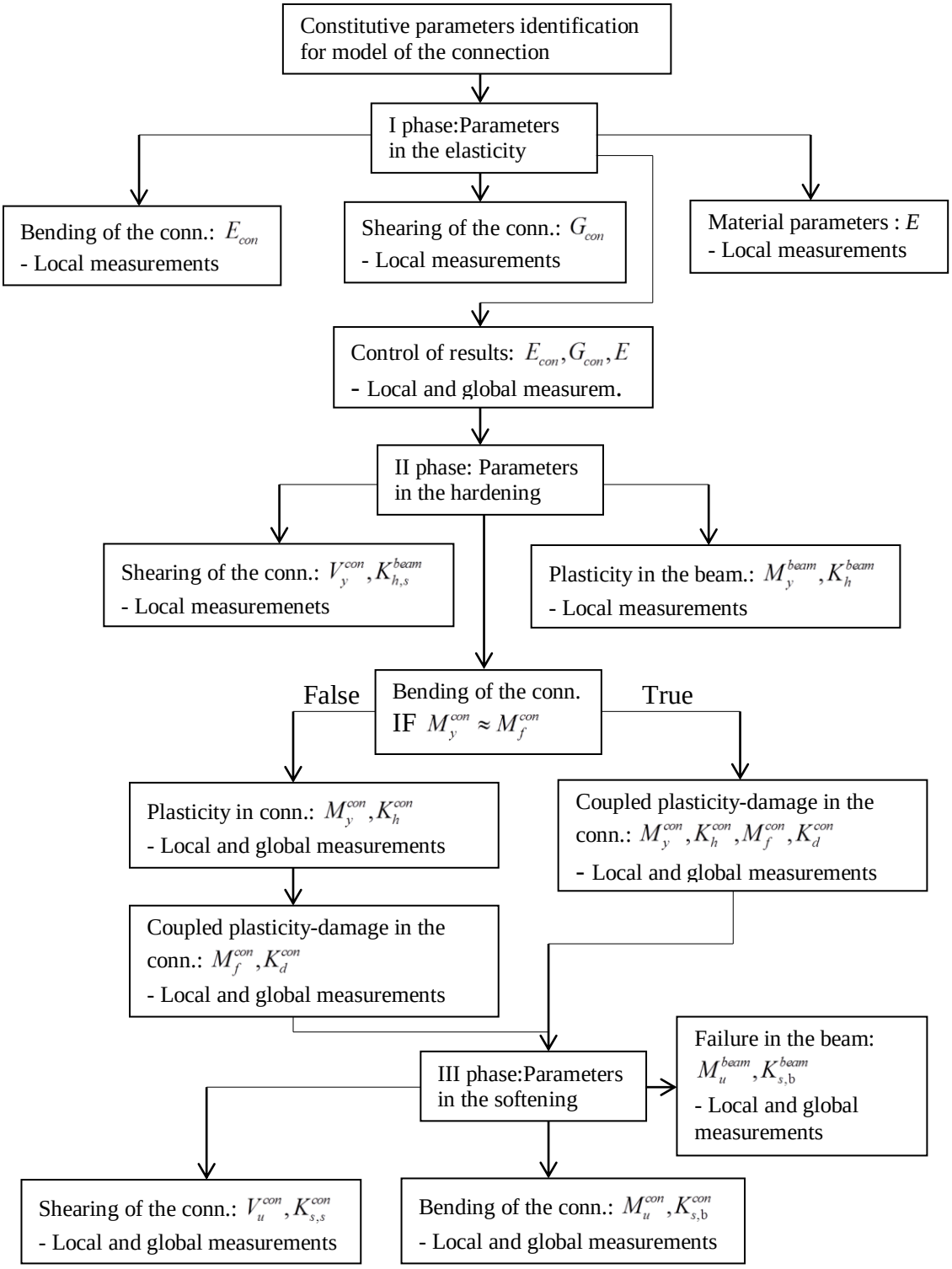

Figure 3.4 Flow chart of parameters identification

The general identification procedure of the connection model parameters is presented in the

flowchart in Figure 3.4. The process is split into three phases, with every phase further splits into few cases. For every case, local and global measurements are required.

Local measurements depend only on one constitutive model, while the global ones depend on all models. This objective function is defined in a detail for different cases of the identification, in the first example, where experimental results are replaced by those obtained from FEM model.

Unconstrained minimization methods included in Matlab are used to solve the identification problem. In particular, we use four methods: BFGS (Broyden–Fletcher–Goldfarb–Shanno method), DFP (Davidon–Fletcher–Powell method), Trust Region and Steepest Descent. The comparisons between these methods are presented in the examples that follow.

The objective function for the parameters identification of the connection in a general case can be written as:

$$J\left(\mathbf{d}_p\right)=\sum_{1}^{3}a\left(F_{Pi}^{com}-F_{Pi}^{\exp}\right)^2+\sum_{1}^{3}b\left(U_{Pi}^{com}-U_{Pi}^{\exp}\right)^2+\sum_{1}^{3}b\left(U_{S,Pi}^{com}-U_{S,Pi}^{\exp}\right)^2+\sum_{1}^{3}c\left(\psi_{Pi}^{com}-\psi_{Pi}^{\exp}\right)^2+$$
$$+\sum_{1}^{3}c\left(\psi_{Pi'}^{com}-\psi_{Pi'}^{\exp}\right)^2+\sum_{1}^{2}d\left(\Delta\psi_{Pi}^{com}-\Delta\psi_{Pi}^{\exp}\right)^2+\sum_{1}^{3}e\left(\kappa_{Pi}^{com}-\kappa_{Pi}^{\exp}\right)^2+\sum_{1}^{3}e\left(\kappa_{Pi'}^{com}-\kappa_{Pi'}^{\exp}\right)^2+$$
$$+\sum_{1}^{3}g\left(\Delta\kappa_{Pi}^{com}-\Delta\kappa_{Pi}^{\exp}\right)^2 \tag{3.44}$$

where are: $F_{Pi}^{com},F_{Pi}^{\exp}$ - forces for a different load level (P_i); $U_{Pi}^{com},U_{Pi}^{\exp}$ - displacements (P_i) ; $U_{S,Pi}^{com},U_{S,Pi}^{\exp}$ - shear displacements (P_i); $U_{Pi'}^{com},U_{Pi'}^{\exp}$ - residual displacements (unloaded point $P_{i'}$); $\psi_{Pi}^{com},\psi_{Pi}^{\exp}$ - rotations of the connection (P_i); $\psi_{Pi'}^{com},\psi_{Pi'}^{\exp}$ - residual rotations (unloaded point $P_{i'}$); $\Delta\psi_{Pi}^{com}=\psi_{Pi+1}^{com}-\psi_{Pi}^{com}$ and $\Delta\psi_{Pi}^{\exp}=\psi_{Pi+1}^{\exp}-\psi_{Pi}^{\exp}$ - gradients of rotation between two different load (P_i) ; $\kappa_{Pi}^{com},\kappa_{Pi}^{\exp}$ - curvatures of the section (P_i); $\kappa_{Pi'}^{com},\kappa_{Pi'}^{\exp}$ - residual curvatures of the section (unloaded point $P_{i'}$); $\Delta\kappa_{Pi}^{com}=\kappa_{Pi+1}^{com}-\kappa_{Pi}^{com}$ and $\Delta\kappa_{Pi}^{\exp}=\kappa_{Pi+1}^{\exp}-\kappa_{Pi}^{\exp}$ - gradients of curvature between two different load (P_i); *a, b, c, d, e, g* - constants.

3.4 Numerical examples

In this chapter, we present three numerical examples in order to illustrate the performance of the proposed identification procedure. The first example serves to illustrate all cases of the identification procedure, where the corresponding experimental results are obtained from the refined FEM model. The remaining two examples provide the illustration of the identification procedure of model parameters for real experimental results of the steel connection and the timber connection. Moreover, the examples serve to illustrate that proposed identification procedure applies to parameters identifications in steel and timber structures, the cases of the large practical interest.

3.4.1. Steel structure connection with complete set of failure modes

In this example, we present a methodology for the parameters identification which describes the nonlinear behavior of both the connection and structural members. We need to obtain eighteen unknowns in total. The measurement values in this example were computed on a more refined mesh of beam elements. We practically can test all phases of the proposed identification procedure.

3.4.1.1. Experimental setup and FEM model

In Figure 3.5, experimental setup for testing of the connection between two orthogonal steel beams and corresponding FEM model, is shown. The horizontal beam is chosen as a much stronger than the vertical beam, so that should ensure the linear elastic behavior of the horizontal beam during the test. The equipment for displacements and deformations measurements is arranged, so that gives us sufficient information for the identification of the mechanical properties. The results can be classified as local and global measurements. The global measurements depend on all model parameters, while the local measurements depend on only one model parameter.

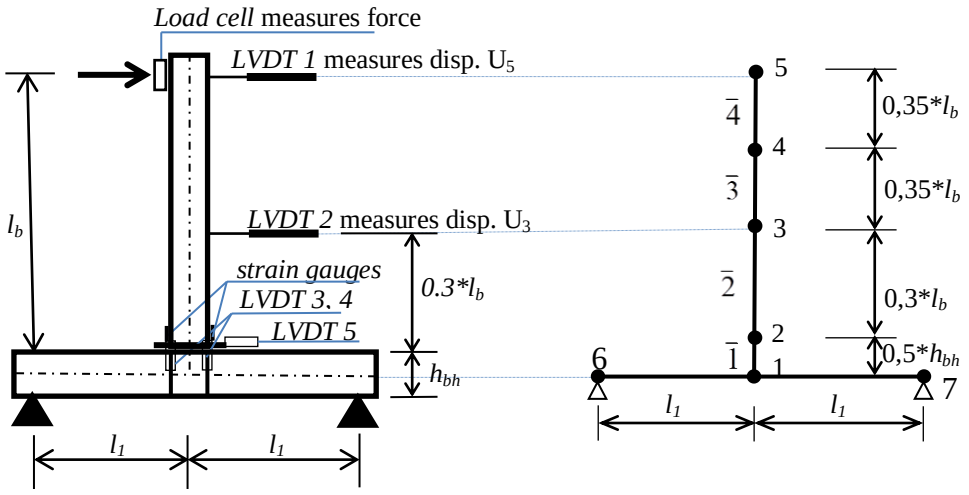

(a) Experimental setup (b) FEM model

Figure 3.5 Experimental setup and FEM model

In particular, the measuring equipment illustrated in Figure 3.5 consists of: LVDT (Linear variable displacement transducer) 1 and 2 measure global displacements of the vertical beam at nodes 3 ($U_{3,Pi}^{\exp}$) and 5 ($U_{5,Pi}^{\exp}$); LVDT 3 and 4 measure relative vertical displacement between the horizontal and the vertical beams, which is later used for a calculation of the connection rotation:

$$\psi^{\exp} = \frac{\Delta v_3^{\exp} - \Delta v_4^{\exp}}{h_{vert.beam}} \tag{3.45}$$

LVDT 5, which measures relative horizontal displacement ($U_{2,Pi}^{\exp} = U_{S,Pi}^{\exp}$) between horizontal and vertical beams, measures transverse (shearing) displacement of connection. Strain gauges measure the deformation at the vertical beam which is later used for calculation of the section curvature near to the connection, assuming the vertical beam is not loaded with axial force:

$$\varepsilon_i^{\exp} = -y \cdot \kappa_i \Rightarrow \kappa_i = -\frac{\varepsilon_i^{\exp}}{y};\ y = \left[-\frac{h}{2}, \frac{h}{2}\right] \Rightarrow \kappa^{\exp} = \frac{\kappa_1 + \kappa_2}{2} \tag{3.46}$$

All the measurements can be taken continuously during the test.

The FEM model is composed of six beam elements. The element number 1 is used for modeling the connection as described in Section 3.2.1., while all other elements (2,3,4,5,6) are chosen as the Euler-Bernoulli beams.

3.4.1.2. Phase I - Elastic parameters identification (E_{con},G_{con}, E)

In this phase, we need to identify three parameters governing the elastic response: E_{con} is the stiffness of the connection for the bending, G_{con} is the stiffness of the connection for the shear response and E is the Young's modulus for steel beams.

Young's modulus E for steel beam can be obtained using the standard material tests. Alternatively, the modulus E can be identified from the local measurement of strain gauges, separately of the other measurements. The shearing stiffness of the connection (G_{con}) can be obtained from the local measurement of LVDT 5. The bending stiffness of the connection (E_{con}) can be identified from the local measurement of the connection rotation.

The loading program for this phase is presented in Figure 3.6. At the time (points: a',b',c'), we measure a residual (plastic) displacement, if these measurements are equal to zero then plasticity is not activated yet.

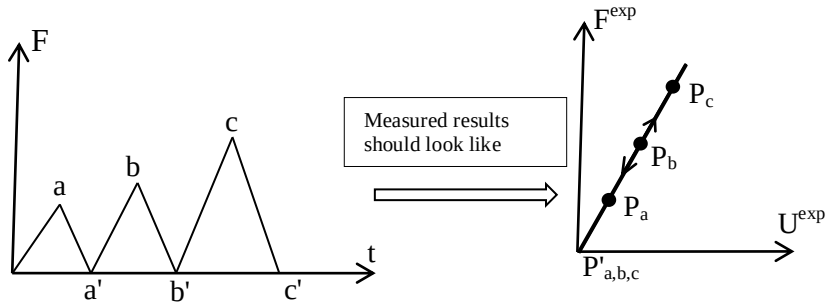

Figure 3.6 Loading program and measurements in the elasticity

By using only measurements of the rotation, we can identify the elastic stiffness (for virgin material) of the connection. The identification problem can be reduced to one unknown if we employ expression, which defines a dependency between elastic and damage stiffness of the connection:

$$E_{con}^{e} = \frac{1}{D_{con}^{d}} \tag{3.47}$$

where E_{con}^{e}, D_{con}^{d} are stiffness coefficients of the linear-elastic and the damage model.

In the elastic phase, the objective function for the parameters identification related to bending of the the connection can be written as:

$$J\left(E_{con}^{e}, D_{con}^{d}\right) = \sum_{1}^{3}\left(\psi_{Pi}^{com} - \psi_{Pi}^{\exp}\right)^{2} \tag{3.48}$$

The shearing stiffness of the connection can be obtained from local measurements of LDVT5, where we measure a relative displacement between the horizontal and the vertical beam, which is triggered by sliding of the connection. The objective function for this identification case can be written as:

$$J\left(G_{con}^{e}\right) = \sum_{1}^{3}\left(U_{2,Pi}^{com} - U_{2,Pi}^{\exp}\right)^{2} \tag{3.49}$$

Young's modulus of the steel beam can be obtained from the local measurements of the strain gauges. The objective function is now defined as:

$$J\left(E^{beam}\right)=\sum_{1}^{3}\left(\kappa_{Pi}^{com}-\kappa_{Pi}^{\exp}\right)^{2} \tag{3.50}$$

At the end of this phase we can control results of the identification using a combination of local and global measurements and identify all parameters simultaneously. A universal objective function can be written as:

$$\begin{aligned} J\left(E_{con}^{e},D_{con}^{d},G_{con}^{e},E^{beam}\right)=&\sum_{1}^{3}\left(U_{5,Pi}^{com}-U_{5,Pi}^{\exp}\right)^{2}+\sum_{1}^{3}\left(U_{3,Pi}^{com}-U_{3,Pi}^{\exp}\right)^{2}\\ &+\sum_{1}^{3}c\left(\psi_{Pi}^{com}-\psi_{Pi}^{\exp}\right)^{2}+\sum_{1}^{3}d\left(\kappa_{Pi}^{com}-\kappa_{Pi}^{\exp}\right)^{2}\end{aligned} \tag{3.51}$$

where *c* and *d* are constants defining the weights of global and local displacement measurements.

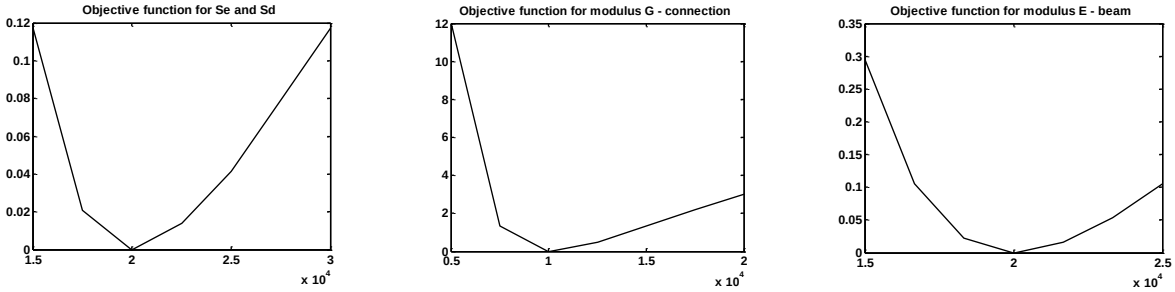

(a) OF: $J\left(E_{con}^{e},D_{con}^{d}\right)$ (b) OF: $J\left(G_{con}^{e}\right)$ (c) OF: $J\left(E^{beam}\right)$

Figure 3.7 Objective functions

3.4.1.3. Phase II of identification procedure for coupled plasticity-damage model constitutive parameters

In this phase, we need to identify eight parameters: M_{y}^{con} - bending moment of the plastic yielding of the connection; $K_{b,h}^{con}$ - plastic hardening modulus for the bending of the connection; M_{f}^{con} - bending moment of the damage yielding of the connection; K_{d}^{con} - damage hardening modulus for the bending of the connection; V_{y}^{con} - shearing force of the plastic yielding of the connection; $K_{s,h}^{con}$ - plastic hardening modulus for the shear response of the connection; M_{y}^{beam} - bending moment of the plastic yielding of the beam; K_{h}^{beam} - plastic hardening modulus for bending of the beam. For identification procedure, these parameters can be divided into three groups: the beam parameters ($M_{y}^{beam},K_{h}^{beam}$), shearing in the connection ($\mathrm{V}_{y}^{con},K_{s,h}^{con}$) and bending in the connection ($M_{y}^{con},K_{b,h}^{con},M_{f}^{con},K_{d}^{con}$).

3.4.1.3.1. Plasticity model for the beam failure

The model parameters of a plasticity related to the beam failure can be obtained from the local measurements by the strain gauges. The strain gauges provide the measurements throughout the loading program. When the plasticity is activated, we need to have values of a deformation for three loading-unloading cycles.

The identification can be completed successfully with this kind of measurements. The objective function for this identification case can be written as:

$$J\left(K_h^{beam}, M_y^{beam}\right) = \sum_1^3 \left(\kappa_{Pi}^{com} - \kappa_{Pi}^{\exp}\right)^2 + \sum_1^3 \left(\kappa_{Pi'}^{com} - \kappa_{Pi'}^{\exp}\right)^2 + \sum_1^2 \left(\Delta\kappa_{Pi}^{com} - \Delta\kappa_{Pi}^{\exp}\right)^2 \tag{3.52}$$

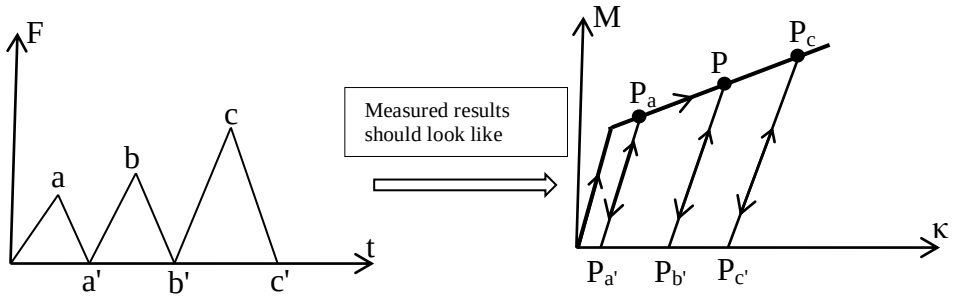

Figure 3.8 Loading program and results of measuring in the hardening response

The objective function is shown in Figure 3.9a, where we can see that the function is convex, which allows to obtain its minimum easily. The minimization of the objective function was done using different methods: BFGS, DFP, Trust Region and Steepest Descent. Comparison of efficiency of these methods is presented in Table 3.1:

Table 3.1 Efficiency of different methods for minimization of $J\left(K_h^{beam}, M_y^{beam}\right)$

Applied method for minimization	Number of		Time of computation	Max. error of the Identification [%]
	Iterations	Evolutions		
BFGS	11	21	50 s	0,00
DFP	45	57	95 s	0,00
Trust Region	22	23	125 s	0,00
Steepest Descent	5	48	108 s	12,55

3.4.1.3.2. Plasticity model for shearing of the connection

Parameters of the plasticity model for the shear response of the connection can be identified from local measurement LVDT 5. In this part we use the analogy in the loading program presented previously in this chapter. More precisely, the loading program and expected results of measurements look the same as presented. The chosen objective function can be written as:

$$J\left(F_y, K_{hs}^{con}\right) = \sum_1^3 \left(U_{2,Pi}^{con} - U_{2,Pi}^{\exp}\right)^2 + \sum_1^3 \left(U_{2,Pi'}^{con} - U_{2,Pi'}^{\exp}\right)^2 + \sum_1^3 \left(\Delta U_{2,Pi}^{con} - \Delta U_{2,Pi}^{\exp}\right)^2 \tag{3.53}$$

Table 3.2 The efficiency of different methods for minimization of $J\left(F_y, K_{hs}^{con}\right)$

Applied Method for Minimization	Number of		Time of computation	Max. error of the Identification [%]
	Iterations	Evolutions		
BFGS	13	19	34 s	0,10
DFP	16	45	75 s	3,35
Trust Region	171	171	780 s	0,59
Steepest Descent	37	150	380 s	0,04

The shape of this objective function is shown in Figure 3.9b. This function is convex and has a minimum. Results of comparison of different methods for minimization of this function are

presented in Table 3.2.

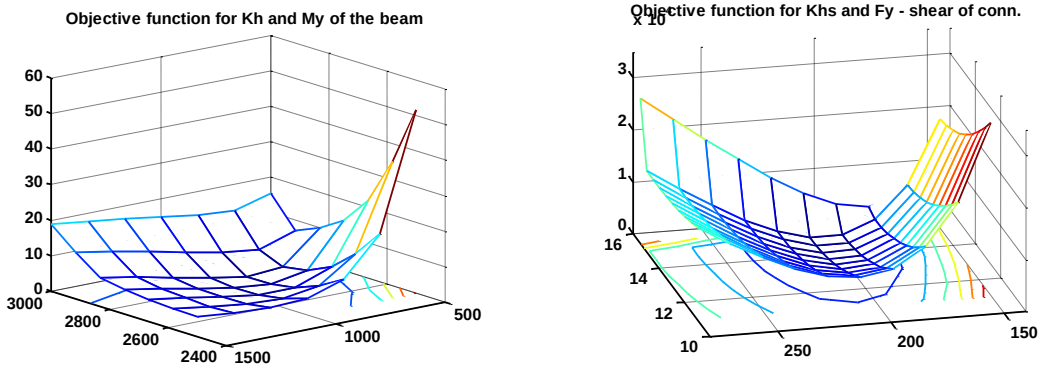

(a) OF: $J\left(K_h^{beam}, M_y^{beam}\right)$ (b) OF: $J\left(F_y, K_{hs}^{con}\right)$

Figure 3.9 Shapes of Objective Functions

3.4.1.3.3. Coupled plasticity-damage model for the bending of the connection

Parameters of the coupled-plasticity model for the bending of the connection can be obtained from all measurements. This task is the most complex, where we need to exploit measurements at the both global and local levels, as well as previously identified values ($V_y^{con}, K_{s,h}^{con}, M_y^{beam}, K_h^{beam}$). Here we can have two different cases. In the first case, the value of the damage moment is significantly larger than a yielding moment in the plasticity. In the second case, both bending moments have close values.

The first case is simpler for the identification because we can first identify parameters for plasticity and then for the damage model. We consider having this case when minimum three cycles occur with a typical plasticity type response (the unloading lines parallel with the first loading line). The measured values should look like those in the diagram in Figure 3.10.

The objective function for the identification of parameters of plasticity models for connection can be written as:

$$J\left(K_{h,b}^{con}, M_y^{con}\right) = \sum_1^3 \left(U_{5,Pi}^{com} - U_{5,Pi}^{\exp}\right)^2 + \sum_1^3 \left(U_{3,Pi}^{com} - U_{3,Pi}^{\exp}\right)^2 + \sum_1^3 m\left(\psi_{Pi}^{com} - \psi_{Pi}^{\exp}\right)^2 + \sum_1^3 m\left(\psi_{Pi'}^{com} - \psi_{Pi'}^{\exp}\right)^2 + \sum_1^2 n\left(\Delta\psi_{Pi}^{com} - \Delta\psi_{Pi}^{\exp}\right)^2 \tag{3.54}$$

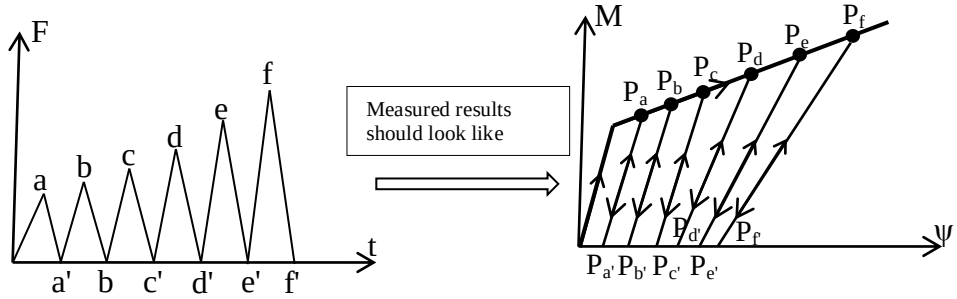

Figure 3.10 Loading program and results of measurements in the coupled plasticity-damage model

The shape of the objective function is shown in Figure 3.12a. This surface is convex, and it can easily be minimized. The minimization is performed by using four different methods. The comparison of the results is shown in Table 3.3.

Table 3.3 Efficiency of different methods for minimization of $J\left(M_y^{con}, K_{h,b}^{con}\right)$

Applied Method for Minimization	Number of		Time of computation	Max. error of the Identification [%]
	Iterations	Evolutions		
BFGS	12	27	53 s	0,00
DFP	39	51	91 s	0,00
Trust Region	71	72	402 s	1,33
Steepest Descent	13	69	120 s	14,80

Afterward, we start the identification of parameters for the damage model (M_f^{con}, K_d^{con}), where the previously identified parameters for the plasticity are kept. The identification problem is reduced to two parameters. The objective function is the same, while only load level is different therefore we use measured values from last three cycles (Figure 3.10).
This objective function is convex, and we can see the shape in Figure 3.12b. The minimization is performed by using four methods. The efficiency of these methods is presented in Table 3.4.

Table 3.4 Efficiency of different methods for minimization of $J\left(M_f^{con}, K_d^{con}\right)$

Applied Method for Minimization	Number of		Time of computation	Max. error of the Identification [%]
	Iterations	Evolutions		
BFGS	14	29	64 s	0,00
DFP	50	66	137 s	0,00
Trust Region	34	35	231 s	10,14
Steepest Descent	9	48	87 s	20,75

The second case is the most complex, where the identification cannot be split into two parts. The damage moment and the yielding moment have close values (Figure 3.11) and we need to identify four parameters simultaneously. The identification of four parameters is possible with the same objective function, where we use results of local and global measurements. The efficiency and the accuracy in the minimization process depend on first guess values. If we have good starting values we can obtain parameters with acceptable errors. Results of the minimization of the objective function for four unknowns with four different methods are presented in the Table 3.5. In this minimization, we used starting values, which are not close to the correct values. From these results, we can conclude that only BFGS method gives results with acceptable errors (2,79 < 3%).

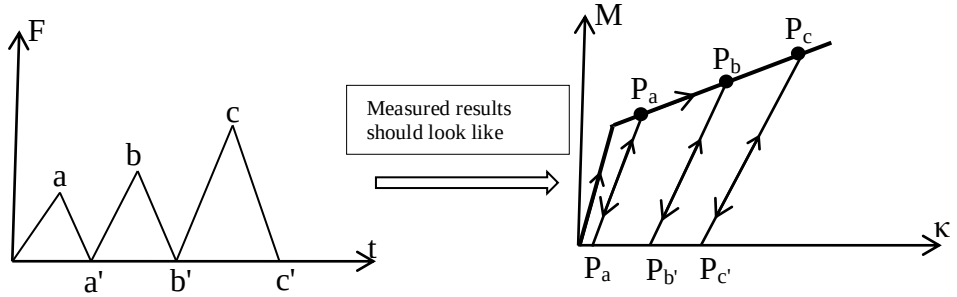

Figure 3.11 Loading program and results of measurements in the coupled plasticity-damage response

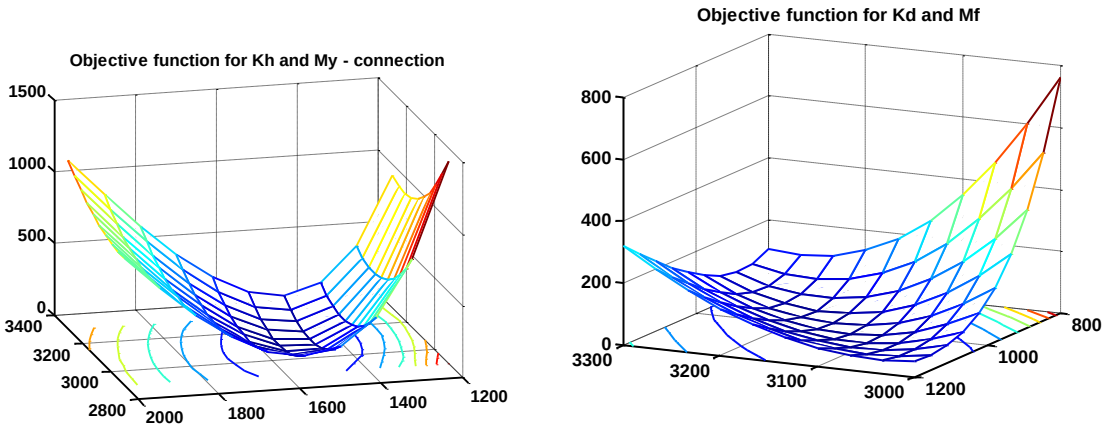

(a) OF: $J\left(M_y^{con}, K_{h,b}^{con}\right)$ (b) OF: $J\left(M_f^{con}, K_d^{con}\right)$

Figure 3.12 Shapes of Objective Functions

To reduce these errors, we can make control identification two by two parameters. First, we can identify parameters for the plasticity model ($M_y^{con}, K_{h,b}^{con}$), while damage parameters are taken as known. Afterword, parameters for the damage model ($M_f^{con}, K_{d,b}^{con}$) are unknown and for the plasticity known. In these two control identifications were determined practically same values of model parameters, but all methods for minimization gave us acceptable errors.

Table 3.5 Efficiency of different methods for minimization of $J\left(M_y^{con}, K_{h,b}^{con}, M_f^{con}, K_d^{con}\right)$

Applied Method for Minimization	Number of		Time of computation	Max. error of the Identification [%]
	Iterations	Evolutions		
BFGS	25	54	161 s	2,79
DFP	58	97	289 s	13,62
Trust Region	81	82	1333 s	6,05
Steepest Descent	22	96	290 s	9,25

3.4.1.4. Phase III of identification procedure for softening model constitutive parameters

In this phase, six parameters can be activated: M_u^{con} - ultimate bending moment of the connection; $G_{f,b}^{con}$ - fracture energy for the bending of the connection; V_u^{con} - ultimate shearing force of the connection; $G_{f,s}^{con}$ - fracture energy for the shearing of the connection; M_u^{beam} - ultimate bending moment of the beam; G_f^{beam} - fracture energy of the beam. These parameters can be obtained for three cases: the failure due to the bending of the connection ($M_u^{con}, G_{f,b}^{con}$), the failure due to the shearing of the connection ($V_u^{con}, G_{f,s}^{con}$) and the failure in the steel beam ($M_u^{beam}, G_{f,b}^{beam}$).

Only one failure mechanism can happen. The local measurements are able to indicate which one of the failure mechanisms is activated. The failure due to the bending the connection can be noted from local measurements LVDT 3 and 4, while the failure due to the shearing of the connection from LVDT 5. The identification can be done for each of these cases.

3.4.1.4.1. First case – softening (failure) due to the bending of the connection

The objective function for this case is a combination of local and global measurements. It can be written as:

$$J\left(M_u^{con}, G_{f,b}^{con}\right) = \sum_1^4 \left(F_{5,Pi}^{com} - F_{5,Pi}^{\exp}\right)^2 + \sum_1^4 \left(U_{5,Pi}^{com} - U_{5,Pi}^{\exp}\right)^2 + \sum_1^4 m\left(\psi_{5,Pi}^{com} - \psi_{5,Pi}^{\exp}\right)^2 \qquad (3.55)$$

The shape of this objective function is shown in Figure 3.13a. We can see that it is a convex function, and thus it has a minimum. The minimization was performed with four methods. Results of the identification procedure are presented in Table 3.6.

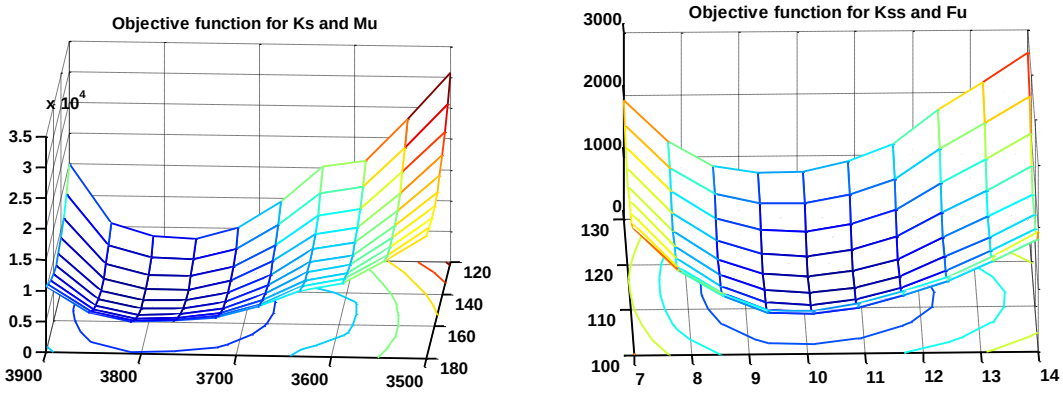

(a) Objective function $J\left(M_u^{con}, G_{f,b}^{con}\right)$ (b) Objective function $J\left(F_u^{con}, G_{f,s}^{con}\right)$

Figure 3.13 Shapes of Objective Functions

Table 3.6 Efficiency of different methods for minimization of $J\left(M_u^{con}, G_{f,b}^{con}\right)$

Applied Method for Minimization	Number of		Time of computation	Max. error of the Identification [%]
	Iterations	Evolutions		
BFGS	7	32	196 s	0,22
DFP	6	35	217 s	0,75
Trust Region	41	42	796 s	0,44
Steepest Descent	28	75	497 s	0,45

3.4.1.4.2. Second case – softening (failure) due to the shearing of the connection

The objective function for this case is a combination of local and global measurements. It can be written as:

$$J\left(F_u^{con}, G_{f,s}^{con}\right) = \sum_1^4 \left(F_{5,Pi}^{com} - F_{5,Pi}^{\exp}\right)^2 + \sum_1^4 \left(U_{5,Pi}^{com} - U_{5,Pi}^{\exp}\right)^2 + \sum_1^4 \left(U_{2,Pi}^{com} - U_{2,Pi}^{\exp}\right)^2 \qquad (3.56)$$

The shape of this objective function is shown in Figure 3.13b. It is a convex function, and the minimization was done with four methods. In Table 3.7, we can see that only results obtained with BFGS method are with acceptable errors.

Table 3.7 Efficiency of different methods for the minimization of $J\left(F_u^{con}, G_{f,s}^{con}\right)$

Applied Method for Minimization	Number of		Time of computation	Max. error of the Identification [%]
	Iterations	Evolutions		
BFGS	2	40	48 s	2,02
DFP	5	34	75 s	3,70
Trust Region	21	22	139 s	5,11
Steepest Descent	3	30	80 s	3,31

3.4.1.4.3. Third case – softening (failure) in the steel beam

This failure mechanism is current if others have not been activated. In this case, we can use only global measurements for the identification of softening parameters of the steel beam. The local measurement of strain gauges is not useful because we do not know where the hinge will be located.

$$J\left(F_u^{beam}, G_{f,s}^{beam}\right) = \sum_1^4 \left(F_{5,Pi}^{com} - F_{5,Pi}^{\exp}\right)^2 + \sum_1^4 \left(U_{5,Pi}^{com} - U_{5,Pi}^{\exp}\right)^2 \tag{3.57}$$

The shape of this objective function is shown in Figure 3.14. This function is convex, but with small irregularities. These irregularities can be reduced if we use more experimental results. In this case we used four reference points (load levels) and the identification procedure was successful.

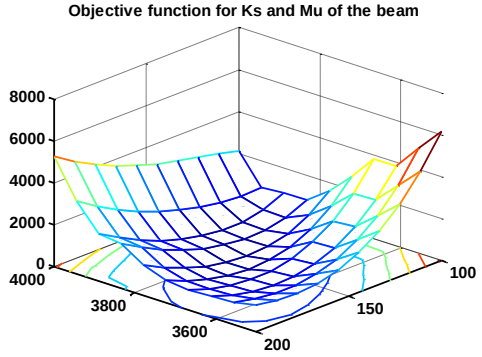

Figure 3.14 The objective function $J\left(M_u^{beam}, G_{f,b}^{beam}\right)$

Table 3.8 Efficiency of different methods for minimization of $J\left(M_u^{beam}, G_{f,b}^{beam}\right)$

Applied Method for Minimization	Number of		Time of computation	Max. error of the Identification [%]
	Iterations	Evolutions		
BFGS	5	27	47 s	0,75
DFP	7	35	68 s	0,70
Trust Region	20	21	146 s	0,88
Steepest Descent	5	31	61 s	0,95

3.4.2. Identification parameters of the steel connection in bending

The presented identification methodology was applied to the experimental results found in the literature. The corresponding hysteresis curve (Gang Shi, 2007) was used for the approximation of a relation bending moment – rotation. For these experimental results, we have tested presented methodology. The hysteresis curve of the end plate connection and approximation of test results are shown in Figure. 3.15.

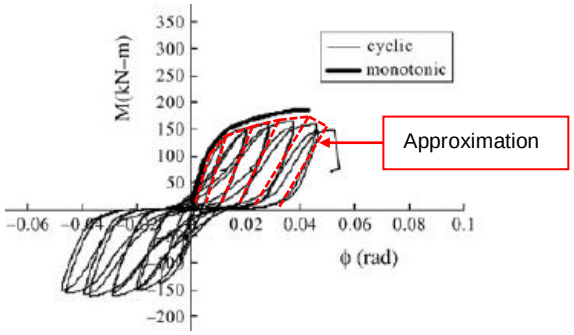

Figure 3.15 Typical hysteresis curve and approximation of the test results **(Gang Shi, 2007)**

The identification of the model parameters starts with the elastic phase, where we need to identify the bending stiffness in the elastic response. Namely, coupled plasticity-damage model is composed of two serially connected models, so that the bending stiffness can be calculated as:

$$\left.\begin{aligned} S_{j,b} &= \frac{E_{con}D_{con}^{-1}}{E_{con}+D_{con}^{-1}} \\ E_{con} &= D_{con}^{-1} \end{aligned}\right\} S_{j,b} = \frac{1}{2}E_{con} \tag{3.58}$$

where E_{con}, D_{con}^{-1} are stiffness of the linear-elastic and the damage model. This expression reduces identification to one parameter.

The objective function for this case can be written:

$$J\left(E_{con}, D_{con}\right) = \left(\psi_{P1}^{com} - \psi_{P1}^{\exp}\right)^2 \tag{3.59}$$

The objective function (Figure 3.16a) is convex and parameters were identified successfully.

In the second phase of the identification, we should identify constitutive parameters of the coupled plasticity-damage model. The procedure begins with the simultaneous identification of four unknown parameters.

The objective function for the this case of identification can be written as :

$$\begin{aligned} J\left(K_{h,b}^{con}, M_{y}^{con}, K_{d,b}^{con}, M_{f}^{con}\right) = \sum_{1}^{3} m\left(\psi_{Pi}^{com} - \psi_{Pi}^{\exp}\right)^2 + \sum_{1}^{3} m\left(\psi_{Pi'}^{com} - \psi_{Pi'}^{\exp}\right)^2 + \\ + \sum_{1}^{3} n\left(\Delta\psi_{Pi}^{com} - \Delta\psi_{Pi}^{\exp}\right)^2 \end{aligned} \tag{3.60}$$

The objective function is convex for all parameters and process was done successfully.
The control of identified parameters was made in two split processes of the identification. In the

first, we identify two unknowns for plasticity model while damage parameters are fixed and known. In the second cases, we use an analogy where two damage parameters are unknown and plasticity known. The shapes of objective functions for both cases are presented in the Figure 3.16.

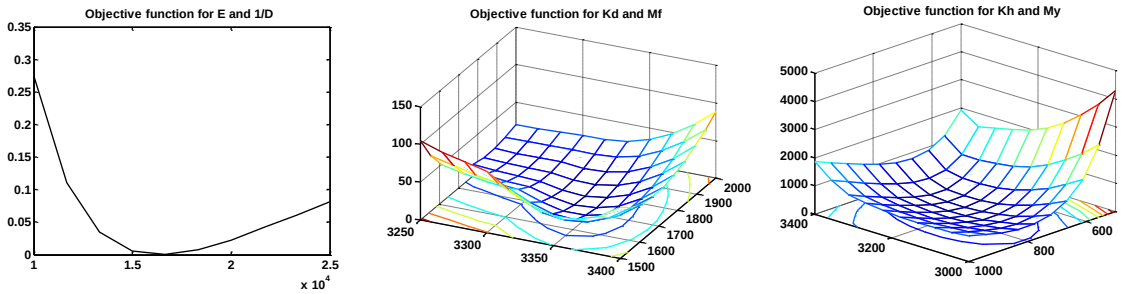

(a) OF: $J\left(E_{con}, D_{con}\right)$ (b) OF: $J\left(K_d^{con}, M_f^{con}\right)$ (c) OF: $J\left(K_h^{con}, M_y^{con}\right)$

Figure 3.16 Shapes of Objective Functions

The proposed objective functions (Figures 3.16b and 3.16c) are convex. These control results are matched with results of the simultaneous identification for all parameters.
Results of the identification are presented in Figure 3.19a where we can see very good matching between the experimental and the computed results. The computed results were obtained using FEM element model with identified constitutive parameters.

3.4.3. Identification parameters of the connection in Timber structure

In the second example, presented methodology is tested at the connection between two wooden elements. The hysteresis curve (Mesic, 2003) and approximation of experimental results are showed in Figure 3.17. This hysteresis curve has been measured with large increment steps of the imposed displacement. In the middle of the curve we can see gap without unloading lines, but this enables to test the quality of the proposed methodology.

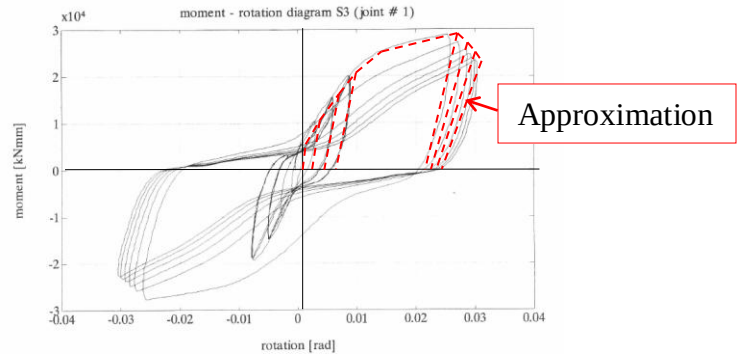

Figure 3.17 Typical hysteresis curve and approximation of the test results

The identification of models parameters begins with the elastic phase, same as in the last example.
The objective function can be written as (Figure 3.18a):

$$J\left(E_{con}, D_{con}\right) = \left(\psi_{P1}^{com} - \psi_{P1}^{\exp}\right)^2 \tag{3.61}$$

In second phase of the identification for the coupled plasticity-damage model, we start with simultaneous identification of four parameters.
The objective function can be written as:

$$J\left(K_{h,b}^{con}, M_{y}^{con}, K_{d,b}^{con}, M_{f}^{con}\right) = \sum_{1}^{3} m\left(\psi_{Pi}^{com} - \psi_{Pi}^{\exp}\right)^2 + \sum_{1}^{3} m\left(\psi_{Pi'}^{com} - \psi_{Pi'}^{\exp}\right)^2 + \\ + \sum_{1}^{3} n\left(\Delta\psi_{Pi}^{com} - \Delta\psi_{Pi}^{\exp}\right)^2 \tag{3.62}$$

The objective function is convex for all parameters and process of the identification is done successfully.

Same as in the last example, a control of identified parameters can be performed in two split processes of the identification. In the first, we have identified two unknowns for the plasticity model while damage parameters were fixed and known. In this case, the objective function is good conditioned (Figure 3.18b). In the second case, the objective function is convex but poorly conditioned. However, with the good start values in the minimization, we can obtain good results.

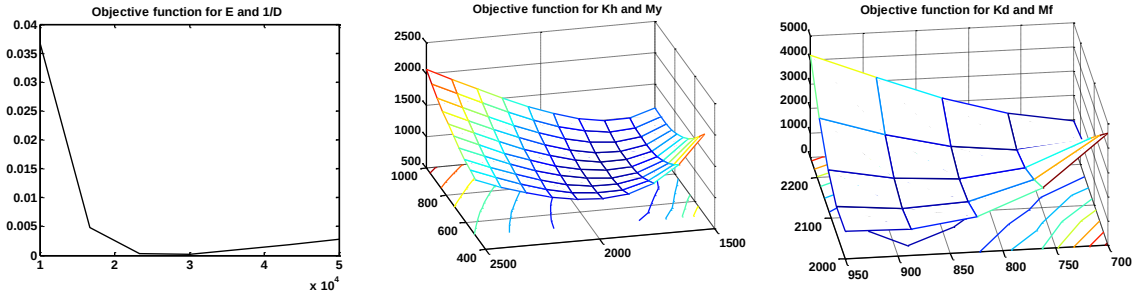

(a) OF: $J\left(E_{con}, D_{con}\right)$ (b) OF: $J\left(K_{h}^{con}, M_{y}^{con}\right)$ (c) OF: $J\left(K_{d}^{con}, M_{f}^{con}\right)$

Figure 3.18 Shapes of Objective function

Results of the identification are presented in the Figure 3.19b, where we can see good matching between the experimental and the computed results. The computed results have been obtained by using FEM element model with identified constitutive parameters.

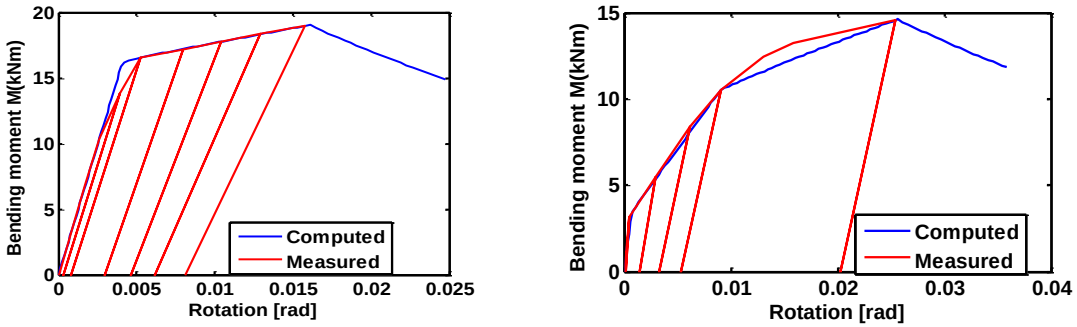

(a) Steel connection (b) Timber connection

Figure 3.19 Matching results: experimental vs. computed

3.5 Concluding remarks

We have proposed a methodology for the identification of constitutive parameters of the connection and the material. The constitutive model of connection contains coupled plasticity-damage in hardening and nonlinear law in the softening with different mechanisms of the failure. The hardening behavior is split to the bending and the shearing, but all combinations are included. The most important conclusions can be stated as follows:

- The proposed methodology is able to identify all unknown parameters (eighteen) when these parameters are split in three phases: elastic, hardening and softening. In every phase, we use local and global measurements.

- Successful identification is conditioned with enough measurements during the experimental test and adequate loading program. In this work, requirements for measurements (Figure 3.3) and loading program, were presented. The loading program contains cycles of loading-unloading, and in the hardening, we need to have minimum three cycles for every case.

- The focus of this chapter was positioned at the behavior of the constitutive models and the choice of the objective function. In the chapter, we showed that using loading and unloading cycles we can obtain all unknown constitutive parameters. These cycles are needed to make a difference between plasticity and damage model. The both models can describe same behavior in the loading regime, but in unloading, we can see the difference between them.

- All cases of identification were presented in the Section 3.3. For an illustration of the complete procedure, we first used the academic example of an inverse analysis and all results of experiments were obtained by FEM model. Then, two practical examples were shown in Section 3.4, but only for partial measurements that pertain to the bending of connection, as the only results found in literature.

Chapter 4

Nonlinear kinematics Reissner's beam with combined hardening/softening elastoplasticity

Abstract

In this chapter, we present geometrically nonlinear beam finite element with embedded discontinuity which can represent elastoplastic constitutive behavior with both hardening and softening response. The constitutive equations are presented in rate form by using the multiplicative decomposition of deformation gradient. Formulation of elastoplastic response is presented in terms of stress resultants including the interaction between axial force, shear force and bending moment appropriate for metallic materials. The softening response is used to model the failure in connections, introducing displacement field discontinuity or a rotational hinge. The hinges or displacement discontinuity are presented in the framework of incompatible modes that can handle three different failure modes dealing with bending, shearing or axial deformation. With several numerical simulations, the FEM implementation is proven very robust for solving the problems of practical interest, such as push-over analysis.

Contents of Chapter 4

4.1. Introduction

The model capable of predicting the complete failure (collapse) of a frame structure is very important in the limit load design. A typical application is push-over analysis used in earthquake engineering; a nonlinear static analysis of a building structure subjected to an equivalent static load that is pushing a structure towards the limit capacity. This type of the analysis was developed in work (Dujc et al., 2010) as incompatible modes in the small displacement framework. During push-over analysis of a structure, there are hinges that develop, in a step-by-step manner, leading to the failing mechanism. In structural analysis those hinges can be included by using static condensation method (Medic et al., 2013). The incompatible mode method is more robust, while the static condensation method is more efficient. For improved prediction, it is necessary (Dujc et al., 2010) to include geometric nonlinearities of the second order, indicating the need for improvement.

The truly large kinematics of steel frame structures combined with elastoplastic hardening/softening is the main novelty of this work. The ductile material like steel can handle large displacements and deformation of a structure during the limit load analysis. The geometrically exact beam with nonlinear kinematics and nonlinear constitutive behavior should be capable of following response of a structure to the complete failure (collapse). In this work, we propose elastoplastic beam element in geometrically nonlinear regime (Ibrahimbegovic & Frey, 1993a) that can handle softening response, which is included in the framework of incompatible modes.

In the formulation of the proposed beam element we use, as the starting point, the previous works, (Ibrahimbegovic & Frey, 1993a) and (Simo et al., 1984). The proposed beam element includes nonlinear kinematics and nonlinear constitutive response. The constitutive behavior is defined as plasticity with linear hardening that includes interaction between axial force, shear force and bending moment. The evolution equations for internal variables are developed in rate form, imposing the need to employ a numerical time integration scheme, -here chosen as the backward Euler scheme.

The main novelty concerns the beam model's ability to reach the ultimate capacity of a cross section, activating one of three failure modes, which represent non-linear softening response in either bending moment, shear or axial force. These failure modes are handled by field discontinuity as incompatible modes, see (Ibrahimbegovic & Frey, 1993b). In this work, we presume that only one softening failure mechanism can be activated at the time. The outline of the chapter is as follows.

In the next section, we present the main ingredients of the geometrically exact beam with the elastoplastic constitutive response. The interaction between axial force, shear force and bending moment is taken in the elastoplastic regime, while the axial response remains elastic. The second section presents corresponding kinematic enhancement in terms of "discontinuity" or "jump" in the displacement field or the rotational field depending upon the activated failure mode. The enhancement is included as an incompatible mode in the geometrically nonlinear framework. The third section deals the FEM implementation, while the fourth section presents the results of several numerical simulations. The last section contains the conclusions.

4.2. Reissner's beam with nonlinear kinematics

In this section, we give a detailed formulation of the two-dimensional beam in the framework of large displacement and large elastoplastic strains. The formulation of Reissner's beam (Reissner,

1972) kinematics equations employs rotated strain measure. The linearization of these strain measures reduces to strains of the Timoshenko beam (Ibrahimbegovic & Frey, 1993a) and (Nikolic et al., 2015). The plastic strains corresponding to stress resultant follow from yield criterion introducing the interaction between axial force, shear force and bending moment. The equations are expressed in rate form (Simo et al., 1984). The consistent linearization of the weak form of equilibrium equations provides tangent stiffness matrix, for both material and geometric part.
Providing the beam element with the embedded discontinuity within the framework of a large displacement is needed for modeling softening phase. The later can concern the failure process in the connections, modeling the failure in bending, in shearing or in axial force separately. The multiplicative decomposition of the deformation gradient into regular and irregular parts corresponds to the additive decomposition of the rotated strain measure proposed by Reissner (Reissner, 1972). Moreover, the weak form of equilibrium equation has to be recast within the framework of incompatible modes (Ibrahimbegovic & Frey, 1993b) , which allows handling of the embedded discontinuity calculation at the element level.

4.2.1. Geometrically nonlinear kinematics

In the framework of large displacement gradient theory, the position vector in deformed configuration can be written as

$$\boldsymbol{\varphi} := \boldsymbol{\varphi}_0 + \zeta \mathbf{t} = \begin{pmatrix} x+u \\ y+v \end{pmatrix} + \zeta \begin{pmatrix} -\sin\psi \\ \cos\psi \end{pmatrix} \tag{4.1}$$

where x and y are coordinates in the reference configuration, u and v are displacement components in the global coordinate system, ζ is the coordinate along the normal to the beam axis in the reference configuration and ψ is the rotation. The corresponding form of the deformation gradient $\mathbf{F}$ can be split into displacement part $\mathbf{F}_{u,v}$ and rotation part $\mathbf{F}_{\psi}$ as:

$$\mathbf{F} := \nabla\boldsymbol{\varphi} = \underbrace{\begin{bmatrix} 1+\dfrac{du}{dx} & 0 \\ \dfrac{dv}{dx} & 0 \end{bmatrix}}_{\mathbf{F}_{u,v}=\mathbf{I}+\nabla\mathbf{u}} + \underbrace{\begin{bmatrix} -\zeta\dfrac{d\psi}{dx}\cos\psi & -\sin\psi \\ -\zeta\dfrac{d\psi}{dx}\sin\psi & \cos\psi \end{bmatrix}}_{\mathbf{F}_{\psi}=\mathbf{I}+\nabla\boldsymbol{\psi}} \tag{4.2}$$

The failure mode in connection can be represented by jump in displacement components u , v and in the rotation ψ , with the corresponding kinematic enhancement in terms of the "discontinuity". In the finite deformation framework, such a displacement discontinuity has to be introduced in deformed configuration (Ibrahimbegovic & Frey, 1993a). This splits displacement field into the regular part $\left(\tilde{\bullet}\right)$ and the „enhanced" part $\left(\bar{\bullet}\right)$ representing the corresponding displacement or rotation „jump". By introducing $\delta_{\bar{x}}$ as the Dirac function where the jump occurs, the additive decomposition of displacements and rotation gradient fields can be written as:

$$
\begin{aligned}
u(x,t) &= \tilde{\bar{u}}(x,t) + \left(N_a(x) + H(x)\right)\bar{\bar{u}}(t) \rightarrow \frac{\partial u}{\partial x} = \frac{\partial \tilde{\bar{u}}}{\partial x} + G_a(x)\bar{\bar{u}} + \delta_{\bar{x}}\bar{\bar{u}} = \frac{\partial \bar{u}}{\partial x} + \delta_{\bar{x}}\bar{\bar{u}} \\
v(x,t) &= \tilde{\bar{v}}(x,t) + \left(N_a(x) + H(x)\right)\bar{\bar{v}}(t) \rightarrow \frac{\partial v}{\partial x} = \frac{\partial \tilde{\bar{v}}}{\partial x} + G_a(x)\bar{\bar{v}} + \delta_{\bar{x}}\bar{\bar{v}} = \frac{\partial \bar{v}}{\partial x} + \delta_{\bar{x}}\bar{\bar{v}} \\
\psi(x,t) &= \tilde{\bar{\psi}}(x,t) + \left(N_a(x) + H(x)\right)\bar{\bar{\psi}}(t) \rightarrow \frac{\partial \psi}{\partial x} = \frac{\partial \tilde{\bar{\psi}}}{\partial x} + G_a(x)\bar{\bar{\psi}} + \delta_{\bar{x}}\bar{\bar{\psi}} = \frac{\partial \bar{\psi}}{\partial x} + \delta_{\bar{x}}\bar{\bar{\psi}}
\end{aligned}
\tag{4.3}
$$

where $N_a(x)$ is interpolation function, $H(x)$ is Heaviside function and $G_a(x)$ is the first derivative of the interpolation function $N_a(x)$. By using last result (4.3) we can write the deformation gradient for both the displacement and the rotation fields, in terms of the multiplicative decomposition of:

$$
\begin{aligned}
&\mathbf{F} = \mathbf{I} + \nabla\bar{\mathbf{u}} + \delta_{\bar{x}}\nabla\bar{\bar{\mathbf{u}}} + \mathbf{I} + \nabla\bar{\psi} + \delta_{\bar{x}}\nabla\bar{\bar{\psi}} = \\
&= \left(\mathbf{I} + \nabla\bar{\mathbf{u}}\right)\left(\mathbf{I} + \delta_{\bar{x}}\frac{\nabla\bar{\bar{\mathbf{u}}}}{I + \nabla\bar{\mathbf{u}}}\right) + \left(\mathbf{I} + \nabla\bar{\psi}\right)\left(\mathbf{I} + \delta_{\bar{x}}\frac{\nabla\bar{\bar{\psi}}}{I + \nabla\bar{\psi}}\right) = \bar{\mathbf{F}}_{u,v}\bar{\bar{\mathbf{F}}}_{u,v} + \bar{\mathbf{F}}_{\psi}\bar{\bar{\mathbf{F}}}_{\psi}
\end{aligned}
\tag{4.4}
$$

From the polar decomposition of the deformation gradient $\mathbf{F}$, into rotation $\mathbf{R}$ and stretch $\mathbf{U}$, we define the rotated strain measure $\mathbf{H}$:

$$
\mathbf{F} = \mathbf{RU} \rightarrow \mathbf{U} = \mathbf{R}^T\mathbf{F},\ \mathbf{R} = \begin{bmatrix} \cos\psi & -\sin\psi \\ \sin\psi & \cos\psi \end{bmatrix} \rightarrow \mathbf{H} = \mathbf{U} - \mathbf{I}
\tag{4.5}
$$

where $\mathbf{I}$ is identity tensor. With the results (4.4) and (4.5), we can obtain the corresponding additive decomposition of the stretch tensor:

$$
\mathbf{U} = \mathbf{R}^{\mathbf{T}}\left(\mathbf{I} + \nabla\bar{\mathbf{u}} + \delta_{\bar{x}}\nabla\bar{\bar{\mathbf{u}}}\right) + \mathbf{R}^{\mathbf{T}}\left(\mathbf{I} + \nabla\bar{\psi} + \delta_{\bar{x}}\nabla\bar{\bar{\psi}}\right) = \underbrace{\bar{\mathbf{U}}^{u,v} + \delta_{\bar{x}}\bar{\bar{\mathbf{U}}}^{u,v}}_{\mathbf{U}^{u,v}} + \underbrace{\bar{\mathbf{U}}^{\psi} + \delta_{\bar{x}}\bar{\bar{\mathbf{U}}}^{\psi}}_{\mathbf{U}^{\psi}}
\tag{4.6}
$$

where:

$$
\bar{\mathbf{U}}^{u,v} = \begin{bmatrix} \left(1 + \dfrac{\partial\bar{u}}{\partial x}\right)\cos\psi + \dfrac{\partial\bar{v}}{\partial x}\sin\psi & 0 \\ -\left(1 + \dfrac{\partial\bar{u}}{\partial x}\right)\sin\psi + \dfrac{\partial\bar{v}}{\partial x}\cos\psi & 1 \end{bmatrix};\ \bar{\bar{\mathbf{U}}}^{u,v} = \begin{bmatrix} \bar{\bar{u}}\cos\psi + \bar{\bar{v}}\sin\psi & 0 \\ -\bar{\bar{u}}\sin\psi + \bar{\bar{v}}\cos\psi & 0 \end{bmatrix}\delta_{\bar{x}}
$$

$$
\bar{\mathbf{U}}^{\psi} = \begin{bmatrix} -\zeta\dfrac{\partial\bar{\psi}}{\partial x} & 0 \\ 0 & 1 \end{bmatrix};\ \bar{\bar{\mathbf{U}}}^{u,v} = \begin{bmatrix} -\zeta\bar{\bar{\psi}} & 0 \\ 0 & 0 \end{bmatrix}\delta_{\bar{x}}
$$

Finally, we can write the internal virtual work in an alternative form that is more in line with the corresponding 3D representations (Ibrahimbegovic & Frey, 1993a)

$$
\int_L\int_A \hat{\mathbf{F}}\cdot\mathbf{P}dAdx = \int_L\int_A \hat{\mathbf{H}}\cdot\mathbf{T}dAdx
\tag{4.7}
$$

where $\hat{\mathbf{F}}$ is variation of the deformation gradient, $\mathbf{P}$ is first Piola-Kirchhoff stress. In last equation (4.7), we used the following result for Biot stress tensor $\mathbf{T}$ and corresponding rotated strain measures $\mathbf{H}$ and their variations $\hat{\mathbf{H}}$:

$$\mathbf{T} = \mathbf{R}^{\mathbf{T}}\mathbf{P} \rightarrow \begin{pmatrix} T^{11} \\ T^{21} \end{pmatrix} = \mathbf{R}^{\mathbf{T}} \begin{pmatrix} P^{11} \\ P^{21} \end{pmatrix} \tag{4.8}$$

4.2.2. Constitutive model and its rate form

In the elastic regime the simplest set of constitutive equations for finite strain beam is chosen in terms of Biot stress resultants and rotated strain measure:

$$\mathbf{T} = \mathbf{C}^e\mathbf{H} \tag{4.9}$$

where $\mathbf{C}^e$ is the elastic modulus. In the plastic regime, we can split displacement and rotation gradients into elastic part $\left(\bullet^e\right)$ and plastic part $\left(\bullet^p\right)$:

$$\begin{aligned} &\bar{\mathbf{F}} = \mathbf{I} + \nabla\bar{\mathbf{u}}^e + \nabla\bar{\mathbf{u}}^p + \mathbf{I} + \nabla\bar{\psi}^e + \nabla\bar{\psi}^p = \\ &= \left(\mathbf{I} + \nabla\bar{\mathbf{u}}^e\right)\left(\mathbf{I} + \frac{\nabla\bar{\mathbf{u}}^p}{I + \nabla\bar{\mathbf{u}}^e}\right) + \left(\mathbf{I} + \nabla\bar{\psi}^e\right)\left(\mathbf{I} + \frac{\nabla\bar{\psi}^p}{I + \nabla\bar{\psi}^e}\right) = \bar{\mathbf{F}}^e_{u,v}\bar{\mathbf{F}}^p_{u,v} + \bar{\mathbf{F}}^e_{\psi}\bar{\mathbf{F}}^p_{\psi} \end{aligned} \tag{4.10}$$

Multiplicative decomposition of the deformation gradient corresponds to the additive decomposition of the stretch tensor $\mathbf{U}$:

$$\mathbf{U} = \mathbf{R}^{\mathbf{T}}\left(\mathbf{I} + \nabla\bar{\mathbf{u}}^e + \nabla\bar{\mathbf{u}}^p\right) + \mathbf{R}^{\mathbf{T}}\left(\mathbf{I} + \nabla\bar{\psi}^e + \nabla\bar{\psi}^p\right) = \underbrace{\bar{\mathbf{U}}^e_{u,v} + \bar{\mathbf{U}}^p_{u,v}}_{\bar{\mathbf{U}}_{u,v}} + \underbrace{\bar{\mathbf{U}}^e_{\psi} + \bar{\mathbf{U}}^p_{\psi}}_{\bar{\mathbf{U}}_{\psi}} \tag{4.11}$$

where:

$$\bar{\mathbf{U}}^e_{u,v} = \begin{bmatrix} \left(1 + \dfrac{\partial\bar{u}^e}{\partial x}\right)\cos\psi + \dfrac{\partial\bar{v}^e}{\partial x}\sin\psi & 0 \\ -\left(1 + \dfrac{\partial\bar{u}^e}{\partial x}\right)\sin\psi + \dfrac{\partial\bar{v}^e}{\partial x}\cos\psi & 1 \end{bmatrix}; \bar{\mathbf{U}}^p_{u,v} = \begin{bmatrix} \dfrac{\partial\bar{u}^p}{\partial x}\cos\psi + \dfrac{\partial\bar{v}^p}{\partial x}\sin\psi & 0 \\ -\dfrac{\partial\bar{u}^p}{\partial x}\sin\psi + \dfrac{\partial\bar{v}^p}{\partial x}\cos\psi & 0 \end{bmatrix}$$

$$\bar{\mathbf{U}}^e_{\psi} = \begin{bmatrix} -\zeta\dfrac{\partial\bar{\psi}^e}{\partial x} & 0 \\ 0 & 1 \end{bmatrix}; \bar{\mathbf{U}}^p_{\psi} = \begin{bmatrix} -\zeta\dfrac{\partial\bar{\psi}^p}{\partial x} & 0 \\ 0 & 0 \end{bmatrix}$$

The Helmholtz free energy can be defined as a quadratic form:

$$\bar{\Psi}(\bar{\mathbf{U}}^e, \bar{\xi}^p) = \underbrace{\frac{1}{2}\bar{\mathbf{U}}^{e,T}\cdot\mathbf{C}^e\cdot\bar{\mathbf{U}}^e}_{\bar{\Psi}^e} + \underbrace{\frac{1}{2}\bar{\xi}^{p,T}\cdot\mathbf{K}^h\cdot\bar{\xi}^p}_{\bar{\Xi}^p} \tag{4.12}$$

where $\bar{\mathbf{U}}^e$ is elastic part of the stretch tensor, $\bar{\xi}^p$ is a vector of hardening variables and $\mathbf{K}^h$ are corresponding hardening moduli. The yield criterion condition has to be satisfied:

$$\bar{\phi}(\mathbf{T},\bar{\mathbf{q}}) \le 0 \tag{4.13}$$

where $\bar{\mathbf{q}}$ is a vector of internal hardening stress like variables. The second principle of thermodynamics states that the plastic dissipation must remain non-negative:

$$0 \le \bar{\mathcal{D}} = \underbrace{\left(\mathbf{T} - \frac{d\bar{\Psi}^e}{d\bar{\mathbf{U}}^e}\right)\dot{\bar{\mathbf{U}}}^e}_{\bar{\mathcal{D}}^e=0} + \underbrace{\mathbf{T}\dot{\bar{\mathbf{U}}}^p - \frac{\partial\bar{\Xi}^p}{\partial\bar{\xi}^p}\frac{d\bar{\xi}^p}{dt}}_{\bar{\mathcal{D}}^p} \tag{4.14}$$

The principal of maximum plastic dissipation can be formulated (Hill, 1950) as the constrained minimization, where the constraint is yield function (4.13). This can further be recast as corresponding unconstrained minimization by using Lagrange multiplier method:

$$\min_{\mathbf{T},\bar{\mathbf{q}}} \max_{\dot{\bar{\gamma}}} \left[\bar{L}^p(\mathbf{T},\bar{\mathbf{q}},\dot{\bar{\gamma}}) = -\bar{\mathcal{D}}^p(\mathbf{T},\bar{\mathbf{q}}) + \dot{\bar{\gamma}}\cdot\bar{\phi}(\mathbf{T},\bar{\mathbf{q}}) \right] \tag{4.15}$$

where $\dot{\bar{\gamma}}$ is the Lagrange multiplier. Regarding the Kuhn-Tucker optimality conditions, the result can be used to provide the evolution equations for internal variables in rate form along with the loading/unloading conditions:

$$\begin{aligned}
&\frac{\partial\bar{L}^p}{\partial\mathbf{T}} = -\dot{\bar{\mathbf{U}}}^p + \dot{\bar{\gamma}}\frac{\partial\bar{\phi}}{\partial\mathbf{T}} = 0 \Rightarrow \dot{\bar{\mathbf{U}}}^p = \dot{\bar{\gamma}}\frac{\partial\bar{\phi}}{\partial\mathbf{T}} \\
&\frac{\partial\bar{L}^p}{\partial\bar{\mathbf{q}}} = -\frac{\partial\bar{\xi}^p}{\partial t} + \dot{\bar{\gamma}}\frac{\partial\bar{\phi}}{\partial\bar{\mathbf{q}}} = 0 \Rightarrow \frac{\partial\bar{\xi}^p}{\partial t} = \dot{\bar{\gamma}}\frac{\partial\bar{\phi}}{\partial\bar{\mathbf{q}}} \\
&\dot{\bar{\gamma}} \ge 0, \quad \bar{\phi} \le 0, \quad \dot{\bar{\gamma}}\bar{\phi} = 0
\end{aligned} \tag{4.16}$$

The appropriate value of plastic multiplier $\dot{\bar{\gamma}}$ can be determined from the plastic consistency condition for the case of sustained plastic flow:

$$\dot{\bar{\phi}} = 0 \;\Rightarrow\; \dot{\bar{\gamma}} = \frac{\frac{\partial\bar{\phi}}{\partial\mathbf{T}}\mathbf{C}^e\dot{\bar{\mathbf{U}}}}{\frac{\partial\bar{\phi}}{\partial\mathbf{T}}\mathbf{C}^e\frac{\partial\bar{\phi}}{\partial\mathbf{T}} + \frac{\partial\bar{\phi}}{\partial\bar{\mathbf{q}}}\mathbf{K}^h\frac{\partial\bar{\phi}}{\partial\bar{\mathbf{q}}}} \tag{4.17}$$

By replacing the last result in stress rate equation, we can obtain the elastoplastic modulus $\mathbf{C}^{ep}$ that should replace the elastic modulus $\mathbf{C}^e$ in plastic regime:

$$C^{ep} = \mathbf{C}^e - \frac{\mathbf{C}^e\frac{\partial\bar{\phi}}{\partial\mathbf{T}} \otimes \mathbf{C}^e\frac{\partial\bar{\phi}}{\partial\mathbf{T}}}{\frac{\partial\bar{\phi}}{\partial\mathbf{T}}\mathbf{C}^e\frac{\partial\bar{\phi}}{\partial\mathbf{T}} + \frac{\partial\bar{\phi}}{\partial\bar{\mathbf{q}}^p}\mathbf{K}^h\frac{\partial\bar{\phi}}{\partial\bar{\mathbf{q}}^p}} \tag{4.18}$$

We note in passing that the elastoplastic tangent stiffness above remains the same in the discrete problem, obtained by using the backward Euler time integration scheme.

In the softening regime the Helmholtz free energy can be written as a quadratic form in softening variables:

$$\bar{\bar{\Psi}}\left(\bar{\bar{\xi}}^s\right)=\underbrace{\frac{1}{2}\bar{\bar{\xi}}^s\mathbf{K}_s\bar{\bar{\xi}}^s}_{\bar{\bar{\Xi}}^s};\quad \Psi(\cdot)=\bar{\Psi}(\cdot)+\bar{\bar{\Psi}}(\bar{\bar{\xi}}^s)\delta_{\bar{x}} \tag{4.19}$$

where $\bar{\bar{\xi}}^s$ is a set of internal variables, representing the connection failure and $\bar{\bar{\mathbf{K}}}^s$ is set of softening moduli. The yield function for softening is chosen as a multi-criteria form, related to, bending, shearing and axial force:

$$\dot{\bar{\bar{\gamma}}}_i\bar{\bar{\phi}}_i=0\Rightarrow\bar{\bar{\phi}}^i(t_i,\bar{\bar{q}}_i^s)\le 0 \tag{4.20}$$

where t_i is traction force and $\bar{\bar{q}}_i^s$ is stress-like variables, which are work-conjugated to the softening internal variables at the discontinuity for the corresponding failure mode. Among all admissible values of these variables, the principal of maximum dissipation pertinent to softening states will pick the ones that maximize softening dissipation. This can be solved as an unconstrained minimization problem, to provide the evolution equations for internal variables along with the loading/unloading conditions:

$$\begin{aligned}&\frac{\partial\bar{\bar{L}}^s}{\partial\bar{\bar{\mathbf{q}}}^s}=-\dot{\bar{\bar{\xi}}}^s+\sum\nolimits_1^3\dot{\bar{\bar{\gamma}}}\frac{\partial\bar{\bar{\phi}}}{\partial\bar{\bar{\mathbf{q}}}^s}=0\Rightarrow\dot{\bar{\bar{\xi}}}^s=\sum\nolimits_1^3\dot{\bar{\bar{\gamma}}}_i\frac{\partial\bar{\bar{\phi}}}{\partial\bar{\bar{\mathbf{q}}}^s}\\&\dot{\bar{\bar{\gamma}}}\ge 0,\quad\bar{\bar{\phi}}\le 0,\quad\dot{\bar{\bar{\gamma}}}\bar{\bar{\phi}}=0\end{aligned} \tag{4.21}$$

4.2.3. Stress resultant form

By using the rotated strain measure $\mathbf{H}$, we obtain the only non-zero components, defined as

$$H_{11}=\Sigma-\zeta K,\ H_{21}=\Gamma \tag{4.22}$$

The explicit form of generalized strains can be written as

$$\begin{aligned}\Sigma=H_{11}^{u,v}&=\underbrace{\left(1+\frac{d\bar{u}}{dx}\right)\cos\psi+\frac{d\bar{v}}{dx}\sin\psi-1}_{\bar{\Sigma}}+\underbrace{\left(\frac{d\bar{\bar{u}}}{dx}\cos\psi+\frac{d\bar{\bar{v}}}{dx}\sin\psi\right)}_{\bar{\bar{\Sigma}}}\delta_{\bar{x}}\\\Gamma=H_{21}^{u,v}&=\underbrace{-\left(1+\frac{d\bar{u}}{dx}\right)\sin\psi+\frac{d\bar{v}}{dx}\cos\psi}_{\bar{\Gamma}}+\underbrace{\left(-\frac{d\bar{\bar{u}}}{dx}\sin\psi+\frac{d\bar{\bar{v}}}{dx}\cos\psi\right)}_{\bar{\bar{\Gamma}}}\delta_{\bar{x}}\\K=H_{11}^{\psi}&=\underbrace{\frac{d\bar{\psi}}{dx}}_{\bar{K}}+\underbrace{\frac{d\bar{\bar{\psi}}}{dx}}_{\bar{\bar{K}}}\delta_{\bar{x}}\end{aligned} \tag{4.23}$$

The linearized strain measures (4.23) coincide with the strains of the Timoshenko beam (Ibrahimbegovic & Frey, 1993a). The equation (4.23) can be written in matrix compact form:

$$\bar{\boldsymbol{\Sigma}} = \boldsymbol{\Lambda}^{\mathbf{T}}\left(\mathbf{h}(\bar{\mathbf{a}}) - \mathbf{n}\right) + \boldsymbol{\Lambda}^{\mathbf{T}}\mathbf{h}(\bar{\bar{\mathbf{a}}})\delta_{\bar{x}}$$

$$\boldsymbol{\Sigma} = \begin{pmatrix} \Sigma \\ \Gamma \\ K \end{pmatrix},\ \boldsymbol{\Lambda} = \begin{bmatrix} \cos\psi & -\sin\psi & 0 \\ \sin\psi & \cos\psi & 0 \\ 0 & 0 & 1 \end{bmatrix},\ \mathbf{h}(\bar{\mathbf{a}}) = \begin{pmatrix} 1+\dfrac{d\bar{u}}{dx} \\ \dfrac{d\bar{v}}{dx} \\ \dfrac{d\bar{\psi}}{dx} \end{pmatrix}, \mathbf{h}(\bar{\bar{\mathbf{a}}}) = \begin{pmatrix} \bar{\bar{u}} \\ \bar{\bar{v}} \\ \bar{\bar{\psi}} \end{pmatrix}, \mathbf{n} = \boldsymbol{\Lambda}\mathbf{g}_1,\ \mathrm{g}_1 = \begin{pmatrix} 1 \\ 0 \\ 0 \end{pmatrix} \tag{4.24}$$

By using the same compact notation for the virtual strains (denoted with superposed $(\hat{\bullet})$), we can write the weak form of the equilibrium equation, see (Ibrahimbegovic & Frey, 1993a):

$$G(\mathbf{a}, \hat{\mathbf{a}}) := \int_L \left(\hat{\Sigma}N + \hat{\Gamma}V + \hat{K}M\right)dx - G^{ext}(\hat{\mathbf{a}}) = 0 \tag{4.25}$$

In (4.25) above, N, V and M denote stress resultants, expressed regarding the Biot stress:

$$\boldsymbol{\sigma} = (N, V, M)^T;\ \ N = \int_A T^{11}dA;\ \ V = \int_A T^{21}dA;\ M = -\int_A \zeta T^{11}dA \tag{4.26}$$

The yield function, in the stress resultant form, is defined according to classic works (Simo et al., 1984) and (Neal, 1961), except for a small modification to account for isotropic hardening

$$\begin{aligned} &\bar{\phi}(\bar{\boldsymbol{\sigma}}, \bar{\mathbf{q}}) = |m| + n^2\left(1+v^2\right) + v^4 - 1 \le 0 \\ &m = \frac{M + \bar{q}_M}{M_y};\ v = \frac{V_V + \bar{q}_V}{V_y};\ n = \frac{N + \bar{q}_N}{N_y} \end{aligned} \tag{4.27}$$

where m is a non-dimensional bending moment; v is a non-dimensional shear force; n is a non-dimensional axial force; $\bar{q}_M, \bar{q}_V, \bar{q}_N$ are internal hardening stress like variables; whereas M_y, V_y and N_y denote yield bending moment, yield shear force and yield axial force. The yield function for softening is chosen as a multi-criteria form, pertaining to, bending moment, shear and axial force:

$$\begin{aligned} &\bar{\bar{\phi}}^M(t_M, \bar{\bar{q}}_M^s) = |t_M| - \left(t_{M_y} - \bar{\bar{q}}_M^s\right) \le 0 \\ \dot{\bar{\bar{\gamma}}}_i \bar{\bar{\phi}}_i = 0 \Rightarrow\ \ &\bar{\bar{\phi}}^V(t_V, \bar{\bar{q}}_V^s) = |t_V| - \left(t_{V_y} - \bar{\bar{q}}_V^s\right) \le 0 \\ &\bar{\bar{\phi}}^N(t_N, \bar{\bar{q}}_N^s) = |t_N| - \left(t_{N_y} - \bar{\bar{q}}_N^s\right) \le 0 \end{aligned} \tag{4.28}$$

where t_M, t_V, t_N are traction forces, $t_{M_y}, t_{V_y}, t_{N_y}$ are the corresponding ultimate values where softening starts and $\bar{\bar{q}}_M^s, \bar{\bar{q}}_V^s, \bar{\bar{q}}_N^s$ are stress-like variables work-conjugate to softening variables at the discontinuity.

4.2.4. Consistent linearization of virtual work equations

As shown in (4.7) (Ibrahimbegovic & Frey, 1993a), the virtual work equation can be expressed regarding different stress – strain energy-conjugated pairs. Any of them leads to a nonlinear problem, which requires an iterative solution procedure. With Newton's iterative method, we need

to perform consistent linearization at each iteration.

4.2.4.1. Incompatible modes implementation

The embedded discontinuity formulation that handles the softening is implemented in the framework of incompatible modes (Ibrahimbegovic & Frey, 1993b). Namely, we turn to Hu-Washizu variational formulation, where the weak form is constructed for all three groups of equations: kinematics, constitutive and equilibrium equations. Namely, we choose the spaces of virtual displacements, virtual stress and virtual strain to write:

$$\begin{aligned}
\mathbf{G_a}(\mathbf{u},\mathbf{H},\mathbf{T};\hat{\mathbf{u}}) &:= \int_L\int_A \hat{\mathbf{H}}\mathbf{T}\,dA\,dx - \int_L \hat{\mathbf{u}}^{\mathbf{T}}\mathbf{f}\,dx = 0 \\
\mathbf{G_r}(\mathbf{u},\mathbf{H},\mathbf{T};\hat{\mathbf{T}}) &:= \int_L\int_A \hat{\mathbf{T}}\bar{\bar{\mathbf{H}}}\,dA\,dx = 0 \\
\mathbf{G}_{\hat{\Sigma}}(\mathbf{u},\mathbf{H},\mathbf{T};\hat{\mathbf{H}}) &:= \int_L\int_A \hat{\mathbf{H}}\left(\mathbf{C}^{ep}\mathbf{H}-\mathbf{T}\right)dA\,dx = 0
\end{aligned} \tag{4.29}$$

where virtual fields are denoted with superposed $(\hat{\bullet})$; $\hat{\mathbf{H}}$ - virtual rotated strain field; $\hat{\mathbf{T}}$ - virtual stress field and $\hat{\mathbf{u}}$ - virtual displacements field. Virtual rotated strain measure can be derived by taking the directional derivative of strain measure $\mathbf{U}$ (4.11) and exploiting relation $\mathbf{U}=\mathbf{H}+\mathbf{I}$:

$$\begin{aligned}
\hat{\mathbf{H}} = \hat{\mathbf{U}} = \frac{d}{d\alpha}\left[\mathbf{U}\left(u+\alpha\delta u\right)\right] = &\underbrace{\frac{\partial \mathbf{R}^T}{\partial \psi}\left(\mathbf{I}+\nabla\bar{\mathbf{u}}\right)\hat{\psi} + \mathbf{R}^T\nabla\hat{\mathbf{u}}}_{\hat{\bar{\mathbf{H}}}_{u,v}} + \underbrace{\frac{\partial \mathbf{R}^T}{\partial \psi}\delta_{\bar{x}}\nabla\bar{\bar{\mathbf{u}}}\,\hat{\psi} + \mathbf{R}^T\delta_{\bar{x}}\nabla\hat{\bar{\mathbf{u}}}}_{\hat{\bar{\bar{\mathbf{H}}}}_{u,v}} + \\
&+ \underbrace{\frac{\partial \mathbf{R}^T}{\partial \psi}\left(\mathbf{I}+\nabla\bar{\psi}\right)\hat{\psi} + \mathbf{R}^T\nabla\hat{\bar{\psi}}}_{\hat{\bar{\mathbf{H}}}_{\psi}} + \underbrace{\frac{\partial \mathbf{R}^T}{\partial \psi}\delta_{\bar{x}}\nabla\bar{\bar{\psi}}\hat{\psi} + \mathbf{R}^T\delta_{\bar{x}}\nabla\hat{\bar{\psi}}}_{\hat{\bar{\bar{\mathbf{H}}}}_{\psi}}
\end{aligned} \tag{4.30}$$

In the equation (4.30), the additive decomposition of the displacement gradient field produces an additive decomposition of the virtual strain measure $\hat{\mathbf{H}}$. The virtual stress field can be expressed as:

$$\hat{\mathbf{T}} = \mathbf{C}^{ep}\left(\hat{\bar{\mathbf{H}}} + \delta_{\bar{x}}\hat{\bar{\bar{\mathbf{H}}}}\right) \tag{4.31}$$

By exploiting results (4.22)-(4.25) and (4.29)-(4.31) we can construct the weak form of equilibrium equations in terms of stress resultants:

$$\begin{aligned}
\mathbf{G_a}(\mathbf{a},\boldsymbol{\Sigma},\mathbf{a};\hat{\mathbf{a}}) &:= \int_L\left(\mathbf{d}^{\mathbf{T}}(\bar{\mathbf{a}})\boldsymbol{\Lambda} + \bar{\psi}\mathbf{h}^{\mathbf{T}}(\bar{\mathbf{a}})\frac{d\boldsymbol{\Lambda}}{d\psi}\right)\mathbf{C}^{\mathbf{ep}}\boldsymbol{\Lambda}^{\mathbf{T}}\left(\mathbf{h(a)-n}\right)dx - \int_L \hat{\mathbf{a}}^{\mathbf{T}}\mathbf{f}\,dx = 0 \\
\mathbf{G_r}(\mathbf{a},\boldsymbol{\Sigma},\mathbf{r};\hat{\mathbf{r}}) &:= \int_L \hat{\mathbf{r}}\left(\bar{\boldsymbol{\Sigma}}-\boldsymbol{\Sigma}\right)dx = 0 \\
\mathbf{G}_{\hat{\Sigma}}(\mathbf{a},\boldsymbol{\Sigma},\mathbf{r};\hat{\boldsymbol{\Sigma}}) &:= \int_L \hat{\boldsymbol{\Sigma}}\left(\mathbf{C}^{ep}\boldsymbol{\Sigma}-\mathbf{r}\right)dx = 0
\end{aligned} \tag{4.32}$$

The virtual strain measure $\hat{\boldsymbol{\Sigma}}$ can be derived by taking the directional derivative of the strain measures in (4.23), which can be written explicitly as:

$$
\begin{aligned}
\hat{\bar{\Sigma}} &= \frac{d\hat{\bar{u}}}{dx}\cos\psi + \frac{d\hat{\bar{v}}}{dx}\sin\psi + \hat{\psi}\left[-\left(1+\frac{d\bar{u}}{dx}\right)\sin\psi + \frac{d\bar{v}}{dx}\cos\psi\right] \\
\hat{\bar{\bar{\Sigma}}}\delta_{\bar{x}} &= \hat{\bar{\bar{u}}}\delta_{\bar{x}}\cos\psi + \hat{\bar{\bar{v}}}\delta_{\bar{x}}\sin\psi + \hat{\psi}\left[-\bar{\bar{u}}\sin\psi + \hat{\bar{\bar{v}}}\cos\psi\right]\delta_{\bar{x}} \\
\hat{\bar{\Gamma}} &= -\frac{d\hat{\bar{u}}}{dx}\sin\psi + \frac{d\hat{\bar{v}}}{dx}\cos\psi + \hat{\psi}\left[\left(1+\frac{d\bar{u}}{dx}\right)\cos\psi - \frac{d\bar{v}}{dx}\sin\psi\right] \\
\hat{\bar{\bar{\Gamma}}}\delta_{\bar{x}} &= -\hat{\bar{\bar{u}}}\delta_{\bar{x}}\sin\psi + \hat{\bar{\bar{v}}}\delta_{\bar{x}}\cos\psi + \hat{\psi}\left[\hat{\bar{\bar{u}}}\cos\psi - \hat{\bar{\bar{v}}}\sin\psi\right]\delta_{\bar{x}} \\
\hat{\bar{K}} &= \frac{d\hat{\bar{\psi}}}{dx}; \hat{\bar{\bar{K}}}\delta_{\bar{x}} = \hat{\bar{\bar{\psi}}}\delta_{\bar{x}}
\end{aligned}
\tag{4.33}
$$

The virtual strains components (4.33) can be put in the matrix form as

$$
\hat{\boldsymbol{\Sigma}} = \underbrace{\boldsymbol{\Lambda}^{\mathbf{T}}\mathbf{d}(\hat{\bar{\mathbf{a}}}) + \frac{d\boldsymbol{\Lambda}^{\mathbf{T}}}{d\psi}\mathbf{h}(\bar{\mathbf{a}})\hat{\psi}}_{\hat{\bar{\boldsymbol{\Sigma}}}} + \underbrace{\boldsymbol{\Lambda}^{\mathbf{T}}\mathbf{d}(\hat{\bar{\bar{\mathbf{a}}}})\delta_{\bar{x}} + \frac{d\boldsymbol{\Lambda}^{\mathbf{T}}}{d\psi}\mathbf{h}(\bar{\bar{\mathbf{a}}})\delta_{\bar{x}}\hat{\psi}}_{\hat{\bar{\bar{\boldsymbol{\Sigma}}}}\delta_{\bar{x}}}; \quad \mathbf{d}(\hat{\bar{\mathbf{a}}}) = \begin{pmatrix} \frac{d\hat{\bar{u}}}{dx} \\ \frac{d\hat{\bar{v}}}{dx} \\ \frac{d\hat{\bar{\psi}}}{dx} \end{pmatrix}; \mathbf{d}(\hat{\bar{\bar{\mathbf{a}}}}) = \begin{pmatrix} \hat{\bar{\bar{u}}} \\ \hat{\bar{\bar{v}}} \\ \hat{\bar{\bar{\psi}}} \end{pmatrix} \tag{4.34}
$$

The discrete form can be obtained at the later stage, given that the linearization and discretization commute. The weak form of the virtual work equation can be expressed as:

$$
\mathbf{G}(\mathbf{a}, \hat{\mathbf{a}}) := \int_L \hat{\boldsymbol{\Sigma}} \cdot \boldsymbol{\sigma} dx - \int_L \hat{\mathbf{a}}^{\mathbf{T}}\mathbf{f} dx = 0 \tag{4.35}
$$

where $\mathbf{a}$ is a vector of real displacements, $\hat{\mathbf{a}}$ is a vector of virtual displacements; $\hat{\boldsymbol{\Sigma}}$ is a virtual strain measure; $\boldsymbol{\sigma}$ is a vector of stress resultant forces and $\mathbf{f}$ is a vector of external forces.

The stress resultant forces $\boldsymbol{\sigma}$ for the elastoplastic response can be written as

$$
\boldsymbol{\sigma} = \mathbf{C}^{ep}\boldsymbol{\Lambda}^{\mathbf{T}}\left(\mathbf{h}(\mathbf{a}) - \mathbf{n}\right); \quad \mathbf{C} = diag\left(C_N^{ep}, C_V^{ep}, C_M^{ep}\right) \tag{4.36}
$$

where $C_N^{ep}, C_V^{ep}, C_M^{ep}$ are elastoplastic stiffness of the beam section for an axial force, shear force and bending moment.

By enforcing the orthogonality condition (Ibrahimbegovic, 2009) for the element with incompatible modes, which results in elimination of the stress field and allows us to write the remaining set of equilibrium equations (4.32) as

$$
\begin{aligned}
\mathbf{G}_{\mathbf{a}}(\mathbf{a}, \boldsymbol{\Sigma}, \mathbf{a}; \hat{\mathbf{a}}) &:= \int_L \hat{\bar{\Sigma}}\mathbf{C}^{\mathbf{ep}}\left(\bar{\Sigma} + \bar{\bar{\Sigma}}\delta_{\bar{x}}\right) dx - \int_L \hat{\mathbf{a}}^{\mathbf{T}}\mathbf{f} dx = 0 \\
\mathbf{G}_{\hat{\Sigma}}(\mathbf{a}, \boldsymbol{\Sigma}, \mathbf{r}; \hat{\boldsymbol{\Sigma}}) &:= \int_L \hat{\bar{\boldsymbol{\Sigma}}}\mathbf{C}^{ep}\left(\bar{\boldsymbol{\Sigma}} + \bar{\bar{\boldsymbol{\Sigma}}}\delta_{\bar{x}}\right) dx = 0
\end{aligned}
\tag{4.37}
$$

In the last expression, the virtual strains are obtained explicitly by directional derivative computation:

$$\hat{\boldsymbol{\Sigma}} = (d/d\beta)\left[\tilde{\hat{\boldsymbol{\Sigma}}}\left(\tilde{\mathbf{a}}+\boldsymbol{\beta}\tilde{\hat{\mathbf{a}}}\right)+\bar{\hat{\boldsymbol{\Sigma}}}\left(\bar{\mathbf{a}}+\boldsymbol{\beta}\bar{\hat{\mathbf{a}}}\right)\right]\Big|_{\beta=0}$$
$$= \underbrace{\boldsymbol{\Lambda}^{\mathbf{T}}\mathbf{d}(\hat{\mathbf{a}})+\frac{d\boldsymbol{\Lambda}^{\mathbf{T}}}{d\psi}\mathbf{h}(\bar{\mathbf{a}})\hat{\psi}}_{\tilde{\hat{\boldsymbol{\Sigma}}}} + \underbrace{\boldsymbol{\Lambda}^{\mathbf{T}}\mathbf{d}(\bar{\hat{\mathbf{a}}})\delta_{\bar{x}}+\frac{d\boldsymbol{\Lambda}^{\mathbf{T}}}{d\psi}\mathbf{h}(\bar{\mathbf{a}})\delta_{\bar{x}}\hat{\psi}}_{\bar{\hat{\boldsymbol{\Sigma}}}\delta_{\bar{x}}} \tag{4.38}$$

In order to provide the quadratic convergence of Newton's method, we need to find the consistent tangent stiffness. The latter can be obtained by consistent linearization of the weak form in $(4.37)_1$ resulting with

$$L[G]\big|_{\mathbf{a}} = \mathbf{G}_{\mathbf{a}}(\mathbf{a},\boldsymbol{\Sigma},\mathbf{a};\hat{\mathbf{a}})\big|_a + \frac{d}{d\beta}\left[G(\hat{\mathbf{a}},\mathbf{a}+\beta\Delta\mathbf{a})\right]\Big|_{\beta=0}$$
$$= G(\mathbf{a},\hat{\mathbf{a}}) + \int_L \left(\mathbf{d}(\hat{\mathbf{a}});\hat{\psi}\right)\left[\mathbf{D}_m^K+\mathbf{D}_g^K\right]\begin{pmatrix}\mathbf{d}(\Delta\bar{\mathbf{a}})\\ \Delta\bar{\psi}\end{pmatrix}dx \tag{4.39}$$
$$+\int_L \left(\mathbf{d}(\hat{\mathbf{a}});\hat{\psi}\right)\left[\mathbf{D}_m^F\right]\begin{pmatrix}\mathbf{d}(\Delta\bar{\bar{\mathbf{a}}})\\ \Delta\bar{\bar{\psi}}\end{pmatrix}dx = 0$$

where $\mathbf{D}_m^k$ and $\mathbf{D}_g^k$ are defined in (4.42), along with

$$L[G]\big|_{\Sigma} = G(\mathbf{a},\hat{\boldsymbol{\Sigma}})\big|_{\Sigma} + \frac{d}{d\beta}\left[G(\hat{\boldsymbol{\Sigma}},\mathbf{a}+\beta\Delta\mathbf{a})\right]\Big|_{\beta=0}$$
$$= G(\mathbf{a},\hat{\boldsymbol{\Sigma}}) + \int_L \left(\mathbf{d}(\bar{\hat{\mathbf{a}}});\bar{\hat{\psi}}\right)\left[\mathbf{D}_m^F\right]\begin{pmatrix}\mathbf{d}(\Delta\mathbf{a})\\ \Delta\psi\end{pmatrix}dx + \int_L \left(\mathbf{d}(\bar{\hat{\mathbf{a}}});\bar{\hat{\psi}}\right)\left[\mathbf{D}_m^H+\mathbf{D}_g^H\right]\begin{pmatrix}\mathbf{d}(\Delta\bar{\bar{\mathbf{a}}})\\ \Delta\bar{\bar{\psi}}\end{pmatrix}dx = 0 \tag{4.40}$$

where

$$\mathbf{D}_m^F = \mathbf{D}_m^H = \begin{bmatrix}\boldsymbol{\Lambda}\\ \mathbf{h}^{\mathbf{T}}(\bar{\mathbf{a}})\dfrac{d\boldsymbol{\Lambda}}{d\psi}\end{bmatrix}\mathbf{C}^{\mathbf{ep}}\left[\boldsymbol{\Lambda}^{\mathbf{T}};\quad \frac{d\boldsymbol{\Lambda}^{\mathbf{T}}}{d\psi}\mathbf{h}(\bar{\mathbf{a}})\right];\ \mathbf{D}_g^H = \begin{bmatrix}0 & \dfrac{d\boldsymbol{\Lambda}}{d\psi}\mathbf{r}\\ \mathbf{r}^{\mathbf{T}}\dfrac{d\boldsymbol{\Lambda}^{\mathbf{T}}}{d\psi} & \mathbf{h}^{\mathbf{T}}(\bar{\mathbf{a}})\dfrac{d^2\boldsymbol{\Lambda}}{d\psi^2}\mathbf{r}\end{bmatrix} \tag{4.41}$$

$$\mathbf{D}_m^k = \begin{bmatrix}\boldsymbol{\Lambda}\\ \mathbf{h}^{\mathbf{T}}(\mathbf{a})\dfrac{d\boldsymbol{\Lambda}}{d\psi}\end{bmatrix}\mathbf{C}^{\mathbf{ep}}\left[\boldsymbol{\Lambda}^{\mathbf{T}};\quad \frac{d\boldsymbol{\Lambda}^{\mathbf{T}}}{d\psi}\mathbf{h}(\mathbf{a})\right];\ \mathbf{D}_g^k = \begin{bmatrix}0 & \dfrac{d\boldsymbol{\Lambda}}{d\psi}\mathbf{r}\\ \mathbf{r}^{\mathbf{T}}\dfrac{d\boldsymbol{\Lambda}^{\mathbf{T}}}{d\psi} & \mathbf{h}^{\mathbf{T}}(\mathbf{a})\dfrac{d^2\boldsymbol{\Lambda}}{d\psi^2}\mathbf{r}\end{bmatrix} \tag{4.42}$$

4.3. Finite element approximation

We choose the simplest finite element approximation for the presented beam model with a plasticity that fits within the framework of incompatible modes method. We here provide some details of numerical implementation for a beam element with two nodes and three localized failure

modes. We allow for displacement discontinuity representation for bending moment, shear force and axial force, each with an additional parameter $\boldsymbol{\alpha}_e$:

$$
\begin{aligned}
&x(\xi)=\sum_{a=1}^{2} N_a(\xi)\cdot x_a;\; N_a(\xi)=\frac{1}{2}(1+\xi_a\xi)\\
&u^h(\xi,t_{n+1})=\sum_{a=1}^{2} N_a(\xi)\cdot u_a(t)+M^e(\xi)\alpha_u^e(t);\\
&v^h(\xi,t_{n+1})=\sum_{a=1}^{2} N_a(\xi)\cdot v_a(t)+M^e(\xi)\alpha_v^e(t);\\
&\psi^h(\xi,t_{n+1})=\sum_{a=1}^{2} N_a(\xi)\cdot \psi_a(t)+M^e(\xi)\alpha_\psi^e(t);\\
&M^e(\xi)=\begin{cases} -N_2(\xi)=-\dfrac{1}{2}(1+\xi),\ \text{for } \xi\in[-1,0]\\ H_{\bar{\xi}}(\xi)-N_2(\xi)=\dfrac{1}{2}(1-\xi),\ \text{for } \xi\in[0,1]\end{cases}
\end{aligned}
\tag{4.43}
$$

where $\xi\in[-1,1]$ is natural coordinate at the parent element and $H_{\bar{\xi}}(\xi)$ is Heaviside function related to the point $\bar{\xi}=\xi=0$. The two-node element interpolation is enhanced with the displacement discontinuity, placed in the center of this element. The corresponding approximation of displacements gradient can then be written as:

$$
\begin{aligned}
&\frac{du^h(\xi,t)}{dx}=\sum_{a=1}^{2} B_a(\xi)u_a(t)+G^e(\xi)\alpha_u^e(t)\\
&\frac{dv^h(\xi,t)}{dx}=\sum_{a=1}^{2} B_a(\xi)v_a(t)+G^e(\xi)\alpha_v^e(t)\\
&\frac{d\psi^h(\xi,t)}{dx}=\sum_{a=1}^{2} B_a(\xi)\psi_a(t)+G^e(\xi)\alpha_\psi^e(t)
\end{aligned}
\tag{4.44}
$$

where

$$
\begin{aligned}
&B_a(\xi)=\frac{dN_a(\xi)}{dx};\; B_a(\xi)=\frac{(-1)^a}{l^e}\\
&G^e(\xi)=\frac{dM_a(\xi)}{dx};\; G^e(\xi)=\begin{cases} -\dfrac{1}{l^e},\ \text{for } \xi\in[-1,0)\cup(0,1]\\ -\dfrac{1}{l^e}+\delta_0,\ \text{for } \xi=0\end{cases}
\end{aligned}
$$

with δ_0 the Dirac delta function placed in the center of the element. This choice will ensure that the incompatible mode variation remains orthogonal to the constant stress in each element.

By combining the results in (4.24), (4.43) and (4.44), we can construct strain field approximation. We typically use reduced numerical integration with a single point, $\xi=0$, in order to avoid locking phenomena (Ibrahimbegovic & Frey, 1993a):

$$\Sigma^h(0,t) = \left(\sum_{a=1}^{2} B_a(0)\cdot u_a(t) + G^e(0)\alpha_u^e(t)\right)\cos\left(\sum_{a=1}^{2} N_a(0)\cdot\psi_a(t) + \underbrace{M^e(0)\alpha_\psi^e(t)}_{=0}\right)$$
$$+\left(\sum_{a=1}^{2} B_a(0)\cdot v_a(t) + G^e(0)\alpha_v^e(t)\right)\sin\left(\sum_{a=1}^{2} N_a(0)\cdot\psi_a(t) + \underbrace{M^e(0)\alpha_\psi^e(t)}_{=0}\right)$$
$$\Gamma^h(0,t) = \left(\sum_{a=1}^{2} B_a(0)\cdot u_a(t) + G^e(0)\alpha_u^e(t)\right)\sin\left(\sum_{a=1}^{2} N_a(0)\cdot\psi_a(t) + \underbrace{M^e(0)\alpha_\psi^e(t)}_{=0}\right) \quad (4.45)$$
$$+\left(\sum_{a=1}^{2} B_a(0)\cdot v_a(t) + G^e(0)\alpha_v^e(t)\right)\cos\left(\sum_{a=1}^{2} N_a(0)\cdot\psi_a(t) + \underbrace{M^e(0)\alpha_\psi^e(t)}_{=0}\right)$$
$$-\sum_{a=1}^{2} N_a(0)\cdot\psi_a(t)$$
$$K^h(0,t) = \sum_{a=1}^{2} B_a(0)\cdot\psi_a(t) + G^e(0)\alpha_\psi^e(t)$$

We note that a pure bending deformation mode (Kirchoff's constraint), which imposes that both shear and membrane deformations are equal to zero ($\Sigma^h(\xi)=\Gamma^h(\xi)=0,\forall\xi$), can be obtained if we have one point of integration and $M^e(x)\dot{\alpha}_\psi^e(t)=0$. The stress field approximation can be obtained from the regular part of the strain rate in (4.45) with no contribution from the singular part, which represents softening plastic strain rate. We can write:

$$N^h(0,t_{n+1}) = EA\left(\tilde{\bar{\Sigma}}^h(0,t) + G^e(0)\bar{\bar{\Sigma}}^h(t)\right)$$
$$V^h(0,t_{n+1}) = GA\left(\tilde{\bar{\Gamma}}^h(0,t) + G^e(0)\bar{\bar{\Gamma}}^h(t)\right) \quad (4.46)$$
$$M^h(0,t_{n+1}) = EI\left(\sum_{a=1}^{2} B_a(0)\cdot\psi_a(t) + G^e(0)\alpha_\psi^e(t)\right)$$

where

$$\bar{\bar{\Sigma}}^h(t) = \alpha_u^e(t)\cos\left(\sum_{a=1}^{2} N_a(0)\cdot\psi_a(t)\right) + \alpha_v^e(t)\sin\left(\sum_{a=1}^{2} N_a(0)\cdot\psi_a(t)\right)$$
$$\bar{\bar{\Gamma}}^h(t) = -\alpha_u^e(t)\sin\left(\sum_{a=1}^{2} N_a(0)\cdot\psi_a(t)\right) + \alpha_v^e(t)\cos\left(\sum_{a=1}^{2} N_a(\xi)\cdot\psi_a(t)\right)$$

4.4. *Numerical examples*

Several numerical examples are presented in this section to illustrate the performance of the proposed finite element formulation. All numerical computations are performed with a research version of the computer program FEAP (Taylor, 2008).

4.4.1. Straight cantilever under imposed end rotation

In this example, we present three different types of a response for a cantilever beam under free-end bending load. The geometric properties of the cross section correspond to standard IPE 200 and material properties take values for steel class S235. The initially straight cantilever beam model is constructed with three different meshes of 2, 4 and 8 elements. Each analysis is performed under imposed end rotation $\psi = \pi$. The first analysis represents the linear elastic response (see Figure 4.1), the second analysis represents the elastoplastic response that remains in hardening phase (see Figure 4.2), whereas the third analysis represents the elastoplastic response that goes into the softening phase, failure. The failure is localized in the middle of the cantilever, where one element is weakened (see Figure 4.3). Response diagrams show the mesh indifference of the proposed formulation.

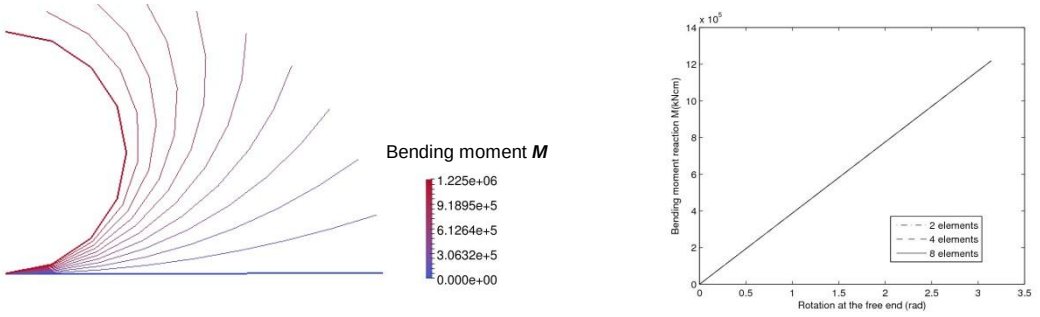

Figure 4.1 Linear elastic analysis: Deformed configuration and diagram $\left(M\left[kNcm\right]-\psi\left[rad\right]\right)$

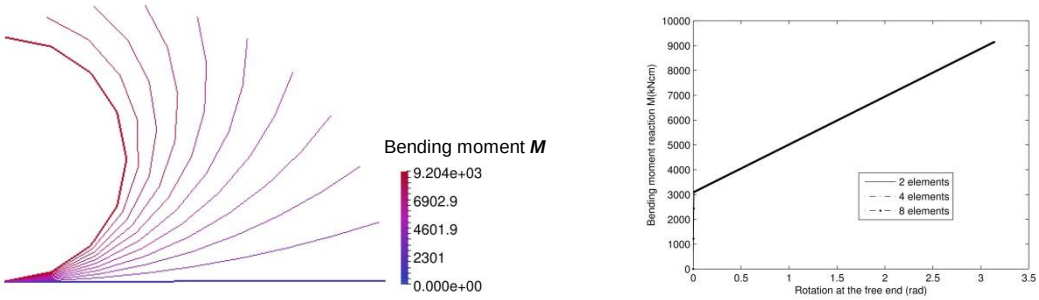

Figure 4.2 Elastic-plastic analysis: Deformed configuration and diagram $\left(M\left[kNcm\right]-\psi\left[rad\right]\right)$

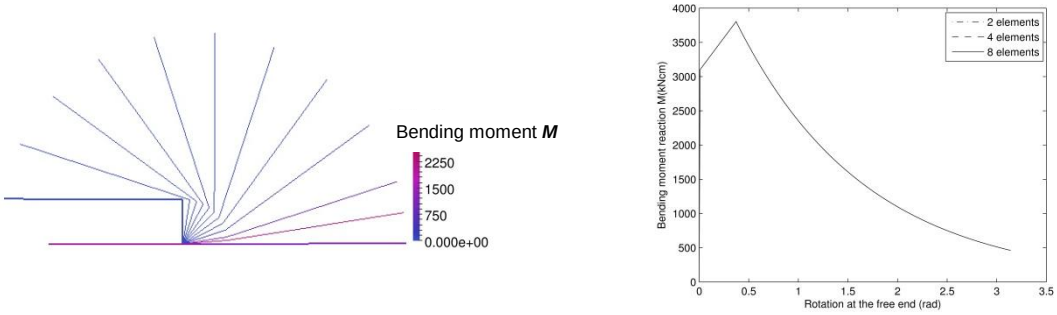

Figure 4.3 Ultimate limit analysis with included failure: Deformed configuration and response curve

For the chosen properties of the cantilever (Young's modulus: $E=2\cdot10^4 kN/cm^2$; Hardening modulus: K=0.05·E; Moment of inertia: $I=1940cm^4$; *Area of the cross section:* $A=28.5cm^2$; *Yield bending moment:* $M_y=3100kNcm$), some of the results can be verified analytically. Namely, the elastic bending moment can be computed as $M_e=\pi\cdot EI/L=1218320kNcm$ and the elastoplastic bending moment as $M_{ep}=(\pi-K_y)\cdot EK/(E+K)L + K_y\cdot EI/L=9145,87kNcm$. The comparison, these reference values versus numerical results computed with a different number of elements, is presented in Table 4.1.

Table 4.1 Cantilever beam under imposed an end rotation

No. of elements	Bending moment	
	Elastic analysis	Elastoplastic anal.
2	1218300 kNcm	9146kNcm
4	1218300 kNcm	9146kNcm
8	1218300 kNcm	9146kNcm
16	1218300 kNcm	9146kNcm
Exact	1218320 kNcm	9145,87kNcm

4.4.2. Straight cantilever under imposed free-end vertical displacement

This example presents two different failure modes under free-end vertical displacement. Namely, by imposing vertical displacement at the free end of a cantilever, we can trigger failure due to either bending moment or shearing force. The type of failure depends on chosen values for constitutive parameters. We first perform analysis (see Figure 4.4) where the ultimate bending M_u is reached before the ultimate shear force V_u (M_u=3800kNcm, V_u=75kN). We then modify the parameters (M_u=3800kNcm, V_u=65kN), see Figure 4.5, in the second analysis, in order to reach the ultimate shear force before the ultimate bending moment. In Table 4.2, we provide the results of studies for the typical rate of convergence.

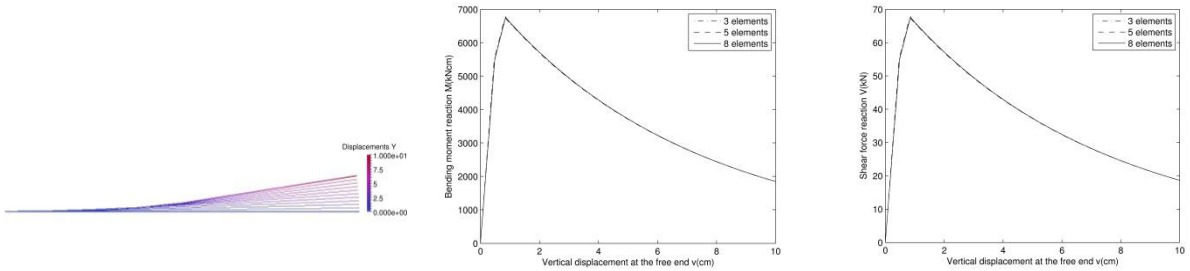

Figure 4.4 Failure in the bending: deformed configuration and response curves

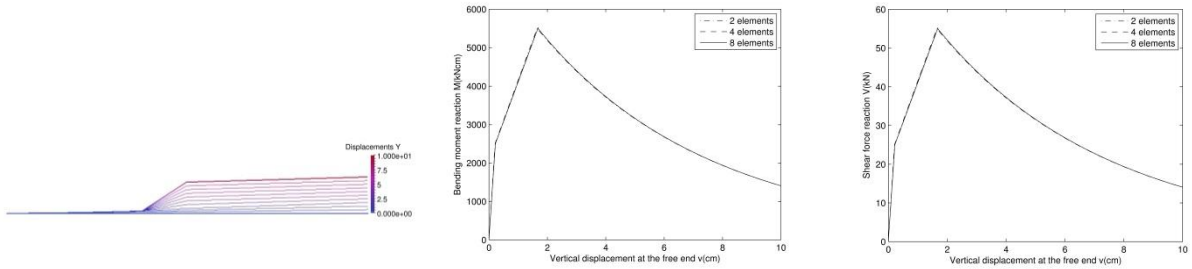

Figure 4.5 Failure in the shearing: deformed configuration and response curves

Table 4.2 Reduction in residual and energy norm in one increment (softening)

No. of iterations	Failure in the bending		Failure in the shearing	
	Residual	Energy	Residual	Energy
1	2.5451184E+03	2.89262392986E+00	2.5617356E+03	2.88022968875E+00
2	1.2603427E-02	7.72176817049E-09	2.2358020E-01	2.94749460179E-08
3	3.1269310E-10	5.37722363293E-25	5.5411964E-05	2.27071800263E-14
4			1.0282664E-07	2.31118241048E-20

4.4.3. Push-over analysis of a symmetric frame

In this example, we present the results of a push-over analysis of symmetric steel frame. The frame geometry is given in Figure 4.6. The material properties for all frame members are equal (Young's modulus: $E=2\cdot10^4 kN/cm^2$; Hardening modulus: K=0.05·E; Moment of inertia: $I=1940cm^4$; *Area of the cross section:* $A=28.5cm^2$; *Yield bending moment:* $M_y=3100kNcm$; *Ultimate bending moment:* $M_u=3100kNcm$; *Yield shear force:* $V_y=355kN$; *Ultimate shear force:* $V_u=400kN$, *Fracture energies:* $G_{f,M}=550$ *and* $G_{f,V}=450$), except the fact that the cross-section properties of the columns are 10% stronger then cross-section properties of the beams.

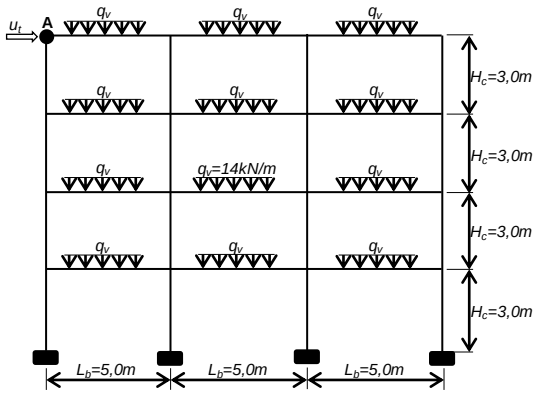

Figure 4.6 a) Frame geometry and loading

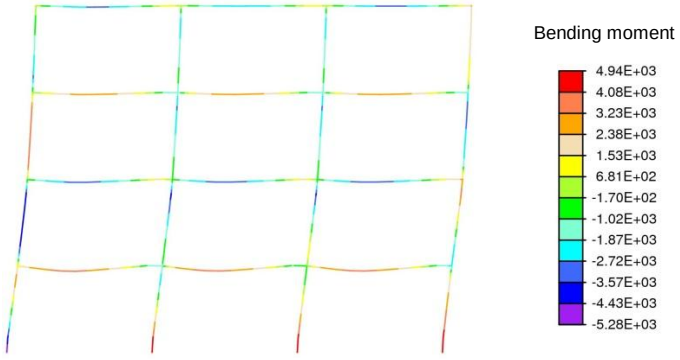

b) Deformed shape and bending moment distribution

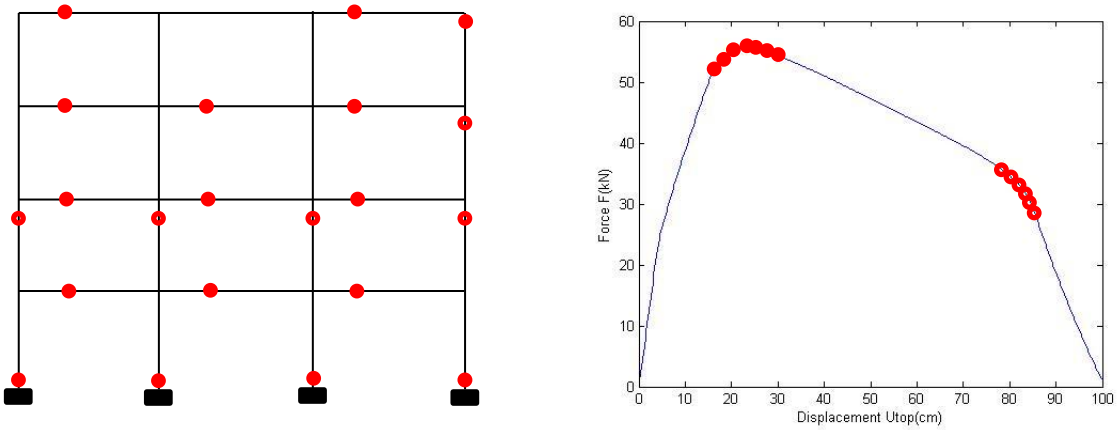

Figure 4.7 Locations of softening plastic hinges and load versus displacement ($u_{top}=100cm$)

The elements which connect beams to columns are 10% weaker than cross-section properties of beams; these elements are chosen to simulate the behavior of connections in the global analysis of

the steel frame structure. The vertical load was applied to all beam members. This load is kept constant throughout pushover analysis in order to simulate the dead load effect. The lateral loading is applied regarding an imposed incremental displacement (u_{top}) at the upper corner (point A, see Figure 4.6). In Figure 4.6b, we present the deformed configuration of the steel frame and the corresponding distribution of the bending moments. In Figure 4.7, we present the position of activated plastic hinges in the final stage of failure, along with the computed softening response in terms of the force – displacement diagram. In Figure 4.7b, the force denotes reaction in the corner A, where is imposed the displacement.

4.4.4. Push-over analysis of a simple frame

In this example, we present ability to capture different failure modes of the frame. We consider a simple steel frame presented in Figure 4.8, where the span is 5,0m and height is 3,0m. The mesh is composed of 48 elements where the length of each element is 0,25m. The material properties of all frame members are equal (Young's modulus: $E=2\cdot10^4 kN/cm^2$; Hardening modulus: K=0.05·E; Moment of inertia: $I=1940cm^4$; *Area of cross section:* $A=28.5cm^2$; *Yield bending moment:* $M_y=3100kNcm$; *Ultimate bending moment:* $M_u=3100kNcm$; *Yield shear force:* V_y=355kN; *Ultimate shear force:* $V_u=400kN$, *Fracture energies:* $G_{f,M}=550$ *and* $G_{f,V}=450$), but elements which connect beams and columns are defined according to connection behavior see (Imamovic et al., 2015).

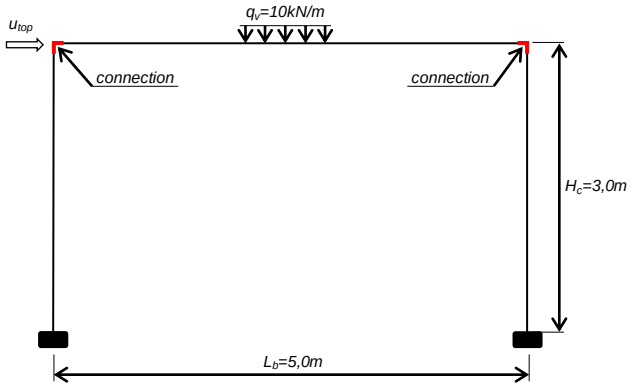

Figure 4.8 Frame geometry and loading

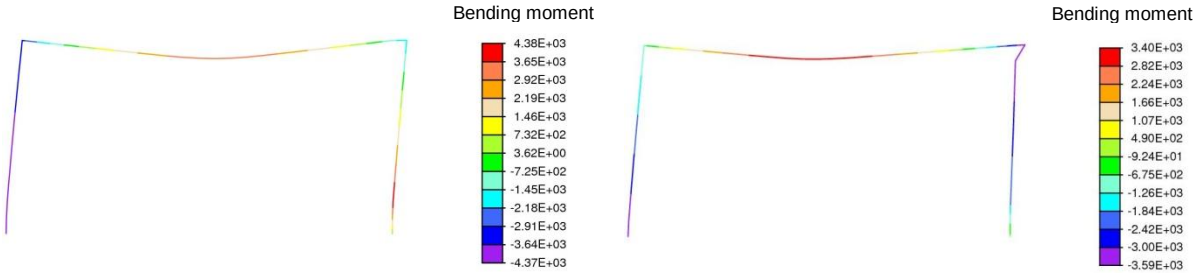

a) Failure in the bending *b) Failure in the shearing*

Figure 4.9 Deformed Configuration

Two cases are considered, in the first, connections are defined properly. In the second case, right connection is defined with very low capacity regard to the shear force ($V_u=30kN$), which can be caused by poor construction during building. This construction error is assumed in the right corner of the steel frame. Deformed configurations of the frame for both cases are presented in Figure 4.9.

The results of the analysis for both cases are shown in Figure 4.10, showing a significant reduction in a frame limit load that can be brought by construction errors. Figure 4.10b shows this reduction of the limit load, caused by construction errors during building.

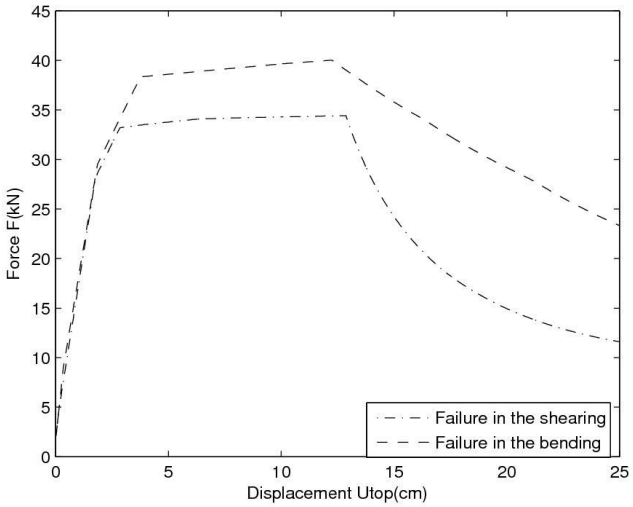

Figure 4.10 Response of the frame

4.5. *Concluding remarks*

The presented geometrically non-linear planar beam model provides the main novelty with its ability to account for both bending and shear failure. The proposed constitutive model contains both coupled plasticity with isotropic hardening and nonlinear law for softening with three different failure mechanisms. The hardening response providing the interaction between bending moment, shear force, and axial force can be calibrated against damage of beams or columns in a steel frame. The softening response can be activated to model the failure mode in the connections with different failure mechanisms. Which of mechanisms will be activated depends on interplay and stress redistribution during the limit load analysis.

By using the proposed beam element, we can perform ultimate limit analysis of any frame planar steel structure, including the second order effects as well as different failure mechanisms. The geometrically nonlinear analysis allows the ultimate limit analysis with large displacement without any need for correction of the proposed property (Dujc et al., 2010). This advantage is significant in a steel frame structure because of a large ductility of steel.

The results for all numerical examples illustrate an excellent performance of the proposed beam element.

Chapter 5

Experimental testing of structural steel connections and constitutive parameters identification

Abstract

The moment-resistant steel frames are frequently used as a load-bearing structure of buildings. Global response of a moment-resistant frame structure strongly depends on connections behavior, which can significantly influence the response and load-bearing capacity of a steel frame structure. The analysis of a steel frame with included joints behavior is the main focus of this work. In particular, we analyze the behavior of three connection types through experimental tests, and we propose numerical beam model capable of representing connection behavior. The experimental tests are performed for three different types of structural connections: end plate connection with an extended plate, end plate connection and moment resistant connection with angles. The proposed beam model is Reissner beam with the ability to capture both hardening and softening response, which has 17 constitutive parameters. The identification of those constitutive parameters requires an elaborate procedure, which we illustrate in this work. We also illustrate that the constitutive parameters successfully identification requires the well-designed experimental testing program. We finally illustrate that the steel structure connections are very important for correct prediction of the global response of steel frame structure. A detailed analysis is presented in several practical examples.

Contents of Chapter 5

5.1. Introduction

The moment-resistant steel frame is frequently used as a bearing structure, especially in seismic regions. They provide a very ductile response and a large potential to dissipate energy, which is crucial in the case of earthquakes. These characteristics provide the economical design of the structure and increase resistance with respect to the seismic security. Structural connections between beams and columns play a crucial role in the response of a steel frame structure. They can significantly change the response of the structure, sometimes up to 30%.

The analysis of a steel structure with connection behavior can be performed with many nonlinear FEM commercial programs, using 3D solid finite elements. The refined nonlinear model can predict the behavior of a joint, but those computations are often too costly and not practical for the design of the whole structure. For this reason, we propose the use of beam element as a better choice regarding computational efficiency and reduced costs. It is well known that geometrically nonlinear elastoplastic beam elements are able to represent the behavior of a steel structure including material nonlinearities and buckling (Imamovic et al., 2017; Dujc et al., 2010). We postulate that every connection in steel frame structure can be modeled with beam element. The geometrically nonlinear beam element with bilinear hardening and the linear softening response is used to represent connection behavior. For the steel members, a simpler beam element with linear hardening and softening is proposed. The constitutive parameters of the beam element are determined from the connection behavior of steel bulk material. The constitutive model, which we propose is much more refined than the bilinear plasticity model proposed in EC 3 (EC3, 2005), where after reaching an ultimate bending moment, the connection response corresponds to perfect plasticity model with a constant value that remains permanently. The EC 3 connection does not consider the shear response. The main novelty of the proposed beam model with the connection is to be able to capture bending and shearing inelastic response with both hardening and softening response until the complete failure is reached.

The proposed Reissner beam model contains 17 constitutive parameters that need to be identified. The parameters identification represents a challenge, which can be raised by done using well-designed experimental tests of a structural connection. In this chapter, experimental testing related to loading program and measurement equipment is designed according to (Imamovic et al., 2015). The loading program was defined as cycles of a loading/unloading. The measurements were split into the set of local and the set of global measurements. Such experimental testing gives us sufficient information for the identification of the seventeen constitutive parameters. Six experimental tests were performed for three different connection types: end plate connection with the extended plate, end plate connection and moment resistant connection with angles. The testing structures were designed so that the joint represents the weakest element of the structure. Every connection type is tested for two different bolt classes. This difference should change failure model of connection according to EC3 (EC3, 2005), but experimental testing does not confirm that.

The outline of the chapter is as follows. In the next section, we describe the experimental testing methodology and present main experimental results. The third section gives a brief overview of the main ingredients of the proposed beam model and corresponding FEM implementation. The constitutive parameters identification of the proposed beam element is shown in the fourth section. In the fifth section, we present results of two numerical simulations of the steel frame structures with and without included connection behavior. The last section contains the conclusions.

5.2. The experimental testing of structural connections

Experimental tests on three types of moment-resistant connection have been conducted with the aim to identify constitutive parameters of the proposed beam model. The tested moment-resistant connection types are: end plate connection with the extended plate, end plate connection and moment resistant connection with angles. In the experimental structures, connection represents the weakest element where plastic deformations and failure are expected to occur. The vertical and the horizontal beams, chosen as IPE 200 and IPE 400, respectively, are deemed sufficiently strong to remain linear elastic throughout the loading program.

In total, six experimental tests have been performed. Every connection type has been tested for two different bolt classes (10.9. and 8.8.). The experimental tests were performed at the Laboratory for materials and structures of the University of Sarajevo.

According to EC3, the difference in bolt classes should result in different failure mechanisms. EC3 predicts failure in the T-stub (Abidelah et al., 2014) for the higher class bolts, and the failure in bolts for the lower class bolts (EC3, 2005).

5.2.1. Experimental setup

Figure 5.1 shows the experimental setup for testing connection between two orthogonal steel beams. The horizontal beam is chosen much stronger than the vertical beam, which should ensure the linear elastic behavior of the horizontal beam during the test. The equipment for displacements measurements are arranged so that sufficient information for identification of mechanical properties can be obtained. The experimental data can be classified as the local and the global measurements. The global measurements depend mainly on all model parameters, while the local measurements depend on only one model parameter.

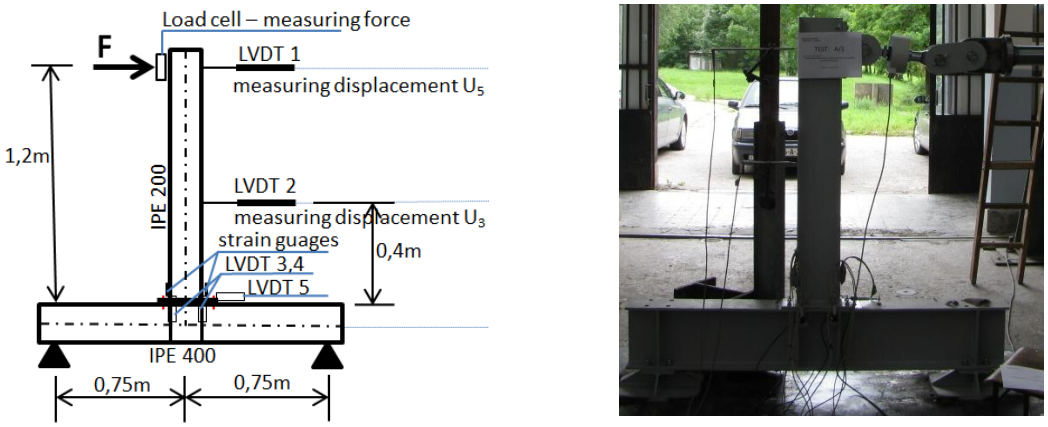

Figure 5.1 Experimental setup

The Figure 5.1a illustrates the measuring equipment, where LVDT is an abbreviation for the "Linear variable displacement transducer", which measures displacements. The LVDT 1 and 2 measure horizontal displacements of the vertical beam ($U_{3,Pi}^{\exp}$) and ($U_{5,Pi}^{\exp}$), which can be classified as the global measurements. All other measurements are classified as local. LVDT 3 and 4 measure relative vertical displacement between horizontal and vertical beams, which we use for calculating the rotation of the connection:

$$\psi^{\exp} = \frac{\Delta v_3^{\exp} - \Delta v_4^{\exp}}{h_{vert.beam}} \tag{5.1}$$

LVDT 5 measures relative horizontal displacement ($U_{2,Pi}^{\exp} = U_{S,Pi}^{\exp}$) between horizontal and vertical beams, which corresponds to transverse (shearing) displacement of the connection. The strain gauges measure deformation at the vertical beam, which we use for calculating the curvature of the section near to the connection:

$$\varepsilon_i^{\exp} = -y \cdot \kappa_i \Rightarrow \kappa_i = -\frac{\varepsilon_i^{\exp}}{y};\ y = \left[-\frac{h}{2}, \frac{h}{2}\right] \Rightarrow \kappa^{\exp} = \frac{\kappa_1 + \kappa_2}{2} \tag{5.2}$$

The force F is applied by using a hydraulic pump. The value of the force is measured with load cell placed between the hydraulic pump and the loading point, in the experimental structure. The measuring equipment is controlled with experimental device *Spider 8* and monitored with software *Catman* 5.

Table 5.1 Geometrical characteristics of experimental structures

Joint	Vertical beam	Horizontal beam	End plate dimension/Angles	Bolts
A1	IPE 200 – S275	IPE 400 – S275	≠ 340x130x10 – S275	8M12-class 8.8.
A2	IPE 200 – S275	IPE 400 – S275	≠ 340x130x10 – S275	8M12-class 10.9.
B1	IPE 200 – S275	IPE 400 – S275	≠ 220x130x10 – S275	4M16-class 8.8.
B2	IPE 200 – S275	IPE 400 – S275	≠ 220x130x10 – S275	4M16-class 10.9.
C1	IPE 240 – S275	IPE 400 – S275	L 100x100x10 – S235	17M12-class 8.8.
C2	IPE 240 – S275	IPE 400 – S275	L 100x100x10 – S235	17M12-class 10.9.

5.2.2. *Experimental testing*

The experimental data have been collected during load application, with all results recorded during the complete loading program. Figure 5.2 shows loading program, which contains several cycles of loading and unloading. The benefits of this loading program are presented in (Imamovic et al., 2015), where we elaborated that unloading points are important for the potential existence of connection damage. Namely, plasticity and damage models can represent the same behavior in the loading regime, but the unloading shows the difference between them. The same loading program has been used for all experimental testing, with only step size adjusted to the connection behavior.

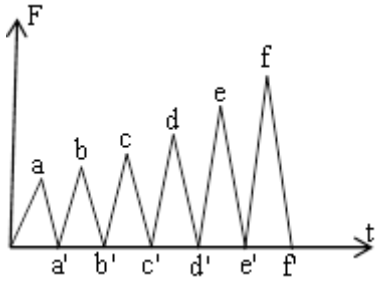

Figure 5.2 Loading program

5.2.2.1. End plate connection with extended end plate

The end plate connection type with the extended plate is constructed from the plate (340x130x10mm) welded to the vertical beam and eight bolts (M12) connecting the plate to the horizontal beam. The bolts were preloaded with 50% of prestressing force according to EC3. Two experimental tests have been performed for this type of connection; the first is A1 (bolt class 8.8.) and the second is A2 (bolt class 10.9.).

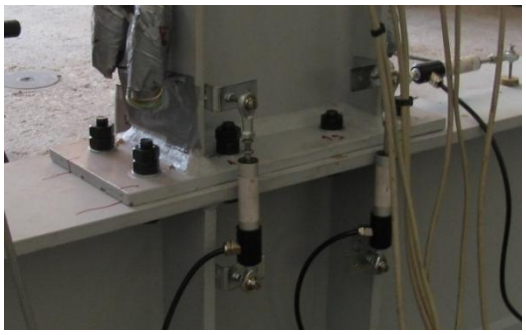

Figure 5.3 End plate connection with extended end plate

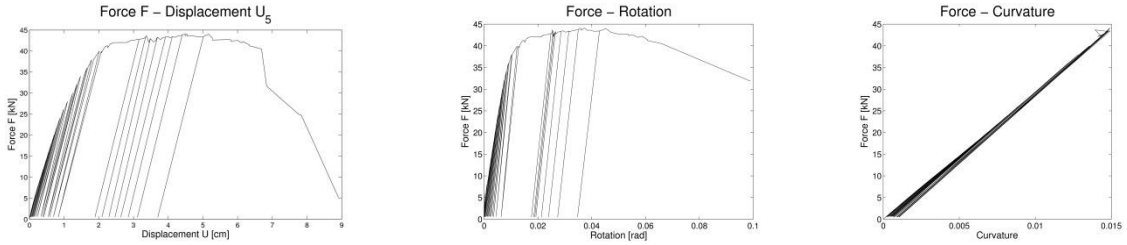

Figure 5.4 Experimental results for connection A1

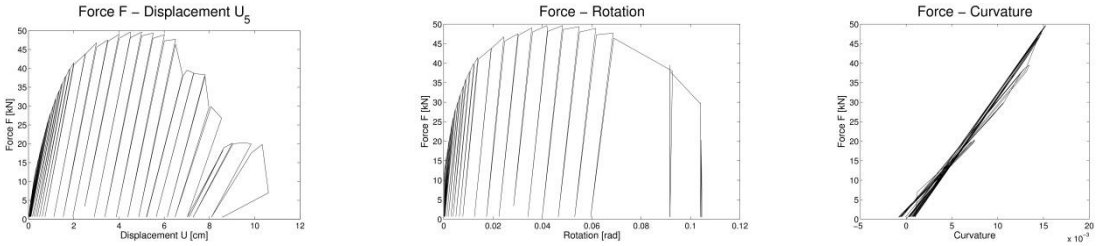

Figure 5.5 Experimental results for connection A2

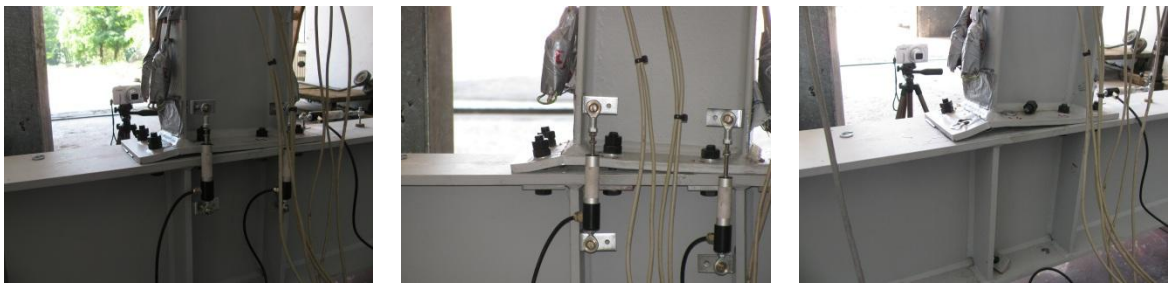

Figure 5.6 Deformation of connection elements during experimental testing

The testing results are shown in Figure 5.4 and Figure 5.5, where we can see that vertical beam remains in the elastic response. The relative horizontal displacement between vertical and

horizontal beams does not exist ($U_{2,Pi}^{\exp} = U_{S,Pi}^{\exp}$). The unloading lines at diagrams are parallel to first loading line, which indicates that plasticity model can represent the behavior of the connection. The photographs in Figure 5.6 show deformation of connection elements during experimental testing.

In both experimental structures (A1 and A2), failure has progressively occurred in the bolts, where the inner row of bolts broke before the outer row of bolts.

5.2.2.2. End plate connection

The end plate connection is constructed from the plate (220x130x10mm) welded to the vertical beam and four bolts (M16), connecting the plate to the horizontal beam. A total of two experimental tests have been conducted; the first is B1 (bolt class 8.8.) and the second is B2 (bolt class 10.9.).

Figures 5.8 and 5.9 show testing results, where we can see that sliding displacement between vertical and horizontal beam exists. The strain gauges have not measured residual strains which indicate that vertical beam has remained in the linear elastic part of the response. The diagrams show that plasticity model can appropriately represent connection behavior because the subsequent loading/ unloading lines are parallel to the first loading line.

Figure 5.7 End plate connection

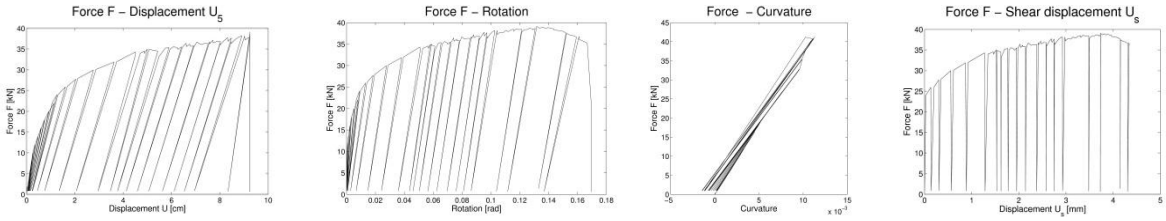

Figure 5.8 Experimental results for connection B1

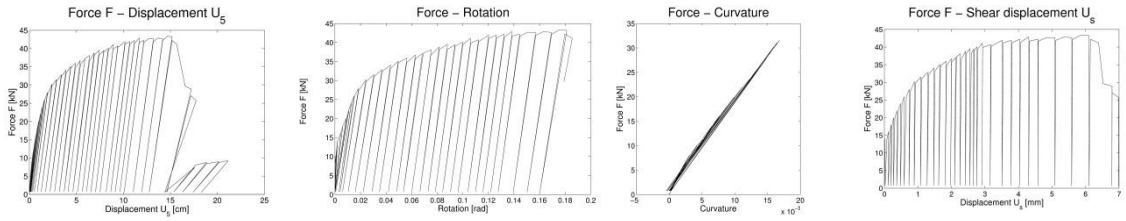

Figure 5.9 Experimental results for connection B2

In both experimental structures (B1 and B2), failure has occurred in bolts, see Figure 4.10. In the

B1 test, both bolts in the tension zone broke at the same moment, while in the B2 experimental structure bolts gradually broke. Regarding the failure mechanism in the B1 test, where the brittle failure happened, we were not able to measure the softening response.

Figure 5.10 Deformation of connection elements during the experimental testing

5.2.2.3. Moment resistant connection with angles

The moment resistant connection with angles is constructed from four hot rolled angle profiles (L100x100x10mm), where two angles on flanges provide the resistance to the bending moment and angles on the web ensure the shear resistance. A total of two experimental tests have been performed; the first is C1 (bolt class 8.8.) and the second is C2 (bolt class 10.9.).

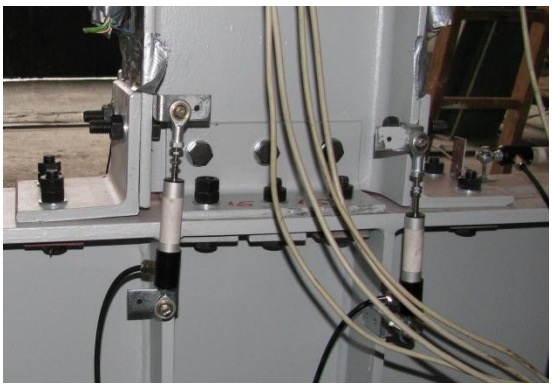

Figure 5.11 Moment resistant the connection with angles

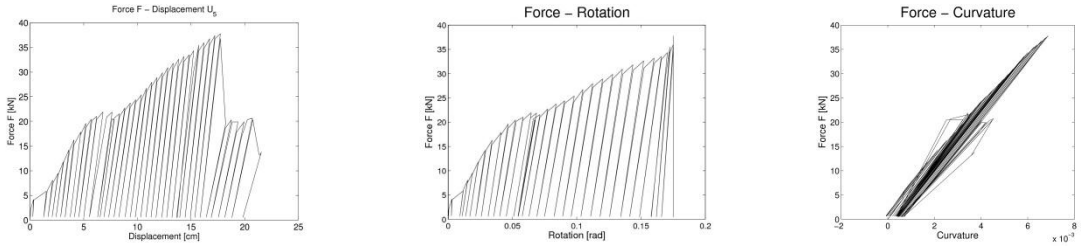

Figure 5.12 Experimental results for the connection C1

Figures 5.12 and 5.13 present testing results, where we can see that vertical beam remains in the elastic response, while the measured sliding deformation between horizontal and vertical beam is very small and can be neglected.

The deformations of connection elements during experimental testing are presented in Figure 4.14. In both experimental structures (C1 and C2), failure has occurred in bolts. The horizontal bolts in tension zone broke under shear stresses. In the C1 test, both bolts in the tension zone broke in the

same moment, while in the C2 test bolts broke one-by-one. Regarding the brittle failure mechanism in the C1 test, we were not able to measure the softening response.

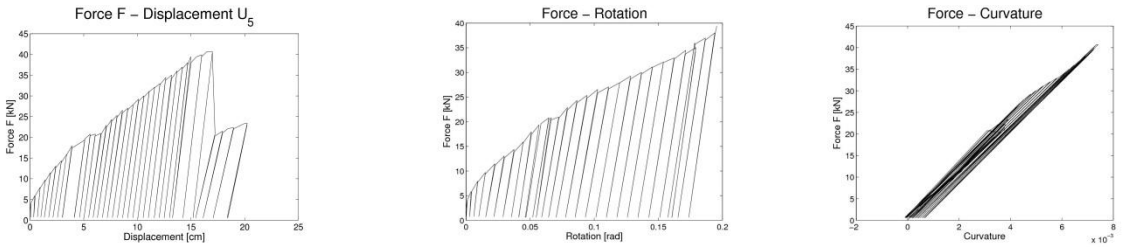

Figure 5.13 Experimental results for connection C2

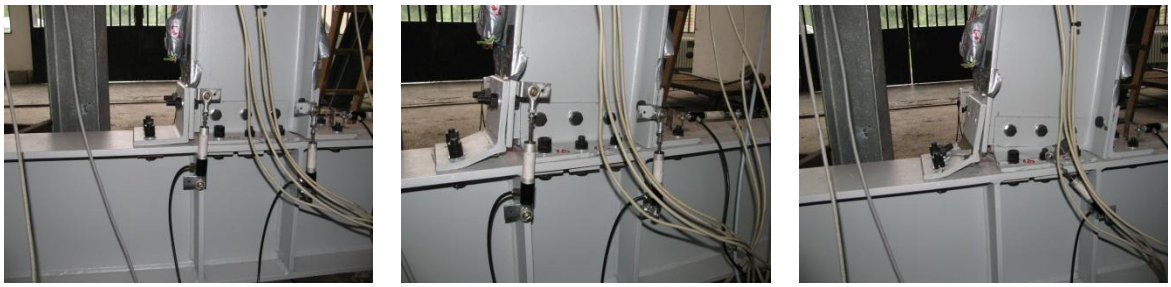

Figure 5.14 Deformation of connection elements during experimental testing

5.3. Finite element beam model: geometrically exact beam with bilinear hardening and nonlinear softening response

The complex response of a steel frame structure with connections is quite a challenge to describe. In this work, we use the geometrically exact beam with bilinear hardening and linear softening response (Imamovic et al., 2017). This model is able to represent many phenomena observed during experimental testing, including the regime of large deformation (Wagner & Gruttmann, 2002) of the tested structure. A brief description of the beam model is given as follows. The Helmholtz free energy can be defined as quadratic form:

$$\bar{\Psi}(\bar{\mathbf{U}}^e, \bar{\boldsymbol{\xi}}^p) = \underbrace{\frac{1}{2}\bar{\mathbf{U}}^{e,T} \cdot \mathbf{C} \cdot \bar{\mathbf{U}}^e}_{\bar{\Psi}^e} + \underbrace{\frac{1}{2}\bar{\boldsymbol{\xi}}_1^{p,T} \cdot \mathbf{K}_1^h \cdot \bar{\boldsymbol{\xi}}_1^p}_{\bar{\Xi}_1^p} + \underbrace{\frac{1}{2}\bar{\boldsymbol{\xi}}_2^{p,T} \cdot \mathbf{K}_2^h \cdot \bar{\boldsymbol{\xi}}_2^p}_{\bar{\Xi}_2^p} \tag{5.3}$$

where $\bar{\mathbf{U}}^e$ is elastic strain measure tensor, $\bar{\boldsymbol{\xi}}_i^p$ are vectors of hardening variables and $\mathbf{K}_i^h$ are corresponding hardening moduli. The yield criterion that has to be satisfied in hardening regime:

$$\bar{\phi}_i(\mathbf{T}, \bar{\mathbf{q}}) \leq 0 \tag{5.4}$$

where $\bar{\mathbf{q}}$ is a vector of internal hardening stress like variables. The second principle of thermodynamics states that the plastic dissipation must remain non-negative:

$$0 \leq \bar{\mathcal{D}} = \underbrace{\left(\mathbf{T} - \frac{d\bar{\Psi}^e}{d\bar{\mathbf{U}}^e}\right)\dot{\bar{\mathbf{U}}}^e}_{\bar{\mathcal{D}}^e = 0} + \underbrace{\mathbf{T}\dot{\bar{\mathbf{U}}}_1^p - \frac{\partial\bar{\Xi}_1^p}{\partial\bar{\boldsymbol{\xi}}_1^p}\frac{d\bar{\boldsymbol{\xi}}_1^p}{dt}}_{\bar{\mathcal{D}}_1^p} + \underbrace{\mathbf{T}\dot{\bar{\mathbf{U}}}_2^p - \frac{\partial\bar{\Xi}_2^p}{\partial\bar{\boldsymbol{\xi}}_2^p}\frac{d\bar{\boldsymbol{\xi}}_2^p}{dt}}_{\bar{\mathcal{D}}_2^p} \tag{5.5}$$

The principle of maximum plastic dissipation can be formulated (Hill, 1950; Ibrahimbegovic & Frey, 1993a) as the minimization problem with the constraint, with the latter being yield function (5.4). This can further be recast as corresponding unconstrained minimization by using the Lagrange multiplier method:

$$\min_{\mathbf{T},\bar{\mathbf{q}}} \max_{\dot{\bar{\gamma}}} \left[\bar{L}^p(\mathbf{T},\bar{\mathbf{q}},\dot{\bar{\gamma}}) = -\bar{\mathcal{D}}^p(\mathbf{T},\bar{\mathbf{q}}) + \dot{\bar{\gamma}}_i \cdot \bar{\phi}_i(\mathbf{T},\bar{\mathbf{q}}) \right] \tag{5.6}$$

where $\dot{\bar{\gamma}}_i$ are Lagrange multipliers. The Kuhn-Tucker optimality conditions provide the evolution equations for internal variables in rate form along with the loading/unloading conditions:

$$\begin{aligned}
&\frac{\partial \bar{L}_i^p}{\partial \mathbf{T}} = -\dot{\bar{\mathbf{U}}}_i^p + \dot{\bar{\gamma}}_i \frac{\partial \bar{\phi}_i}{\partial \mathbf{T}} = 0 \Rightarrow \dot{\bar{\mathbf{U}}}_i^p = \dot{\bar{\gamma}}_i \frac{\partial \bar{\phi}_i}{\partial \mathbf{T}} \\
&\frac{\partial \bar{L}_i^p}{\partial \bar{\mathbf{q}}_i} = -\frac{\partial \bar{\boldsymbol{\xi}}_i^p}{\partial t} + \dot{\bar{\gamma}}_i \frac{\partial \bar{\phi}_i}{\partial \bar{\mathbf{q}}_i} = 0 \Rightarrow \frac{\partial \bar{\boldsymbol{\xi}}_i^p}{\partial t} = \dot{\bar{\gamma}}_i \frac{\partial \bar{\phi}_i}{\partial \bar{\mathbf{q}}_i} \\
&\dot{\bar{\gamma}}_i \geq 0, \quad \bar{\phi}_i \leq 0, \quad \dot{\bar{\gamma}}_i \bar{\phi}_i = 0
\end{aligned} \tag{5.7}$$

The appropriate value of plastic multiplier $\dot{\bar{\gamma}}$ can be determined from the plastic consistency condition for the case of sustained plastic flow:

$$\dot{\bar{\phi}}_i = 0 \;\Rightarrow\; \dot{\bar{\gamma}}_i = \frac{\dfrac{\partial \bar{\phi}_i}{\partial \mathbf{T}} \mathbf{C}^e \dot{\bar{\mathbf{U}}}}{\dfrac{\partial \bar{\phi}_i}{\partial \mathbf{T}} \mathbf{C}^e \dfrac{\partial \bar{\phi}_i}{\partial \mathbf{T}} + \dfrac{\partial \bar{\phi}_i}{\partial \bar{\mathbf{q}}_i} \mathbf{K}_i^h \dfrac{\partial \bar{\phi}_i}{\partial \bar{\mathbf{q}}_i}} \tag{5.8}$$

By replacing the last result in stress rate equation, we can obtain the elastoplastic modulus $\mathbf{C}^{ep}$ that should replace the elastic modulus $\mathbf{C}$ in plastic regime:

$$C_i^{ep} = \mathbf{C}^e - \frac{\mathbf{C}^e \dfrac{\partial \bar{\phi}_i}{\partial \mathbf{T}} \otimes \mathbf{C}^e \dfrac{\partial \bar{\phi}_i}{\partial \mathbf{T}}}{\dfrac{\partial \bar{\phi}_i}{\partial \mathbf{T}} \mathbf{C}^e \dfrac{\partial \bar{\phi}_i}{\partial \mathbf{T}} + \dfrac{\partial \bar{\phi}_i}{\partial \bar{\mathbf{q}}_i} \mathbf{K}_i^h \dfrac{\partial \bar{\phi}_i}{\partial \bar{\mathbf{q}}_i}} \tag{5.9}$$

We note in passing that the elastoplastic tangent above remains the same in the discrete problem, obtained by using the backward Euler time integration scheme.

In the softening regime the Helmholtz free energy can be written as a quadratic form in softening variables:

$$\bar{\bar{\Psi}}\left(\bar{\bar{\boldsymbol{\xi}}}^s\right) = \underbrace{\frac{1}{2} \bar{\bar{\boldsymbol{\xi}}}^s \mathbf{K}_s \bar{\bar{\boldsymbol{\xi}}}^s}_{\bar{\bar{\Xi}}^s}; \quad \Psi(\cdot) = \bar{\Psi}(\cdot) + \bar{\bar{\Psi}}(\bar{\bar{\boldsymbol{\xi}}}^s)\delta_{\bar{x}} \tag{5.10}$$

where $\bar{\bar{\boldsymbol{\xi}}}^s$ is a set of internal variables representing the connection failure and $\bar{\bar{\mathbf{K}}}^s$ is a set of softening moduli. The yield function for softening is chosen as a multi-criteria pertaining to bending, shearing and axial force:

$$\dot{\bar{\bar{\gamma}}}_i \bar{\bar{\phi}}_i = 0 \Rightarrow \bar{\bar{\phi}}^i(t_i, \bar{\bar{q}}_i^s) \leq 0 \tag{5.11}$$

where t_i is the traction force and $\bar{\bar{q}}_i^s$ are stress-like variables work-conjugate to softening variables at the discontinuity for the corresponding failure mode. The principal of maximum dissipation (Hill, 1950) that applies to softening states will pick the ones that maximize softening dissipation, among all admissible values of these variables. That can be solved as an unconstrained minimization problem, to provide the evolution equations for internal variables along with the loading/unloading conditions:

$$\frac{\partial \bar{\bar{L}}^s}{\partial \bar{\bar{\mathbf{q}}}^s} = -\dot{\bar{\bar{\boldsymbol{\xi}}}}^s + \sum_1^3 \dot{\bar{\bar{\gamma}}} \frac{\partial \bar{\bar{\phi}}}{\partial \bar{\bar{\mathbf{q}}}^s} = 0 \Rightarrow \dot{\bar{\bar{\boldsymbol{\xi}}}}^s = \sum_1^3 \dot{\bar{\gamma}}_i \frac{\partial \bar{\bar{\phi}}}{\partial \bar{\bar{\mathbf{q}}}^s} \qquad \dot{\bar{\bar{\gamma}}} \geq 0, \;\; \bar{\bar{\phi}} \leq 0, \;\; \dot{\bar{\bar{\gamma}}} \bar{\bar{\phi}} = 0 \tag{5.12}$$

The beam kinematics equations can be written by using the rotated strain measure: $\mathbf{H} = \mathbf{U} - \mathbf{I}$, where the only non-zero components are defined as:

$$H_{11} = \Sigma - \zeta K, \; H_{21} = \Gamma \tag{5.13}$$

The explicit form of generalized strains can be written as

$$\begin{aligned}
\Sigma = H_{11}^{u,v} &= \underbrace{\left(1 + \frac{d\bar{u}}{dx}\right)\cos\psi + \frac{d\bar{v}}{dx}\sin\psi - 1}_{\bar{\Sigma}} + \underbrace{\left(\frac{d\bar{\bar{u}}}{dx}\cos\psi + \frac{d\bar{\bar{v}}}{dx}\sin\psi\right)}_{\bar{\bar{\Sigma}}}\delta_{\bar{x}} \\
\Gamma = H_{21}^{u,v} &= \underbrace{-\left(1 + \frac{d\bar{u}}{dx}\right)\sin\psi + \frac{d\bar{v}}{dx}\cos\psi}_{\bar{\Gamma}} + \underbrace{\left(-\frac{d\bar{\bar{u}}}{dx}\sin\psi + \frac{d\bar{\bar{v}}}{dx}\cos\psi\right)}_{\bar{\bar{\Gamma}}}\delta_{\bar{x}} \\
K = H_{11}^{\psi} &= \underbrace{\frac{d\bar{\psi}}{dx}}_{\bar{K}} + \underbrace{\frac{d\bar{\bar{\psi}}}{dx}}_{\bar{\bar{K}}}\delta_{\bar{x}}
\end{aligned} \tag{5.14}$$

The linearized form of strain measures in (5.14) coinciding with the strains of the Timoshenko beam (Ibrahimbegovic & Frey, 1993a; Nikolic et al., 2015), which allow for the additive split into elastic and plastic components. The equation (5.14) can be written in compact matrix notation:

$$\bar{\boldsymbol{\Sigma}} = \boldsymbol{\Lambda}^{\mathrm{T}}\left(\mathbf{h}(\bar{\mathbf{a}}) - \mathbf{n}\right) + \boldsymbol{\Lambda}^{\mathrm{T}}\mathbf{h}(\bar{\bar{\mathbf{a}}})\delta_{\bar{x}}$$

$$\boldsymbol{\Sigma} = \begin{pmatrix} \Sigma \\ \Gamma \\ K \end{pmatrix}, \; \boldsymbol{\Lambda} = \begin{bmatrix} \cos\psi & -\sin\psi & 0 \\ \sin\psi & \cos\psi & 0 \\ 0 & 0 & 1 \end{bmatrix}, \; \mathbf{h}(\bar{\mathbf{a}}) = \begin{pmatrix} 1 + \frac{d\bar{u}}{dx} \\ \frac{d\bar{v}}{dx} \\ \frac{d\bar{\psi}}{dx} \end{pmatrix}, \mathbf{h}(\bar{\bar{\mathbf{a}}}) = \begin{pmatrix} \bar{\bar{u}} \\ \bar{\bar{v}} \\ \bar{\bar{\psi}} \end{pmatrix}, \mathbf{n} = \boldsymbol{\Lambda}\mathbf{g}_1, \; \mathrm{g}_1 = \begin{pmatrix} 1 \\ 0 \\ 0 \end{pmatrix} \tag{5.15}$$

By using the same compact notation for the virtual strains (denoted with superposed $(\hat{\bullet})$), we can write the weak form of equilibrium equation, see (Ibrahimbegovic & Frey, 1993a):

$$G(\mathbf{a}, \hat{\mathbf{a}}) := \int_L \left(\hat{\Sigma}N + \hat{\Gamma}V + \hat{K}M\right)dx - G^{ext}(\hat{\mathbf{a}}) = 0 \tag{5.16}$$

In (5.16) above, N, V and M denote stress resultants regarding the Biot stress:

$$\boldsymbol{\sigma} = \left(N, V, M\right)^T ; \;\; N = \int_A T^{11} dA; \;\; V = \int_A T^{21} dA; \; M = -\int_A \zeta T^{11} dA \tag{5.17}$$

The yield function for softening is chosen as a multi-criteria form, pertaining respectively, to bending moment, shear and axial force:

$$\begin{aligned} & \bar{\phi}^M (M, \bar{q}_M^p) = |M| - \left(M_y - \bar{q}_M^p\right) \le 0 \\ \dot{\bar{\gamma}}_i \bar{\phi}_i = 0 \Rightarrow \quad & \bar{\phi}^V (V, \bar{q}_V^p) = |V| - \left(V_y - \bar{q}_V^p\right) \le 0 \\ & \bar{\phi}^N (N, \bar{q}_N^p) = |N| - \left(N_y - \bar{q}_N^p\right) \le 0 \end{aligned} \tag{5.18}$$

where M is a bending moment; V is a shear force; N is an axial force; $\bar{q}_M^p, \bar{q}_V^p, \bar{q}_N^p$ are internal hardening stress like variables; whereas M_y, V_y and N_y denote yield bending moment, shear force and axial force. The internal variable q_M^p provides bilinear hardening related to bending moment, which can be written as:

$$q_M^p = \begin{cases} -K_{M,1}^h \bar{\xi}_M^p; \;\; 0 \le \bar{\xi}_M^p < \bar{\xi}_{M_y}^p \\ -K_{M,2}^h \bar{\xi}_M^p; \;\; \bar{\xi}_{M_y}^p \le \bar{\xi}_M^p < \infty \end{cases} \tag{5.19}$$

where $K_{M,1}^h$ and $K_{M,2}^h$ are hardening moduli. The yield function for softening is also chosen as a multi-criteria form:

$$\begin{aligned} & \bar{\bar{\phi}}^M (t_M, \bar{\bar{q}}_M^s) = |t_M| - \left(t_{M_y} - \bar{\bar{q}}_M^s\right) \le 0 \\ \dot{\bar{\bar{\gamma}}}_i \bar{\bar{\phi}}_i = 0 \Rightarrow \quad & \bar{\bar{\phi}}^V (t_V, \bar{\bar{q}}_V^s) = |t_V| - \left(t_{V_y} - \bar{\bar{q}}_V^s\right) \le 0 \\ & \bar{\bar{\phi}}^N (t_N, \bar{\bar{q}}_N^s) = |t_N| - \left(t_{N_y} - \bar{\bar{q}}_N^s\right) \le 0 \end{aligned} \tag{5.20}$$

where t_M, t_V, t_N are traction forces, $t_{M_y}, t_{V_y}, t_{N_y}$ are the corresponding ultimate values where softening starts and $\bar{\bar{q}}_M^s, \bar{\bar{q}}_V^s, \bar{\bar{q}}_N^s$ are stress-like variables work-conjugate to softening variables at the discontinuity.

5.4. Identification of the constitutive model parameters

In the case of connection testing, the global response of a specimen can be represented with load-displacement (*F-u)* diagram. Any such curve can be related to the three phases of the connection response: elastic, hardening and softening part (Figure 5.15). The used plasticity model, which represents connection behavior, contains the bilinear hardening and the linear softening response. For the most general case, we need to identify three parameters in the elastic phase, eight in the hardening phase and six unknown parameters in the softening phase.

The identification in general case is performed in two steps: i) definition of an objective function based on some experimental measurements; ii) minimization of this objective function in order to find values of constitutive parameters used in the model.

The choice of the objective function is a crucial step to ensure the success of the minimization. In general case, the objective function can be defined as the gap between measured and computed response values (displacement, stress, deformation, reaction force, etc.):

$$J(\mathbf{d}_\mathrm{p}) = \sum_{j \in J} n\left(\mathbf{u}_j^{com}(\mathbf{d}_\mathrm{p}) - \mathbf{u}_j^{\exp}\right)^2 \tag{5.21}$$

where $\mathbf{d}_\mathrm{p}$ are the model parameters that we seek to identify, $\frac{dv}{dx}$ and $\mathbf{u}_j^{\exp}$ are, respectively, computed and experimentally measured values of displacements/stresses/strains, and n is the weighting factor for different terms of objective function.

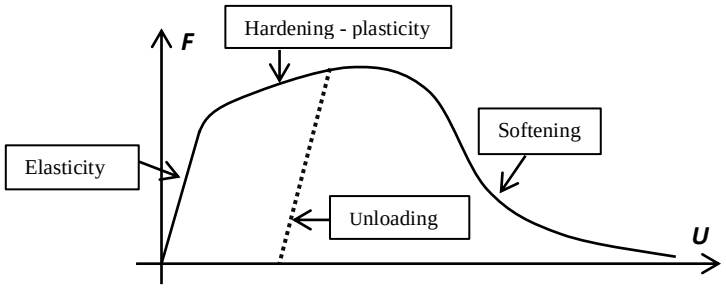

Figure 5.15 General relation: force F – displacement U

Minimization of the objective function can formally be written as minimization under constraint:

$$\min_{G(\sigma;\delta w)=0} J(\mathbf{d}_\mathrm{p}) = \sum_{j \in J} n\left(\mathbf{u}_j^{com}(\mathbf{d}_\mathrm{p}) - \mathbf{u}_j^{\exp}\right)^2 \tag{5.22}$$

where the weak form of equilibrium equations $G(\varepsilon, \zeta^p, \zeta^d; \delta w) = 0$ is the corresponding constraint. Namely, the weak form of equilibrium equations has to be satisfied at every time step. The constrained minimization of the objective function can be transferred into unconstrained minimization by using the Lagrange multiplier method (Ibrahimbegovic et al., 2004):

$$\max_{\forall \lambda} \min_{G(\sigma;\mathbf{d}_p)=0} L(\sigma, \mathbf{d}_\mathrm{p}, \lambda) = J(\mathbf{d}_p) + \mathrm{G}(\sigma, \mathbf{d}_\mathrm{p}, \lambda) \tag{5.23}$$

where λ are Lagrange multipliers inserted into the weak form of equilibrium equations instead of virtual displacements. This type of minimization of the objective function is very complex for seventeen unknown parameters. However, if we split an unconstrained minimization of the objective function into several phases, then we will decrease the number of unknown to maximal of two parameters in each phase (Kucerova et al., 2009).

The general identification procedure of the connection model parameters is presented in the flowchart in Figure 5.16. The process is split into three phases, with every phase further split into few cases. The first phase seeks to identify the three constitutive parameters related to elastic response: S_{jb}^{in} - initial rotational stiffness, S_{js}^{in} - initial shearing stiffness and S_{ja}^{in} - initial axial stiffness.

The second phase deals with eight unknown parameters related to hardening plasticity: V_y^{con} - yield shear force; S_{js}^{p} - hardening stiffness modulus with respect to shear force; N_y^{con} - yield axial force; S_{ja}^{p} - hardening stiffness modulus with respect to axial force; $M_{y,1}^{con}$ - first yield bending moment; $S_{jb,1}^{p}$ - first hardening stiffness modulus with respect to bending moment; $M_{y,2}^{con}$ - second yield bending

moment; $S_{jb,2}^{p}$ - the second hardening stiffness modulus with respect to bending moment.

The last phase deals with six softening constitutive parameters: N_u^{con} - ultimate axial force, S_{ja}^{s} - the softening modulus with respect to axial force, V_u^{con} - ultimate shear force, S_{js}^{s} - softening stiffness modulus with respect to shear force, M_u^{con} - an ultimate bending moment and S_{jb}^{s} - softening modulus with respect to bending moment.

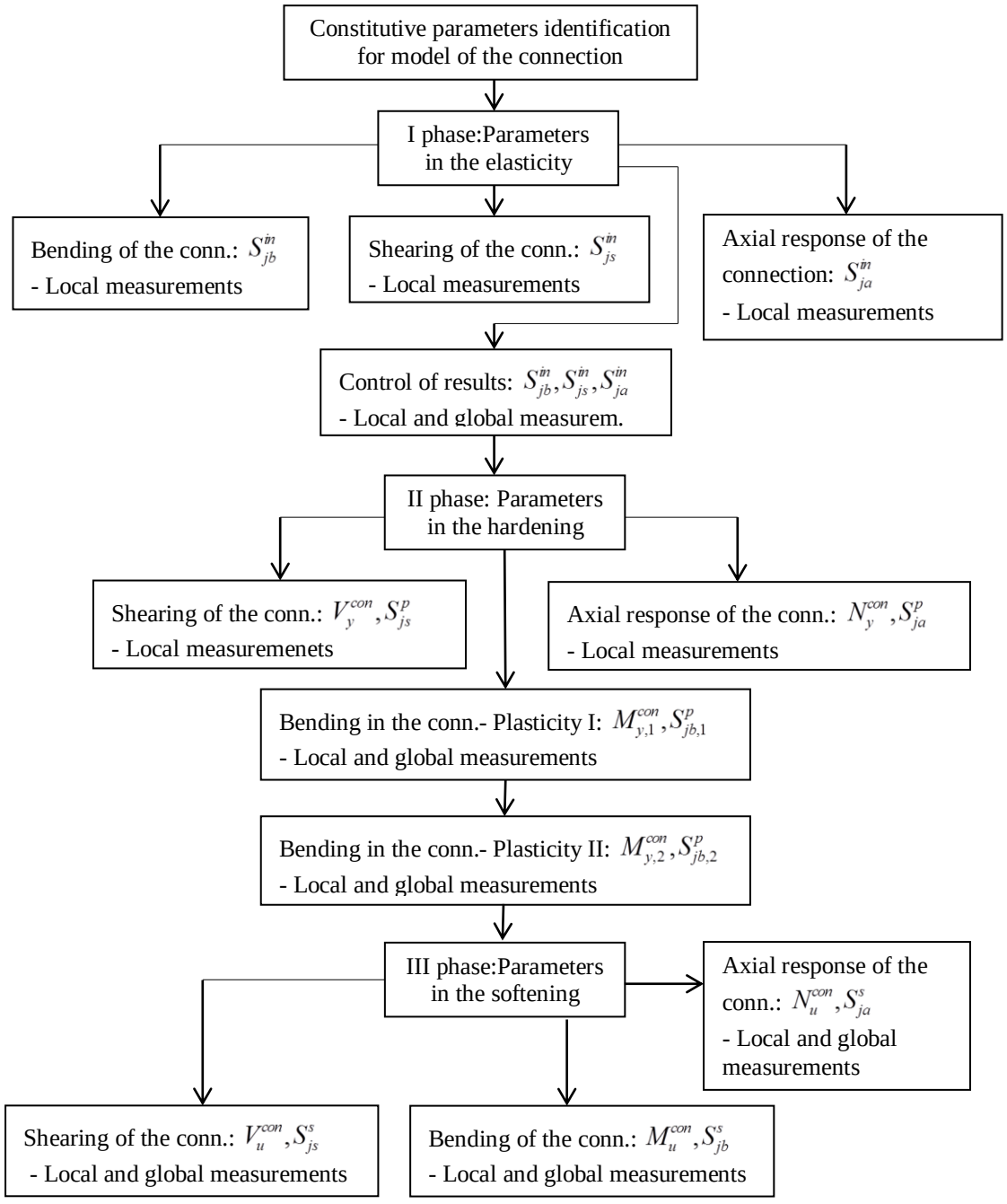

Figure 5.16 Flow chart of parameters identification

The stiffnesses can be obtained from the identified constitutive parameters of the proposed beam,

as follows:

$$S_{jb}^{in}=\frac{EI}{L};\ S_{jb,i}^{p}=\frac{K_{M,1}^{h}I}{L};\ S_{js}^{in}=\frac{GA_s}{L};\ S_{js}^{p}=\frac{K_s^h A_s}{L};\ S_{ja}^{in}=\frac{EA}{L};\ S_{ja}^{p}=\frac{K_a^h A}{L} \tag{5.24}$$

where E, G are Young's-like modulus and shear-like modulus, respectively; I, A_s, A are geometric characteristics of the cross section; $K_{M,1}^h, K_s^h, K_a^h$ are hardening-like moduli; while L is the length of the beam.

For every case in the second and the third identification phase, local and global measurements are required. The local measurements depend mainly on one material parameter, while the global measurements depend on practically all parameters of constitutive models.

The standard algorithms for unconstrained minimization included in Matlab are sufficient to solve the identification problems for each and every phase. The key step to facilitate this is a pertinent choice of the objective function for the parameters identification with the general format that can be written as (Imamovic et al., 2015):

$$\begin{aligned} J\left(\mathbf{d}_p\right)=&\sum_1^3 a\left(F_{Pi}^{com}-F_{Pi}^{\exp}\right)^2+\sum_1^3 b\left(U_{Pi}^{com}-U_{Pi}^{\exp}\right)^2+\sum_1^3 b\left(U_{S,Pi}^{com}-U_{S,Pi}^{\exp}\right)^2+\sum_1^3 c\left(\psi_{Pi}^{com}-\psi_{Pi}^{\exp}\right)^2+\\ &+\sum_1^2 d\left(\Delta\psi_{Pi}^{com}-\Delta\psi_{Pi}^{\exp}\right)^2+\sum_1^3 e\left(\kappa_{Pi}^{com}-\kappa_{Pi}^{\exp}\right)^2+\sum_1^3 g\left(\Delta\kappa_{Pi}^{com}-\Delta\kappa_{Pi}^{\exp}\right)^2 \end{aligned} \tag{5.25}$$

where: $F_{Pi}^{com}, F_{Pi}^{\exp}$ are forces for different load level (P_i); $U_{Pi}^{com}, U_{Pi}^{\exp}$ are the corresponding displacements (P_i); $U_{S,Pi}^{com}, U_{S,Pi}^{\exp}$ are shear displacements (P_i); $\psi_{Pi}^{com}, \psi_{Pi}^{\exp}$ are rotations of the connection (P_i); $\Delta\psi_{Pi}^{com}=\psi_{Pi+1}^{com}-\psi_{Pi}^{com}$ and $\Delta\psi_{Pi}^{\exp}=\psi_{Pi+1}^{\exp}-\psi_{Pi}^{\exp}$ are gradients of rotation between two different load (P_i); $\kappa_{Pi}^{com}, \kappa_{Pi}^{\exp}$ are curvatures of the section (P_i); $\Delta\kappa_{Pi}^{com}=\kappa_{Pi+1}^{com}-\kappa_{Pi}^{com}$ and $\Delta\kappa_{Pi}^{\exp}=\kappa_{Pi+1}^{\exp}-\kappa_{Pi}^{\exp}$ are gradients of curvature between two different load (P_i); while *a, b, c, d, e, g* are constants.

By respecting experimental testing described in the second section of the chapter, we are not able to identify parameters related to the axial force. However, we have exploited the design principle "strong columns - weak beams" in which the axial force behavior can be neglected. Some of the experimental measurements show that relative shear displacement between horizontal and vertical beams are too small. For these experimental tests, parameters related to shear force are not identified but assumed as rigid.

5.4.1. *Experimental tests: A1 and A2*

The experimental equipment in tests A1 and A2 (Figures 5.4 and 5.5) has not measured relative shear displacement $U_{3,Pi}^{\exp}$. This fact reduces identification problem to seven unknowns, where all parameters are related to rotational response. In the first elastic phase, we have only one unknown constitutive parameter. In the second phase, four constitutive parameters are unknown, and only two parameters are unknown in the last third phase. The identification procedure uses the same objective function (5.25) for every case. In Figures 5.17 and 5.18 are shown the shapes of the objective function for performed phases and cases of the identification.

Results of the identification procedure are presented in Figure 5.19 where we can see good match between the experimental and the computed results. Computed results were obtained by using FEM

model and identified constitutive parameters. Comparing the experimental response of the connection against the response predicted by EC3, we can see a fairly good match for elastic response but a significant difference in load-bearing capacities of the connections. Namely, we have measured values of load-bearing capacities that are almost 44% higher than the corresponding values provided by EC3.

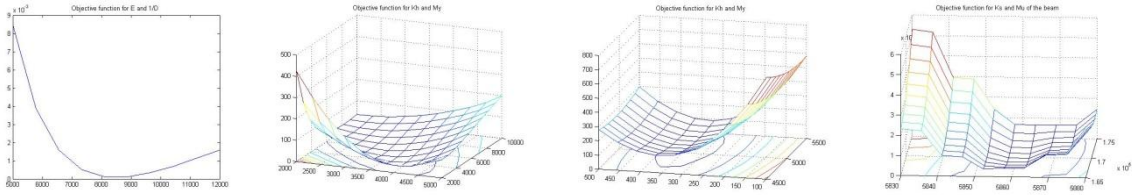

a) Elasticity: S_{jb}^{in} *b) Plasticity- first hardening:* $M_{y,1}^{con}, S_{jb,1}^{p}$ c) *Plasticity - second hardening:* $M_{y,2}^{con}, S_{jb,2}^{p}$ *d) Softening:* M_{u}^{con}, S_{jb}^{s}

Figure 5.17 Objective function shapes for eight unknowns related to bending – Experimental structure A1

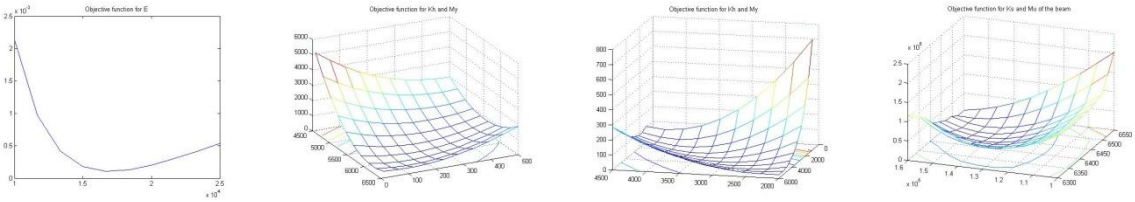

a) Elasticity: S_{jb}^{in} b) *Plasticity- first hardening:* $M_{y,1}^{con}, S_{jb,1}^{p}$ c) *Plasticity - second hardening:* $M_{y,2}^{con}, S_{jb,2}^{p}$ *d) Softening:* M_{u}^{con}, S_{jb}^{s}

Figure 5.18 Objective function shapes for eight unknowns related to bending – Experimental structure A2

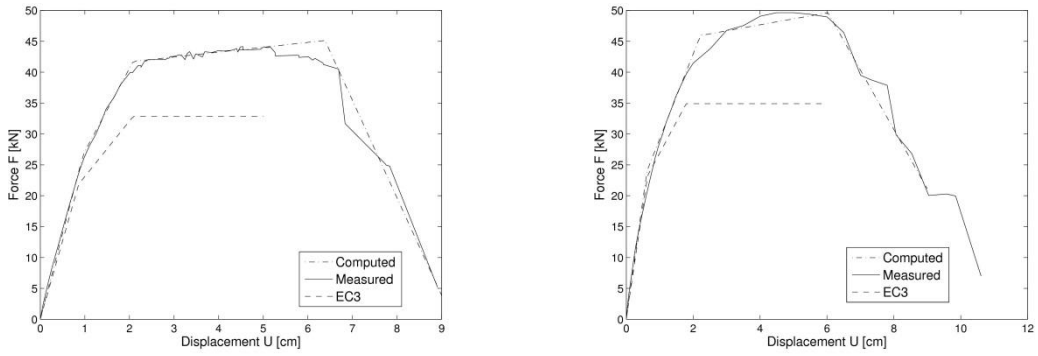

a) *Experimental structure A1* b) *Experimental structure A2*

Figure 5.19 Computed vs. experimental responses of the connections: A1 and A2

Table 5.2 Values of the constitutive parameters for connection A1

	S_{jb}^{in} [kNm/rad]	S_{js}^{in} [kN/rad]	$M_{y,1}^{con}$ [kNm]	$S_{jb,1}^{p}$ [kNm/rad]	$M_{y,2}^{con}$ [kNm]	$S_{jb,2}^{p}$ [kNm/rad]	M_{u}^{con} [kNm]	S_{jb}^{s} [kNm/rad]	θ_c [rad]
Experiment	8235,3	∞	32,0031	3362,99	50,12	137,1	54,0937	-1699,99	0,0679
Eurocode 3	7506	-	26,25	2501,35	39,375	0	39,375	-	0,0165

In Table 5.2 and Table 5.3, the values of identified constitutive parameters are shown and compared with the corresponding parameter values obtained by using the EC3 procedure.

Table 5.3 Values of the constitutive parameters for connection A2

	S_{jb}^{in} [kNcm/rad]	S_{js}^{in} [kN/rad]	$M_{y,1}^{con}$ [kNcm]	$S_{jb,1}^{p}$ [kNcm/rad]	$M_{y,2}^{con}$ [kNcm]	$S_{jb,2}^{p}$ [kNcm/rad]	M_{u}^{con} [kNcm]	S_{jb}^{s} [kNcm/rad]	θ_c [rad]
Experiment	8191,65	∞	31,15	3699,8	55,15	173,47	59,45	-1250,0	0,0755
Eurocode 3	7506	-	27,91	2501,35	41,87	0	41,87	-	0,01785

5.4.2. *Experimental tests: B1 and B2*

The experimental responses (Figures 5.8 and 5.9) of end plate connections (B1 and B2) show that shear displacement exists. Therefore, in this connection type, we have twelve unknowns, seven related to bending moment and five related to shear force. The number of unknowns can be reduced to ten if we recall the assumption that failure of connection can happen due to the bending moment, or due to the shear force. Experimental measurements show that failures in both tests (B1 and B2) have happened due to the bending moment. In Figures 5.20 and 5.21 shapes of the objective function (5.25) for the connections B1 and B2 are shown. In test B1 brittle failure happened where both bolts in tension zone broke at the same moment of time. Here, we are not able to identify the constitutive parameters related to the softening response since sudden drop occurs.

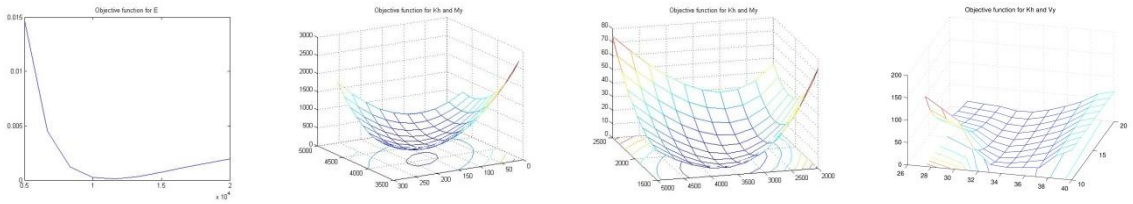

a) *Elasticity (bending):* S_{jb}^{in} b) *Plasticity(bending) - first hardening:* $M_{y,1}^{con}, S_{jb,1}^{p}$ c) *Plasticity(bending) - second hardening:* $M_{y,2}^{con}, S_{jb,2}^{p}$ d) *Plasticity:* V_{y}^{con}, S_{js}^{p} *(shear force)*

Figure 5.20 Objective function shapes for ten unknowns – Experimental structure B1

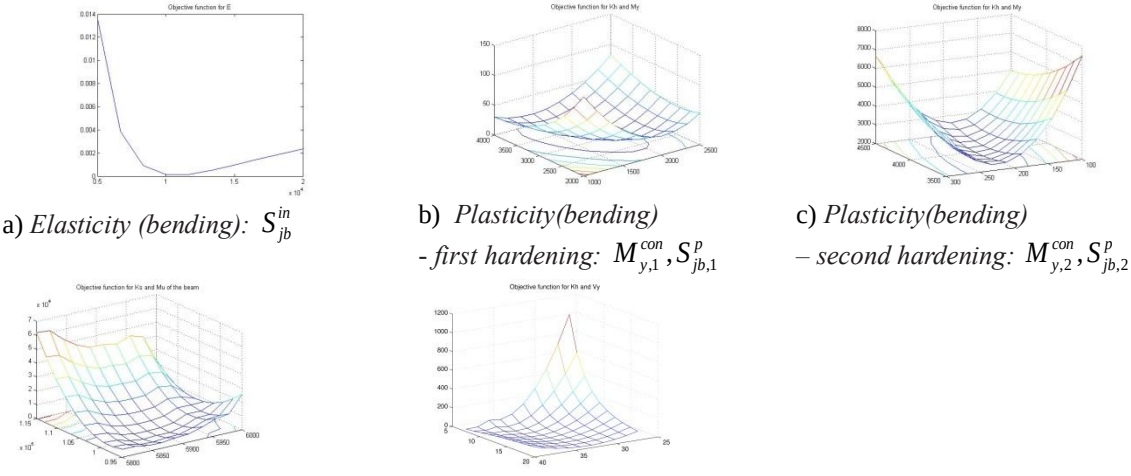

a) *Elasticity (bending):* S_{jb}^{in} b) *Plasticity(bending) - first hardening:* $M_{y,1}^{con}, S_{jb,1}^{p}$ c) *Plasticity(bending) – second hardening:* $M_{y,2}^{con}, S_{jb,2}^{p}$ d) *Softening(bending):* M_{u}^{con}, S_{jb}^{s} e) *Plasticity(shear force):* V_{y}^{con}, S_{js}^{p}

Figure 5.21 Objective function shapes for ten unknowns – Experimental structure B2

Results of the identification are presented in Figure 5.22, where we can see good matching between the experimental and the computed results. Computed results were obtained by using FEM model and identified constitutive parameters. Comparing the experimental responses of connections B1 and B2 against the EC3 responses, we can see a significant difference. Namely, we have measured

almost 90% bigger load-bearing capacities of the connections than the corresponding capacities according to EC3.

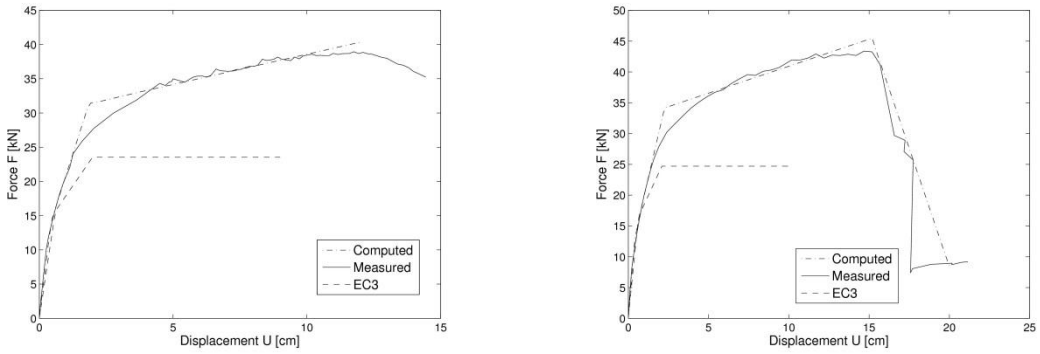

a) *Experimental structure B1* b) *Experimental structure B2*

Figure 5.22 Computed vs. experimental responses of the connections: B1 and B2

The values of identified constitutive parameters are shown in Table 5.4 and Table 5.5. These values are compared with the corresponding parameters obtained using the EC3 procedure. The EC3 procedure gives a very good prediction for the elastic response and bending of the connection.

According to EC3, the elastic response of this joint type can be assumed for the load values lower than the 66% of the load-bearing capacity. Experimental testing confirms this hypothesis.

Table 5.4 Values of the constitutive parameters for connection B1

	S_{jb}^{in} [kNm/rad]	S_{js}^{in} [kN/rad]	$M_{y,1}^{con}$ [kNm]	$S_{jb,1}^{p}$ [kNm/rad]	$M_{y,2}^{con}$ [kNm]	$S_{jb,2}^{p}$ [kNm/rad]	V_{y}^{con} [kN]	S_{js}^{p} [kN/m]	M_{u}^{con} [kNm]	θ_c [rad]
Experimental	5398,05	∞	16,88	3317,11	37,62	161,0	33,03	16102	54,0937	0,1161
Eurocode 3	3784	-	18,83	1260,24	28,25	0	-	-	28,25	0,02384

Table 5.5 Values of the constitutive parameters for connection B2

	S_{jb}^{in} [kNm/rad]	S_{js}^{in} [kN/rad]	$M_{y,1}^{con}$ [kNm]	$S_{jb,1}^{p}$ [kNm/rad]	$M_{y,2}^{con}$ [kNm]	$S_{jb,2}^{p}$ [kNm/rad]	V_{y}^{con} [kN]	S_{js}^{p} [kN/m]	M_{u}^{con} [kNm]	S_{jb}^{s} [kNm/rad]	θ_c [rad]
Experimental	5165,25	∞	16,47	2939,10	38,11	217,21	35,17	21721	54,40	-1043,67	0,1651
Eurocode 3	3784	-	19,75	1260,24	29,625	0	-	-	29,625	-	0,0251

5.4.3. *Experimental tests: C1 and C2*

5he experimental responses of moment-resistant connections with angles (C1 and C2) are shown in Figures 5.12 and 5.13. The relative shear displacement between horizontal and vertical beams is not measured. We can only identify seven unknown constitutive parameters related to bending moment. Shapes of the objective function for all analyzed cases of the identification are shown in Figures 5.23 and 5.24.

The comparisons of computed results and experimental results are shown in Figure 5.25, where we can see good matching of these results. The computed results have been obtained using proposed FEM model and identified constitutive parameters. We have obtained connection responses by using commercial computer's program *PowerConnect*. Contrary to the first comparison, the EC3 procedure underestimates stiffness and bearing capacity of this connection type. Practically, we have measured 155% bigger bearing capacity of the connections than EC3 predicts.

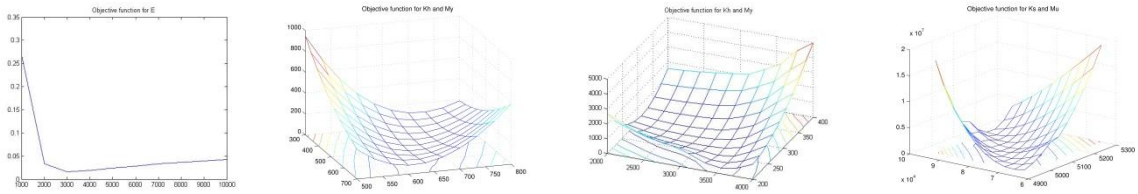

a) *Elasticity:* S_{jb}^{in} b) *Plasticity- first hardening:* S_{js}^{in} c) *Plasticity - second hardening:* $M_{y,2}^{con}, S_{jb,2}^{p}$ d) *Softening:* M_u^{con}, S_{jb}^{s}

Figure 5.23 Objective function shapes for eight unknowns related to bending – Experimental structure C1

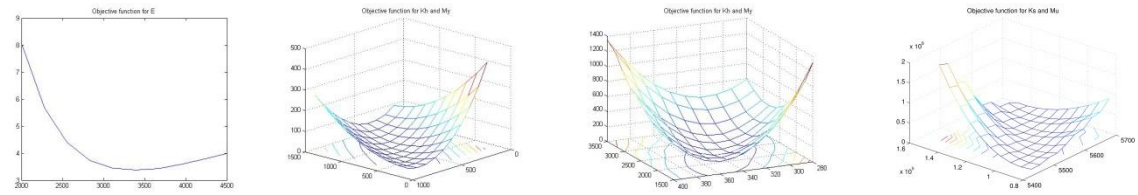

a) Elasticity: S_{jb}^{in} *b) Plasticity- first hardening:* S_{js}^{in} *c) Plasticity - second hardening:* $M_{y,2}^{con}, S_{jb,2}^{p}$ *d) Softening:* M_u^{con}, S_{jb}^{s}

Figure 5.24 Objective function shapes for eight unknowns – Experimental structure C1

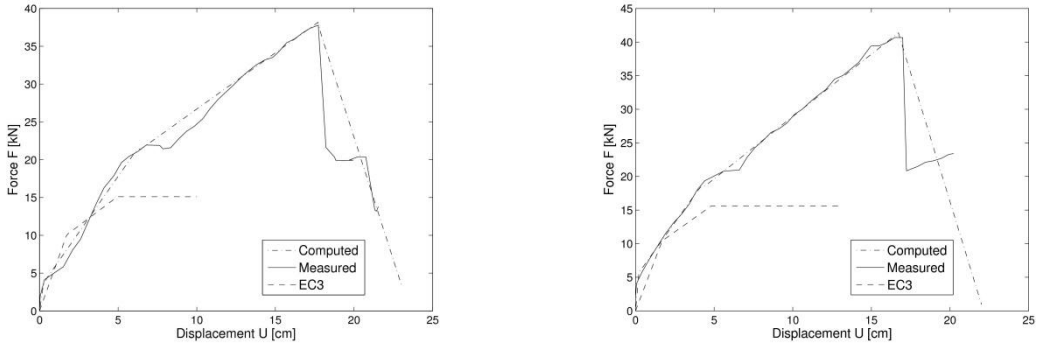

c) *Experimental structure C1* d) *Experimental structure C2*

Figure 5.25 Computed vs. experimental responses of the connections: C1 and C2

The identified constitutive parameter values are shown in Tables 5.6 and 5.7. By comparing these parameters with corresponding parameters obtained by EC3 procedure, we can notice significant differences.

Table 5.6 Values of the constitutive parameters for connection C1

	S_{jb}^{in} [kNm/rad]	S_{js}^{in} [kN/rad]	$M_{y,1}^{con}$ [kNm]	$S_{jb,1}^{p}$ [kNm/rad]	$M_{y,2}^{con}$ [kNm]	$S_{jb,2}^{p}$ [kNm/rad]	M_u^{con} [kNm]	θ_c [rad]
Experimental	1527,45	∞	4,49	635,83	25,22	281,12	44,87	0,1893
Eurocode 3	1118	-	12,08	372,77	18,125	0	18,125	0,02384

Table 5.7 Values of the constitutive parameters for connection C2

	S_{jb}^{in} [kNm/rad]	S_{js}^{in} [kN/rad]	$M_{y,1}^{con}$ [kNm]	$S_{jb,1}^{p}$ [kNm/rad]	$M_{y,2}^{con}$ [kNm]	$S_{jb,2}^{p}$ [kNm/rad]	M_u^{con} [kNm]	S_{jb}^{s} [kNm/rad]	θ_c [rad]
Experimental	1638,86	∞	5,66	595,27	33,88	332,71	47,48	-452,95	0,1812
Eurocode 3	1192	-	12,5	397,36	18,75	0	18,75	-	0,0502

5.5. Numerical examples

Two numerical examples are presented in this section to illustrate the effects of connections behavior to the global steel frame structure response. The global response of the steel frame structure with included connection behavior is compared with the global response of the same steel frame structure without included connection behavior. The comparison quantifies the connection behavior influence on the global response of the structure. All numerical computations are performed with a research version of the computer program FEAP (Taylor, 2008).

5.5.1. The ultimate analysis of a simple steel frame structure

In this example, we analyze the influence of the connection behavior on the structure response. We consider a simple steel frame shown in Figure 5.26a, where the span is 5,0m and height is 3,0m. The mesh is composed of 48 beam elements where the length of each element is 0,25m. The material properties of all frame members are the same (Young's modulus: $E=2\cdot10^4 kN/cm^2$; hardening modulus: $K=0.05\cdot E$;). The geometric properties of the beam cross section corresponds to the I 200 (*Moment of Inertia: $I=1940cm^4$; Area of cross section: $A=28.5cm^2$; Yield bending moment: My=4655kNcm; Ultimate bending moment: Mu=5280kNcm; Yield shear force: $V_y=252kN$; Ultimate shear force: $V_u=378kN$, Fracture energies: $G_{f,M}=550$ and $G_{f,V}=450$*). The column properties are defined as profile I 300 (*Moment of Inertia: $I=11770cm^4$; Area of cross section: $A=53,8cm^2$; Yield bending moment: My=13368kNcm; Ultimate bending moment: Mu=15080kNcm; Yield shear force: $V_y=471kN$; Ultimate shear force: $V_u=707kN$, Fracture energies: $G_{f,M}=650$ and $G_{f,V}=550$*). Two numerical simulations have been performed. In the first simulation, elements which connect beams and columns are defined according to the behavior of the experimentally tested connection denoted with A1. The second analysis does not include connection behavior.

The results of these two simulations are compared in Figure 5.26b, where we can see a significant effect of connections on the global response of the structure under vertical load. This effect is particularly evident at the level of ultimate forces, close to bearing capacity of the structure.

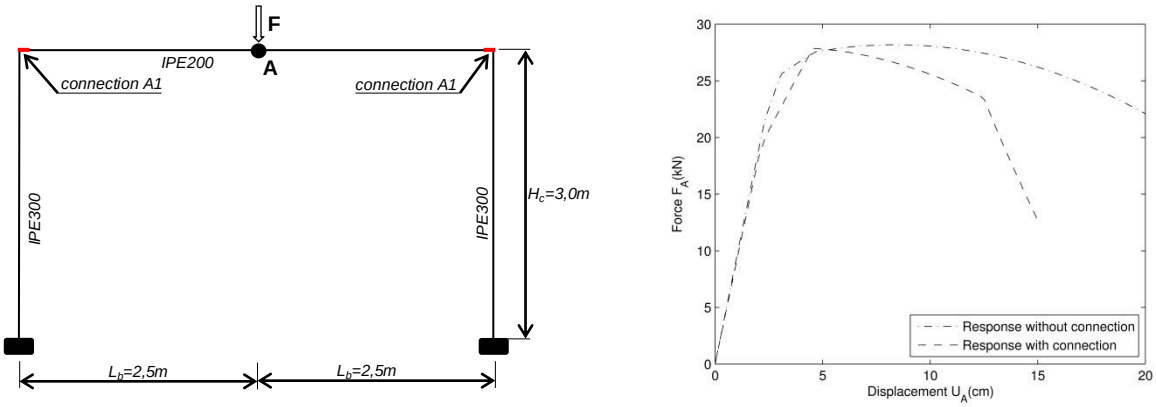

a) Frame structure geometry *b) Response of the frame structure*

Figure 5.26 The simple steel frame

5.5.2. *Pushover analysis of symmetric steel frame*

In this example, we present the results of a push-over analysis of symmetric steel frame with and without included joints behavior. The frame geometry is given in Figure 5.27a. Material properties for all frame members are the same (Young's modulus: $E=2\cdot10^4$kN/cm^2; hardening modulus: $K=0.05\cdot E$). The geometric properties of beams correspond to IPE 200 section; the columns are defined as IPE 300 section. In the first case, the constitutive parameters of elements which connect beams to columns are identified according to experimental test A1, whereas in the second case these elements are defined as IPE 200 section. The vertical load was applied to all beam members. This load is kept constant throughout the pushover analysis to simulate the dead load effect. The lateral loading is applied regarding imposed incremental displacement (u_{top}) at the left upper corner (point A, see Figure 5.27a).

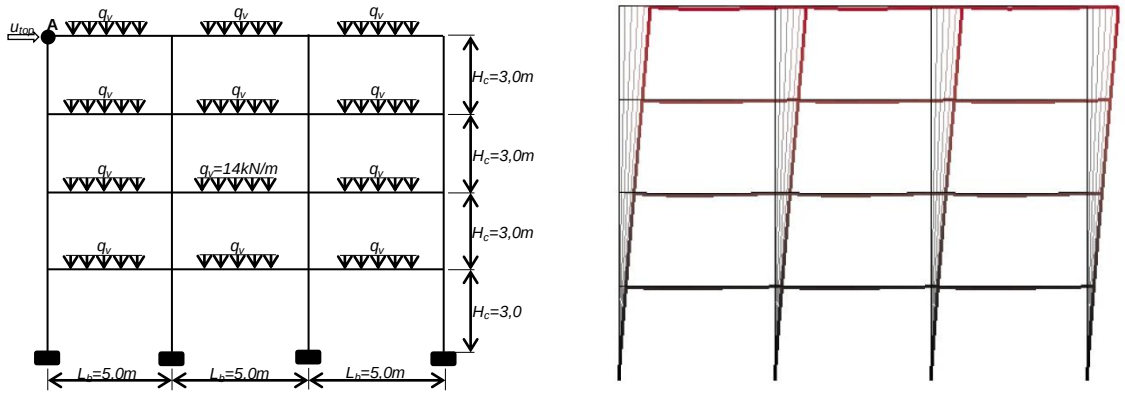

a) *The frame structure geometry* b) *Deformed frame structure (step-by-step)*

Figure 5.27 The symmetric steel frame

The results of numerical simulations are shown in Figure 5.28. These results show a significant influence of the connections behavior on the global response of steel frame structure. This effect is very evident at the level close to the ultimate load. The connections behavior reduces load bearing capacity and changes the global response of the steel structure. Namely, at the lateral displacement of 1m, lateral resistance is reduced by 30% with respect to the structure without connections. Respecting these results, we can mark the importance of connection behavior in the steel structure design related to seismic load.

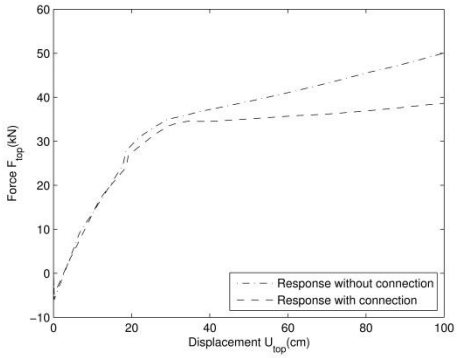

Figure 5.28 Response of the symmetric frame structure

5.6. Concluding remarks

In this chapter we have presented an experimental and numerical study of the moment-resistant connection behavior. A total of three connection types have been analyzed and six experimental tests have been performed. The connection behavior in structural response is included where we model every joint with beam element. The proposed beam element has seventeen unknown constitutive parameters. The identification methodology has been presented and unknown parameters, based on the results of the experimental tests, have been identified. We found that the proposed beam model with identified constitutive parameters can successfully represent connection behavior. The capability of the proposed beam model to represent connection behavior is shown with very good match between experimental and computed results. The set of the constitutive parameters of the proposed beam model can be obtained by using the EC3 procedure, which provides a good prediction of elastic response and bending, while the plastic response prediction is overly conservative, sometimes up to 40%.

The influence of the connection behavior on the steel frame response is shown in two numerical simulations. The numerical results demonstrate the importance of the joints behavior on the steel frame structure response, where we can see a difference in results up to 30%.

Chapter 6

Experimental testing of structural steel connections under cyclic loading

Abstract

The moment-resistant steel frames are frequently used as load-bearing structures of buildings in seismic regions. The earthquake induced inertial forces show cyclic loading pattern. Cyclic loading can significantly change the behavior of the connection in comparison with the monotonic loading. This chapter deals with the experimental testing of two types of structural connections under cyclic loading, and with the constitutive parameters identification. The experimental tests are performed for two different types of structural connections: end plate connection with an extended plate, and end plate connection. Measured data show the change in the behavior of connections in comparison with tests presented in the previous chapter. With the change in the direction of the applied load, the less stiff response of the structural connection has been measured. This phenomenon has a clear physical explanation, which is associated with the loss of the contact between elements of the connection. At the beam element level, this phenomenon can be represented by damage model. In this chapter, we present the theoretical formulation and the numerical implementation of the proposed beam model. The proposed beam model is Reissner beam with the ability to capture both hardening and softening part of the response, and with the constitutive model defined as the coupled plasticity-damage model. The proposed beam model has one constitutive parameter more than the beam model presented in the previous chapter. The identification of this parameter is presented in this chapter. The comparison of the measured and the computed response is given for several numerical simulations, where good matching between results is observed.

Contents of Chapter 6

6.1. Introduction

The moment-resistant steel frames are frequently used as load-bearing structures of buildings in seismic regions. The earthquake induced inertial forces show cyclic loading pattern. Cyclic loading can significantly change the response of the structure in comparison with the monotonic loading. On the one hand, the response of the steel structure under cyclic loading is characterized by Baushinger effect. In a typical cycle with load reversal (from compression to tension or vice versa), the plasticity threshold value is reduced from the previous value. On the other hand, the behavior of the joint is very complex. The behavior of the joint depends on the type of the structural connection and, as experiments have confirmed, the type of the applied load. The behavior of the connection is not the same under the monotonic and the cyclic loading.

The analysis of a structural connection can be performed with many nonlinear FEM commercial programs, using 3D solid finite elements (Imamovic & Mesic, 2014). This type of analysis can represent the response of a structural connection, with included buckling and contact issues. The quality of the predicted connection behavior, obtained by using refined FEM model, is confirmed with experimental tests in many scientific works (Faella et al., 2000; Gang Shi, 2007). The refined nonlinear model can predict the behavior of a joint, but those computations are often too costly and not practical for everyday usage. Modern code (EC3, 2005) proposes the representation of a connection behavior with nonlinear links, but the connection response under cyclic loading is not covered.

This chapter deals with the experimental testing of two types of structural connections under cyclic loading, including the constitutive parameters identification. The experimental tests are performed for two different types of structural connections: end plate connection with an extended plate, and end plate connection. These tests were designed in a way that sufficient information for the identification of constitutive parameters can be obtained from experimental measurements (Imamovic et al., 2015). Experimental observations show the change in the behavior of connections in comparison with tests presented in the previous chapter. With the change in the direction of the applied load, the less stiff response of structural connections has been measured. This phenomenon has a clear physical explanation, which is associated with the loss of the contact between elements of the connection.

6.2. The experimental testing of structural connections

Experimental tests on two types of moment-resistant connection have been conducted with the aim to identify constitutive parameters of the proposed beam model. The tested moment-resistant connection types are: end plate connection with the extended plate, and end plate connection. In these experimental structures, connection represents the weakest element in which plastic deformations and failure are expected to occur. The experimental structures are the same in all as A1 and B1, which are presented in the previous chapter. The loading program has been changed with reversal loading cycles.

The measuring equipment is arranged in the same way as presented in the previous chapter, but with one difference which concerns the measurement of the applied force. The applied force is measured from the values of the pressure in the hydraulic pump. The used hydraulic pump is strong and involves errors in measured force values. These errors are visible in Figures 6.3 and 6.6, where hysteresis curves that are not entirely smooth are shown. However, this does not affect significantly

the results of the identification procedure.

All experimental data have been measured and recorded during the experimental testing. In Figure 6.1, the loading program which contains several cycles of reversal loading is shown. The step size is adjusted to the connection behavior. The geometric characteristics of the experimental structures are shown in Table 6.1. In total, two experimental tests have been performed. The experimental tests were carried out at the Laboratory for materials and structures of the University of Sarajevo.

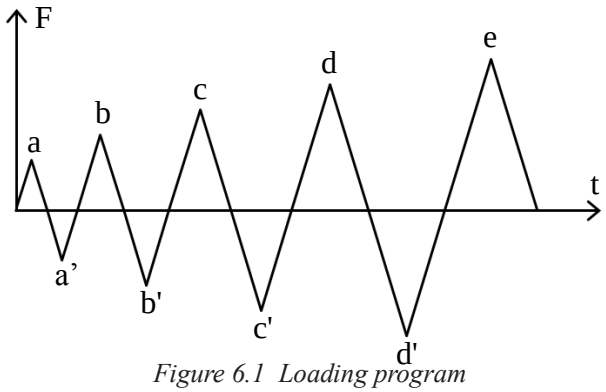

Figure 6.1 Loading program

Table 6.1 Geometrical characteristics of experimental structures

Joint	Vertical beam	Horizontal beam	End plate dimension/Angles	Bolts
A_{cyclic}	IPE 200 – S275	IPE 400 – S275	≠ 340x130x10 – S275	8M12-class 8.8.
B_{cyclic}	IPE 200 – S275	IPE 400 – S275	≠ 220x130x10 – S275	4M16-class 8.8.

6.2.1. End plate connection with extended end plate (A_{cyclic})

The end plate connection type with the extended plate is constructed from the plate (340x130x10mm) welded to the vertical beam and eight bolts (M12) connecting the plate to the horizontal beam, see Figure 6.2. The bolts (class 8.8.) were preloaded with 50% of prestressing force according to EC3.

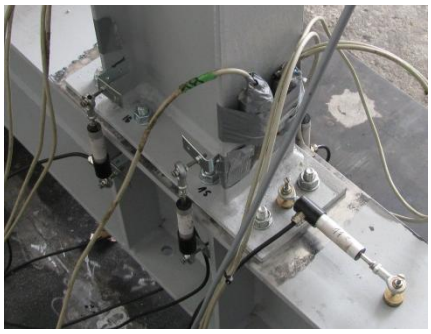

Figure 6.2 End plate connection with extended end plate

The results of the testing are shown in Figure 6.3. The global response, which depends on the behavior of all elements in the connection and all constitutive parameters, is captured through global measurements. The rotation of structural connection is captured through local measurements, see Section 5.2.1. The diagram rotation – force at the top of the experimental structure is shown in Figure 6.3b. Strains in the vertical steel beam are measured with strain gauges, and are shown in the Figure 6.3c. The measurements obtained with strain gauges can be

also classified as local measurements. These measurements show that the response of the vertical beam remains linear elastic. The relative horizontal displacement between vertical and horizontal beam has not been observed during the testing ($U_{2,Pi}^{\exp} = U_{S,Pi}^{\exp}$).

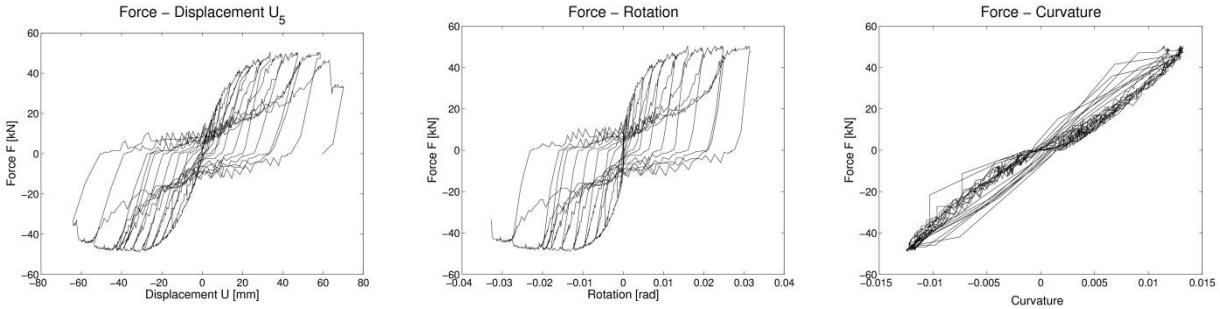

a) Global response *b) Rotational response of the connection* *c) Strains in the vertical steel beam*

Figure 6.3 Experimental results for connection A_{cyclic}

By comparing Figures 6.3a and 6.3b, we can observe that the main source of the nonlinear behavior of the experimental structure are elements of the connection. The deformation of elements of connection during the experimental testing is shown in photographs in Figure 6.4. The failure has progressively occurred in the bolts, where the inner row of bolts broke before the outer row of bolts.

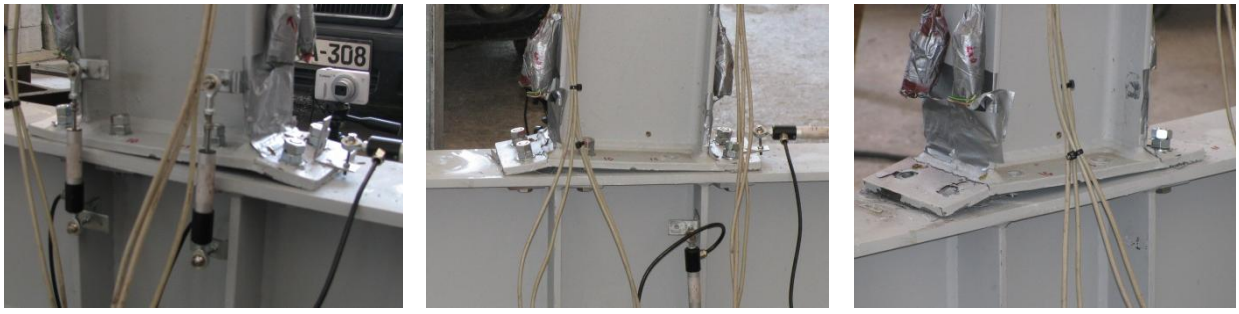

Figure 6.4. Deformation of connection elements during experimental testing

6.2.2. End plate connection (B_{cyclic})

The end plate connection is constructed from the plate (220x130x10mm) welded to the vertical beam and four bolts (M16), connecting the plate to the horizontal beam, see Figure 6.5. The bolts (class 8.8.) have been preloaded with 50% of prestressing force according to EC3.

Figure 6.5 End plate connection

The results of the testing are shown in Figure 6.6. The global response of the experimental structure

and the rotational response of the connection are shown in Figure 6.6a and Figure 6.6b, respectively. Figure 6.6c shows measured strains in the vertical steel beam. The measured strains in vertical steel beam show that the response of the vertical beam remains linear elastic. All presented diagrams are with respect to the force measured at the top of the experimental structure. The relative horizontal displacement between vertical and horizontal beams has not been observed during the testing ($U_{2,Pi}^{\exp} = U_{S,Pi}^{\exp}$).

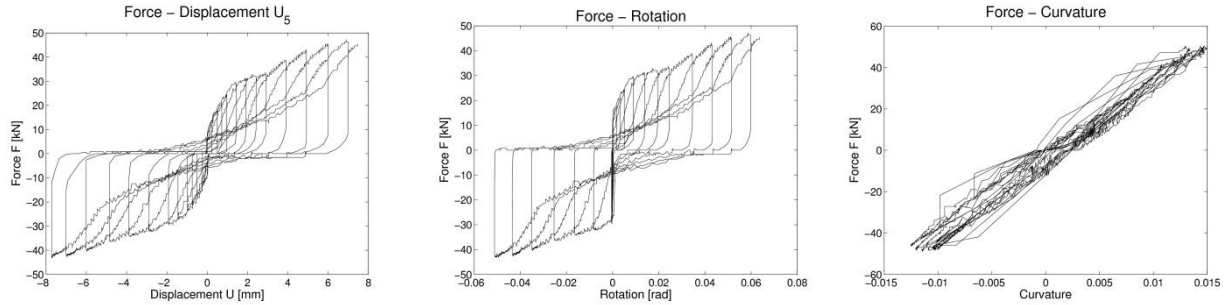

a) Global response *b) Rotational response of the connection* *c) Strains in the vertical steel beam*

Figure 6.6 Experimental results for connection B_{cyclic}

The deformation of elements of connection during the testing are shown in photographs in Figure 6.4. We can conclude that large deformations have occurred in the elements. The failure has not occurred because the displacement limit of the hydraulic pump has been reached.

Figure 6.7 Deformation of connection elements during experimental testing

6.3. Finite element beam model: theoretical formulation and numerical implementation

The complex measured responses of experimental structures under cyclic loading are quite a challenge to describe. The large deformations of the connection elements under cyclic loading cause the loss in the stiffness of the experimental structure. This phenomenon has a physical explanation. During the loading of the experimental structure, large deformations of the welded plate in the tension zone cause partial loss of the contact between the plate and horizontal beam, see Figure 6.8a. With the change in the direction of the applied load, the compression and tension zones will be inverted. The partially lost contact in compression zone causes the reduced stiffness of the connection, see Figure 6.8b. The stiffness will remain reduced until the full contact between the plate and horizontal beam is reached again. After the full contact has been reached, the connection will provide again the full stiffness.

a) 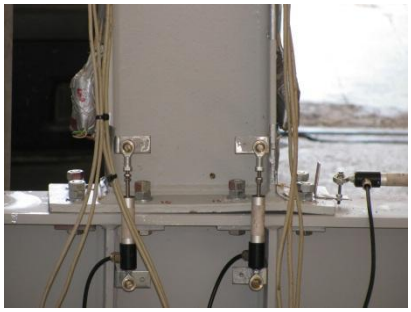 b) 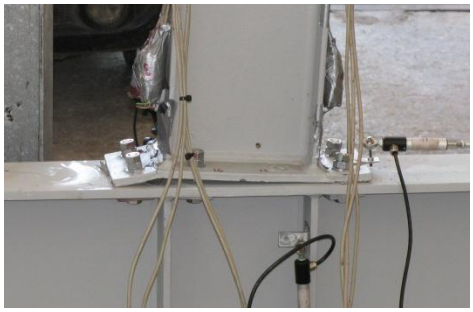

Figure 6.8 Deformation of the connection during a cyclic loading

This phenomenon can be captured with contact and solid elements in refined FEM models. Solid elements are able to represent large deformations and the nonlinear constitutive behavior. However, the refined FEM models are too complex for everyday usage. For this reason, we propose the use of the beam element capable of representing the mentioned phenomenon.

The idea is to use the coupled plasticity-damage model (Imamovic et al., 2015). The plasticity part governs the hardening and unloading phases, whereas the damage part provides the reduced stiffness of the connection after the change in the sign of the bending moment: from positive to negative or vice versa, see Figure 6.9. The damage model governs connection response until full contact between the plate and horizontal beam is reached. After the full contact has been reached, the plasticity model is again activated. The gap δ corresponds to the plastic deformation in bolts.

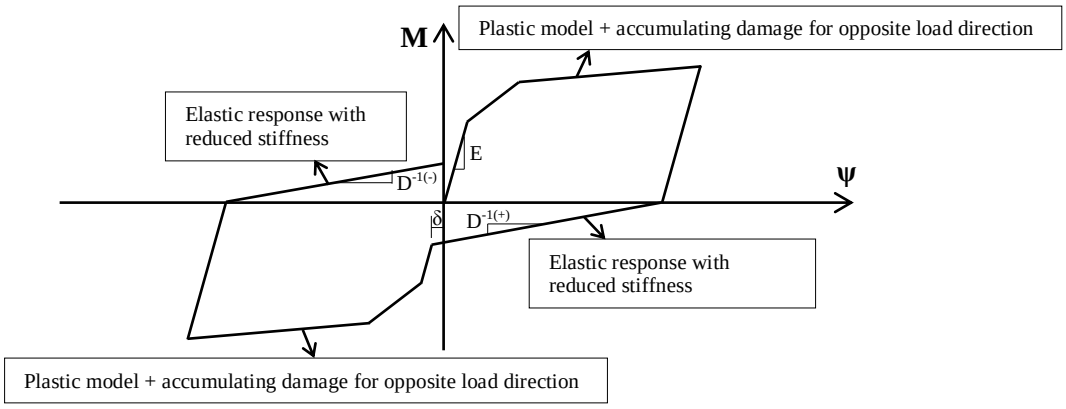

Figure 6.9 Constitutive model

In this section, we use the geometrically exact beam. The constitutive model of the beam consists of bilinear hardening and linear softening (Imamovic et al., 2017). The hardening model is defined as coupled plasticity-damage model. This model is capable of representing previously described phenomena which is commonly observed during experimental testing. A brief description of the beam's constitutive model is given next. The Helmholtz free energy can be defined in a quadratic form, and is split into two part. The first part concerns a positive bending moment $\bar{\Psi}^{(+)}$, and the second part concerns a negative bending moment $\bar{\Psi}^{(-)}$:

$$\bar{\Psi}^{(+)}(\bar{\mathbf{U}}^{e,(+)},\bar{\boldsymbol{\xi}}^{p,(+)},\bar{\mathbf{U}}^{d,(+)},\bar{\boldsymbol{\xi}}^{d,(+)}) = \underbrace{\frac{1}{2}\bar{\mathbf{U}}^{e,T,(+)}\cdot\mathbf{C}^{(+)}\cdot\bar{\mathbf{U}}^{e,(+)}}_{\bar{\Psi}^{e,(+)}} + \underbrace{\frac{1}{2}\bar{\boldsymbol{\xi}}_1^{p,T,(+)}\cdot\mathbf{K}_1^{h,(+)}\cdot\bar{\boldsymbol{\xi}}_1^{p,(+)}}_{\bar{\Xi}_1^{p,(+)}} +$$
$$+\underbrace{\frac{1}{2}\bar{\boldsymbol{\xi}}_2^{p,T,(+)}\cdot\mathbf{K}_2^{h,(+)}\cdot\bar{\boldsymbol{\xi}}_2^{p,(+)}}_{\bar{\Xi}_2^{p,(+)}} + \underbrace{\mathbf{T}\bar{\mathbf{U}}^{d,(+)} - \frac{1}{2}\mathbf{T}D^{(+)}\mathbf{T}}_{\bar{\Psi}^{d,(+)}} + \underbrace{\frac{1}{2}\bar{\xi}^{d,(+)}\bar{K}^{d,(+)}\bar{\xi}^{d,(+)}}_{\bar{\Xi}^{d,(+)}}$$
$$\bar{\Psi}^{(-)}(\bar{\mathbf{U}}^{e,(-)},\bar{\boldsymbol{\xi}}^{p,(-)},\bar{\mathbf{U}}^{d,(-)},\bar{\boldsymbol{\xi}}^{d,(-)}) = \underbrace{\frac{1}{2}\bar{\mathbf{U}}^{e,T,(-)}\cdot\mathbf{C}^{(-)}\cdot\bar{\mathbf{U}}^{e,(-)}}_{\bar{\Psi}^{e,(-)}} + \underbrace{\frac{1}{2}\bar{\boldsymbol{\xi}}_1^{p,T,(-)}\cdot\mathbf{K}_1^{h,(-)}\cdot\bar{\boldsymbol{\xi}}_1^{p,(-)}}_{\bar{\Xi}_1^{p,(-)}} + \tag{6.1}$$
$$+\underbrace{\frac{1}{2}\bar{\boldsymbol{\xi}}_2^{p,T,(-)}\cdot\mathbf{K}_2^{h,(-)}\cdot\bar{\boldsymbol{\xi}}_2^{p,(-)}}_{\bar{\Xi}_2^{p,(-)}} + \underbrace{\mathbf{T}\bar{\mathbf{U}}^{d,(-)} - \frac{1}{2}\mathbf{T}D^{(-)}\mathbf{T}}_{\bar{\Psi}^{d,(-)}} + \underbrace{\frac{1}{2}\bar{\xi}^{d,(-)}\bar{K}^{d,(-)}\bar{\xi}^{d,(-)}}_{\bar{\Xi}^{d,(-)}}$$

where: $\bar{\mathbf{U}}^e, \bar{\mathbf{U}}^d$ are elastic and damage strain measure tensors; $\bar{\boldsymbol{\xi}}_i^p, \bar{\boldsymbol{\xi}}_i^d$ are vectors of hardening variables of the plastic and damage model, respectively; D is the internal damage variable; $\mathbf{K}_i^h, \mathbf{K}^d$ are the corresponding hardening moduli of the plastic and damage model; and $\mathbf{T}$ is Biot's stress tensor. Every symbol contains two symbols. The first corresponds to the positive $(\bullet^{(+)})$, and the second to the negative $(\bullet^{(-)})$ bending moment. The yield criterion, defined as multi - criteria (plasticity and damage), can be completely different for the positive and the negative bending moment. However, in this work we have assumed that the response in the hardening regime is symmetric:

$$\begin{aligned}\bar{\phi}_i^{\,p}(T_i,\bar{q}_i^{\,p}) &\le 0\\ \bar{\phi}_i^{\,d}(T_i,\bar{q}_i^{\,d}) &\le 0\end{aligned} \tag{6.2}$$

where $\bar{\mathbf{q}}$ is the vector of internal hardening stress like variables. The second principle of thermodynamics states that the plastic dissipation must remain non-negative:

$$0 \le \bar{\mathcal{D}} = \underbrace{\dot{\bar{\mathbf{T}}}\left(\frac{\partial\bar{\chi}^e}{\partial\mathbf{T}} - \bar{\mathbf{U}}^e\right) + \dot{\bar{\mathbf{T}}}\left(\frac{\partial\bar{\chi}^d}{\partial\mathbf{T}} - \bar{\mathbf{U}}^d\right)}_{\bar{\mathcal{D}}^e=0} + \underbrace{\mathbf{T}\dot{\bar{\mathbf{U}}}_1^p - \frac{\partial\bar{\boldsymbol{\Xi}}_1^p}{\partial\bar{\boldsymbol{\xi}}_1^p}\frac{d\bar{\boldsymbol{\xi}}_1^p}{dt}}_{\bar{\mathcal{D}}_1^p} +$$
$$+\underbrace{\mathbf{T}\dot{\bar{\mathbf{U}}}_2^p - \frac{\partial\bar{\boldsymbol{\Xi}}_2^p}{\partial\bar{\boldsymbol{\xi}}_2^p}\frac{d\bar{\boldsymbol{\xi}}_2^p}{dt}}_{\bar{\mathcal{D}}_2^p} + \underbrace{\frac{\partial\bar{\mathbf{U}}^d}{\partial\bar{D}}\dot{\bar{D}} - \frac{\partial\bar{\Xi}^d}{\partial\bar{\xi}^d}\dot{\bar{\xi}}^d}_{\bar{\mathcal{D}}^d} \tag{6.3}$$

where $\bar{\chi}$ is complementary energy, see (Ibrahimbegovic, 2009). The principle of maximum plastic dissipation can be formulated (Hill, 1950; Ibrahimbegovic & Frey, 1993a) as the minimization problem with the constraint, with the latter being yield function (6.2). This can further be recast as a corresponding unconstrained minimization by using the Lagrange multiplier method:

$$\min_{\mathbf{T},\bar{\mathbf{q}}}\max_{\dot{\bar{\gamma}}}\left[\bar{L}^p(\mathbf{T},\bar{\mathbf{q}}^p,\dot{\bar{\boldsymbol{\gamma}}}^p) = -\bar{\mathcal{D}}^p(\mathbf{T},\bar{\mathbf{q}}^p) + \dot{\bar{\boldsymbol{\gamma}}}_i^p\cdot\bar{\phi}_i^p(\mathbf{T},\bar{\mathbf{q}}^p)\right] \tag{6.4}$$

where $\dot{\bar{\gamma}}_i^p$ are Lagrange multipliers of the plasticity. The Kuhn-Tucker optimality conditions provide the evolution equations for internal variables in rate form along with the loading/unloading conditions:

$$\begin{aligned}
&\frac{\partial \bar{L}_i^p}{\partial \mathbf{T}} = -\dot{\bar{\mathbf{U}}}_i^p + \dot{\bar{\boldsymbol{\gamma}}}_i^p \frac{\partial \bar{\phi}_i^p}{\partial \mathbf{T}} = 0 \Rightarrow \dot{\bar{\mathbf{U}}}_i^p = \dot{\bar{\boldsymbol{\gamma}}}_i^p \frac{\partial \bar{\phi}_i^p}{\partial \mathbf{T}} \\
&\frac{\partial \bar{L}_i^p}{\partial \bar{\mathbf{q}}_i} = -\frac{\partial \bar{\boldsymbol{\xi}}_i^p}{\partial t} + \dot{\bar{\boldsymbol{\gamma}}}_i^p \frac{\partial \bar{\phi}_i^p}{\partial \bar{\mathbf{q}}_i^p} = 0 \Rightarrow \frac{\partial \bar{\boldsymbol{\xi}}_i^p}{\partial t} = \dot{\bar{\boldsymbol{\gamma}}}_i^p \frac{\partial \bar{\phi}_i^p}{\partial \bar{\mathbf{q}}_i^p} \\
&\dot{\bar{\boldsymbol{\gamma}}}_i^p \geq 0, \quad \bar{\phi}_i^p \leq 0, \quad \dot{\bar{\boldsymbol{\gamma}}}_i^p \bar{\phi}_i^p = 0
\end{aligned} \tag{6.5}$$

The appropriate value of plastic multiplier $\dot{\bar{\boldsymbol{\gamma}}}^p$ can be determined from the plastic consistency condition for the case of sustained plastic flow:

$$\dot{\bar{\phi}}_i^p = 0 \;\Rightarrow\; \dot{\bar{\gamma}}_i^p = \frac{\frac{\partial \bar{\phi}_i^p}{\partial \mathbf{T}} \mathbf{C}^e \dot{\bar{\mathbf{U}}}}{\frac{\partial \bar{\phi}_i^p}{\partial \mathbf{T}} \mathbf{C}^e \frac{\partial \bar{\phi}_i^p}{\partial \mathbf{T}} + \frac{\partial \bar{\phi}_i^p}{\partial \bar{\mathbf{q}}_i^p} \mathbf{K}_i^h \frac{\partial \bar{\phi}_i^p}{\partial \bar{\mathbf{q}}_i^p}} \tag{6.6}$$

By replacing the last result in stress rate equation, we can obtain the elastoplastic modulus $\mathbf{C}^{ep}$ that should replace the elastic modulus $\mathbf{C}$ in the plastic regime:

$$C_i^{ep} = \mathbf{C}^e - \frac{\mathbf{C}^e \frac{\partial \bar{\phi}_i^p}{\partial \mathbf{T}} \otimes \mathbf{C}^e \frac{\partial \bar{\phi}_i^p}{\partial \mathbf{T}}}{\frac{\partial \bar{\phi}_i^p}{\partial \mathbf{T}} \mathbf{C}^e \frac{\partial \bar{\phi}_i^p}{\partial \mathbf{T}} + \frac{\partial \bar{\phi}_i^p}{\partial \bar{\mathbf{q}}_i^p} \mathbf{K}_i^h \frac{\partial \bar{\phi}_i^p}{\partial \bar{\mathbf{q}}_i^p}} \tag{6.7}$$

The principle of maximum damage dissipation states that among all the variables $(T_i, \bar{q}_i^d)$ that satisfy the damage yield criterion $\bar{\phi}_i^d(T_i, \bar{q}_i^d)$, we have to select those that maximize damage dissipation. This can be written as a constrained minimization problem:

$$\min_{\mathbf{T},\bar{\mathbf{q}}} \max_{\dot{\bar{\gamma}}} \left[\bar{L}^d(\mathbf{T}, \bar{\mathbf{q}}^d, \dot{\bar{\gamma}}^d) = -\bar{\mathcal{D}}^d(\mathbf{T}, \bar{\mathbf{q}}^d) + \dot{\bar{\gamma}}_i^d \cdot \bar{\phi}_i^d(\mathbf{T}, \bar{\mathbf{q}}^d) \right] \tag{6.8}$$

where the damage multiplier $\dot{\bar{\gamma}}^d \geq 0$ plays the role of Lagrange multiplier. By appealing to the Kuhn-Tucker optimality conditions, from the last result, we can obtain the evolution equations for internal variables along with the loading/unloading conditions:

$$\begin{aligned}
&\frac{\partial \bar{L}_i^d}{\partial \mathbf{T}} = -\dot{\bar{\mathbf{U}}}_i^d + \dot{\bar{\boldsymbol{\gamma}}}_i^d \frac{\partial \bar{\phi}_i^d}{\partial \mathbf{T}} = 0 \Rightarrow \dot{\bar{\mathbf{U}}}_i^d = \dot{\bar{\boldsymbol{\gamma}}}_i^d \frac{\partial \bar{\phi}_i^d}{\partial \mathbf{T}} \\
&\frac{\partial \bar{L}_i^d}{\partial \bar{\mathbf{q}}_i^d} = -\frac{\partial \bar{\boldsymbol{\xi}}_i^d}{\partial t} + \dot{\bar{\boldsymbol{\gamma}}}_i^d \frac{\partial \bar{\phi}_i^d}{\partial \bar{\mathbf{q}}_i^d} = 0 \Rightarrow \frac{\partial \bar{\boldsymbol{\xi}}_i^d}{\partial t} = \dot{\bar{\boldsymbol{\gamma}}}_i^d \frac{\partial \bar{\phi}_i^d}{\partial \bar{\mathbf{q}}_i^d} \\
&\dot{\bar{\boldsymbol{\gamma}}}_i^d \geq 0, \quad \bar{\phi}_i^d \leq 0, \quad \dot{\bar{\boldsymbol{\gamma}}}_i^d \bar{\phi}_i^d = 0
\end{aligned} \tag{6.9}$$

The appropriate value of the plastic multiplier $\dot{\bar{\boldsymbol{\gamma}}}^p$ can be determined from the damage consistency condition for the case of sustained damage flow:

$$\dot{\overline{\phi}}_i^p = 0 \;\Rightarrow\; \dot{\overline{\gamma}}_i^p = \frac{\dfrac{\partial \overline{\phi}_i^p}{\partial \mathbf{T}} \mathbf{C}^e \dot{\overline{\mathbf{U}}}}{\dfrac{\partial \overline{\phi}_i^p}{\partial \mathbf{T}} \mathbf{C}^e \dfrac{\partial \overline{\phi}_i^p}{\partial \mathbf{T}} + \dfrac{\partial \overline{\phi}_i^p}{\partial \overline{\mathbf{q}}_i^p} \mathbf{K}_i^h \dfrac{\partial \overline{\phi}_i^p}{\partial \overline{\mathbf{q}}_i^p}} \tag{6.10}$$

By replacing the last result in the stress rate equation, we can obtain the damage modulus $\mathbf{C}^{ed}$ that should replace the elastic modulus $\mathbf{C}$ in the damage regime:

$$C_i^{ed} = \mathbf{C}^e - \frac{\mathbf{C}^e \dfrac{\partial \overline{\phi}_i^d}{\partial \mathbf{T}} \otimes \mathbf{C}^e \dfrac{\partial \overline{\phi}_i^d}{\partial \mathbf{T}}}{\dfrac{\partial \overline{\phi}_i^d}{\partial \mathbf{T}} \mathbf{C}^e \dfrac{\partial \overline{\phi}_i^d}{\partial \mathbf{T}} + \dfrac{\partial \overline{\phi}_i^d}{\partial \overline{\mathbf{q}}_i^d} \mathbf{K}_i^d \dfrac{\partial \overline{\phi}_i^d}{\partial \overline{\mathbf{q}}_i^d}} \tag{6.11}$$

The equations (6.2)-(6.11) should be separately written for positive and negative value of the bending moment, but in order to save space, we have expressed them independent of the sign.

We note in passing that the elastoplastic tangent above remains the same in the discrete problem, obtained by using the backward Euler time integration scheme.

In the softening regime, for the both the positive and the negative value of the bending moment, the Helmholtz free energy can be written in a quadratic form in terms of softening variables:

$$\begin{aligned}
&\overline{\overline{\Psi}}^{(+)}\left(\overline{\overline{\boldsymbol{\xi}}}^{s,(+)}\right) = \underbrace{\frac{1}{2}\overline{\overline{\boldsymbol{\xi}}}^{s,(+)} \mathbf{K}_s^{(+)} \overline{\overline{\boldsymbol{\xi}}}^{s,(+)}}_{\overline{\Xi}^{s,(+)}}; \quad \Psi^{(+)}(\cdot) = \overline{\Psi}^{(+)}(\cdot) + \overline{\overline{\Psi}}^{(+)}(\overline{\overline{\boldsymbol{\xi}}}^{s,(+)})\delta_{\bar{x}} \\
&\overline{\overline{\Psi}}^{(-)}\left(\overline{\overline{\boldsymbol{\xi}}}^{s,(-)}\right) = \underbrace{\frac{1}{2}\overline{\overline{\boldsymbol{\xi}}}^{s,(-)} \mathbf{K}_s^{(-)} \overline{\overline{\boldsymbol{\xi}}}^{s,(-)}}_{\overline{\Xi}^{s,(-)}}; \quad \Psi^{(-)}(\cdot) = \overline{\Psi}^{(-)}(\cdot) + \overline{\overline{\Psi}}^{(-)}(\overline{\overline{\boldsymbol{\xi}}}^{s,(-)})\delta_{\bar{x}}
\end{aligned} \tag{6.12}$$

where $\overline{\overline{\boldsymbol{\xi}}}^s$ is a set of internal variables representing the connection failure and $\overline{\overline{\mathbf{K}}}^s$ is a set of the softening moduli. The yield function for softening is chosen in a multi-criteria form pertaining to bending, shearing, and axial force:

$$\begin{aligned}
&\text{Positive value of } M\text{: } \dot{\overline{\overline{\gamma}}}_i^{(+)} \overline{\overline{\phi}}_i^{(+)} = 0 \Rightarrow \overline{\overline{\phi}}_i^{(+)}(t_i^{(+)}, \overline{\overline{q}}_i^{s,(+)}) \le 0 \\
&\text{Negative value of } M\text{: } \dot{\overline{\overline{\gamma}}}_i^{(-)} \overline{\overline{\phi}}_i^{(-)} = 0 \Rightarrow \overline{\overline{\phi}}_i^{(-)}(t_i^{(-)}, \overline{\overline{q}}_i^{s,(-)}) \le 0
\end{aligned} \tag{6.13}$$

where $t_i^{(+)}, t_i^{(-)}$ are traction forces and $\overline{\overline{q}}_i^{s,(+)}, \overline{\overline{q}}_i^{s,(-)}$ are stress-like variables work-conjugate to softening variables at the discontinuity for the corresponding failure mode. The principal of maximum dissipation (Hill, 1950) ,among all admissible values of these variables, will pick the ones that maximize the softening dissipation. This can be solved as an unconstrained minimization problem. The end result are the evolution equations for internal variables along with the loading/unloading conditions:

$$\begin{aligned}
&\frac{\partial \overline{\overline{L}}^s}{\partial \overline{\overline{\mathbf{q}}}^s} = -\dot{\overline{\overline{\boldsymbol{\xi}}}}^s + \sum\nolimits_1^3 \dot{\overline{\overline{\boldsymbol{\gamma}}}} \frac{\partial \overline{\overline{\phi}}}{\partial \overline{\overline{\mathbf{q}}}^s} = 0 \Rightarrow \dot{\overline{\overline{\boldsymbol{\xi}}}}^s = \sum\nolimits_1^3 \dot{\overline{\overline{\gamma}}}_i \frac{\partial \overline{\overline{\phi}}}{\partial \overline{\overline{\mathbf{q}}}^s} \\
&\dot{\overline{\overline{\boldsymbol{\gamma}}}} \ge 0, \quad \overline{\overline{\phi}} \le 0, \quad \dot{\overline{\overline{\boldsymbol{\gamma}}}} \overline{\overline{\phi}} = 0
\end{aligned} \tag{6.14}$$

The last equation (6.14) can be separately written for the positive and the negative values of the

bending moment.

The beam kinematics equations can be written by using the rotated strain measure: $\mathbf{H} = \mathbf{U} - \mathbf{I}$, where the only non-zero components are defined as:

$$H_{11} = \Sigma - \zeta K,\ H_{21} = \Gamma \tag{6.15}$$

The explicit form of generalized strains can be written as

$$\begin{aligned}
\Sigma = H_{11}^{u,v} &= \underbrace{\left(1+\frac{d\bar{u}}{dx}\right)\cos\psi + \frac{d\bar{v}}{dx}\sin\psi - 1}_{\bar{\Sigma}} + \underbrace{\left(\frac{d\bar{\bar{u}}}{dx}\cos\psi + \frac{d\bar{\bar{v}}}{dx}\sin\psi\right)}_{\bar{\bar{\Sigma}}}\delta_{\bar{x}} \\
\Gamma = H_{21}^{u,v} &= \underbrace{-\left(1+\frac{d\bar{u}}{dx}\right)\sin\psi + \frac{d\bar{v}}{dx}\cos\psi}_{\bar{\Gamma}} + \underbrace{\left(-\frac{d\bar{\bar{u}}}{dx}\sin\psi + \frac{d\bar{\bar{v}}}{dx}\cos\psi\right)}_{\bar{\bar{\Gamma}}}\delta_{\bar{x}} \\
K = H_{11}^{\psi} &= \underbrace{\frac{d\bar{\psi}}{dx}}_{\bar{K}} + \underbrace{\frac{d\bar{\bar{\psi}}}{dx}}_{\bar{\bar{K}}}\delta_{\bar{x}}
\end{aligned} \tag{6.16}$$

By using the same notation for the virtual strains (denoted with superposed $(\hat{\bullet})$), we can write the weak form of equilibrium equation, see (Ibrahimbegovic & Frey, 1993a):

$$G(\mathbf{a},\hat{\mathbf{a}}) := \int_L \left(\hat{\Sigma}N + \hat{\Gamma}V + \hat{K}M\right)dx - G^{ext}(\hat{\mathbf{a}}) = 0 \tag{6.17}$$

In (5.16) above, N, V and M denote stress resultants regarding the Biot stress:

$$\boldsymbol{\sigma} = (N,V,M)^T;\ \ N = \int_A T^{11}dA;\ \ V = \int_A T^{21}dA;\ M = -\int_A \zeta T^{11}dA \tag{6.18}$$

The yield function for the hardening is chosen in a multi-criteria form pertaining to the bending moment, shear and axial force, respectively:

$$\begin{aligned}
&\dot{\bar{\gamma}}_i^p \bar{\phi}_i^p = 0 \Rightarrow \begin{cases} \bar{\phi}_M^p(M,\bar{q}_M^p) = |M| - \left(M_y - \bar{q}_M^p\right) \le 0 \\ \bar{\phi}_V^p(V,\bar{q}_V^p) = |V| - \left(V_y - \bar{q}_V^p\right) \le 0 \\ \bar{\phi}_N^p(N,\bar{q}_N^p) = |N| - \left(N_y - \bar{q}_N^p\right) \le 0 \end{cases} \\
&\dot{\bar{\gamma}}_i^d \bar{\phi}_i^d = 0 \Rightarrow \bar{\phi}_M^d(M,\bar{q}_M^d) = |M| - \left(M_f - \bar{q}_M^d\right) \le 0
\end{aligned} \tag{6.19}$$

where M is the bending moment; V is the shear force; M_{ij}^{cm}, S_{ij}^{s} is the axial force; $\bar{q}_M^p, \bar{q}_V^p, \bar{q}_N^p$ and $\bar{q}_M^d$ are internal hardening stress like variables($\bullet^p$ - plasticity; $\bullet^d$ - damage model); whereas M_y, V_y and M_{ij}^{cm}, S_{ij}^{s} denote yield the bending moment, shear force and axial force, while M_f denotes bending moment at the beginning of the damage flow. In this work, we assume that the damage and the plastic flows begin at the same value of a bending moment. The internal variable q_M^p provides bilinear hardening related to the bending moment, which can be written as:

$$q_M^p = \begin{cases} -K_{M,1}^h \bar{\xi}_M^p; \ 0 \le \bar{\xi}_M^p < \bar{\xi}_{M_y}^p \\ -K_{M,2}^h \bar{\xi}_M^p; \ \bar{\xi}_{M_y}^p \le \bar{\xi}_M^p < \infty \end{cases} \tag{6.20}$$

where $K_{M,1}^h$ and S_{ij}^{in} are the hardening moduli. The equations (6.14)-(6.20) should be separately written for positive and negative value of the bending moment, but they are expressed in form independent on sign.

The detailed FEM implementation is presented in previous chapters. At the end of this section, we present the computational procedure (Table 6.2) for a characteristic iteration. This procedure presents the local phase for computing the value of the bending moment. Other internal force can be computed in the same way.

Table 6.2 Computational procedure for a characteristic iteration

<table>
<tr><td colspan="2">Given: $\Delta K_n^{(i)} = K_{n+1}^{(i)} - K_n^{(i)}, K_n^{p,(+)}, D_n^{(-)}, \xi_n^{p,(+)}, K_n^{p,(-)}, D_n^{(+)}, \xi_n^{p,(-)}, M_n$
Find: $M_{n+1}, K_{n+1}^{p(i),(+)}, D_{n+1}^{(i),(-)}, \xi_{n+1}^{p(i),(+)}, K_{n+1}^{p(i),(-)}, D_{n+1}^{(i),(+)}, \xi_{n+1}^{p(i),(-)}$
$IF(\ M_n \ge 0$ and $K_{n+1}^{(i)} \ge \left|\delta^{(-)}\right|$ and ‘damage=false’)
Elastic trial step
$M_{n+1}^{trial} = M_n + EI\left(\Delta K_{n+1}^{(i)} - K_n^{p,(+)}\right)$
damage = false</td></tr>
<tr><td>Plasticity</td><td>Damage</td></tr>
<tr><td>$\bar{\phi}_{M,n+1}^{p,trial}(M, \bar{q}_M^{p,(+)}) = \left|M_{n+1}^{trial}\right| - \left(M_y - \bar{q}_{M,n}^{p,(+)}\right)$
$IF\ \bar{\phi}_{M,n+1}^{p,trial}(M, \bar{q}_M^{p,(+)}) \le 0$
$M_{n+1}^{\ p} = M_{n+1}^{trial}$
$K_{n+1}^{p,(+)} = K_n^{p,(+)}$
$\xi_{n+1}^{p,(+)} = \xi_n^{p,(+)}$
$ELSEIF\ \bar{\phi}_{M,n+1}^{p,trial}(M, \bar{q}_M^{p,(+)}) > 0$
$solve\ \bar{\phi}_{M,n+1}^{p}(M, \bar{q}_M^{p,(+)}) = 0\ with$
$M_{n+1} = M_{n+1}^{trial} - \gamma_{n+1}^p EI \dfrac{\partial \bar{\phi}_{M,n+1}^p}{\partial M}$
$K_{n+1}^{p,(+)} = K_n^{p,(+)} + \gamma_{n+1}^p \dfrac{\partial \bar{\phi}_{M,n+1}^p}{\partial M}$
$\xi_{n+1}^{p,(+)} = \xi_n^{p,(+)} + \gamma_{n+1}^p$</td><td>$\bar{\phi}_{M,n+1}^{d,trial}(M, \bar{q}_M^{d,(+)}) = \left|M_{n+1}^{trial}\right| - \left(M_f - \bar{q}_{M,n}^{d,(+)}\right)$
$IF\ \bar{\phi}_{M,n+1}^{d,trial}(M, \bar{q}_M^{d,(+)}) \le 0$
$M_{n+1}^{\ d} = M_{n+1}^{trial}$
$D_{n+1}^{(+)} = D_n^{(+)}$
$\xi_{n+1}^{d,(+)} = \xi_n^{d,(+)}$
$ELSEIF\ \bar{\phi}_{M,n+1}^{d,trial}(M, \bar{q}_M^{d,(+)}) > 0$
$solve\ \bar{\phi}_{M,n+1}^{d}(M, \bar{q}_M^{d,(+)}) = 0\ with$
$M_{n+1}^{\ d} = M_{n+1}^{trial} - \gamma_{n+1}^d D_n^{-1,(+)} \dfrac{\partial \phi_{M,n+1}^d}{\partial M}$
$D_{n+1}^{(+)} = D_n^{(+)} + \gamma_{n+1}^d \dfrac{1}{\left|M_{n+1}^{\ d}\right|}$
$(\delta^{(+)} =) \xi_{n+1}^{d,(+)} = \xi_n^{d,(+)} + \gamma_{n+1}^d$</td></tr>
<tr><td colspan="2">$ELSEIF(\ \dfrac{M_{n+1}^{trial}}{M_n} < 0$ and $K_{n+1}^{(i)} \ge -\left|\delta^{(+)}\right|)$ or $ELSEIF(\ M_n < 0$ and ‘damage=true’)</td></tr>
</table>

Elastic step with reduced stiffness

$$M_{n+1}^{trial} = M_n + D_n^{-1,(+)} I\left(\Delta K_{n+1}^{(i)} - K_n^{p,(+)}\right)$$

$$M_{n+1} = M_{n+1}^{trial}$$

$$K_{n+1}^{p,(+)} = K_n^{p,(+)}$$

$$\xi_{n+1}^{p,(+)} = \xi_n^{p,(+)}$$

damage = true

ELSEIF($\frac{M_{n+1}^{trial}}{M_n} > 0$ and $K_{n+1}^{(i)} < -\left|\delta^{(+)}\right|$) or *ELSEIF*($M_n < 0$ and 'damage=false')

Elastic trial step

$$M_{n+1}^{trial} = M_n + EI\left(\Delta K_{n+1}^{(i)} - K_n^{p,(-)}\right)$$

damage = false

Plasticity	*Damage*
$\bar{\phi}_{M,n+1}^{p,trial}(M, \bar{q}_M^{p,(-)}) = \left\|M_{n+1}^{trial}\right\| - \left(M_y - \bar{q}_{M,n}^{p,(-)}\right)$	$\bar{\phi}_{M,n+1}^{d,trial}(M, \bar{q}_M^{d,(-)}) = \left\|M_{n+1}^{trial}\right\| - \left(M_f - \bar{q}_{M,n}^{d,(-)}\right)$
IF $\bar{\phi}_{M,n+1}^{p,trial}(M, \bar{q}_M^{p,(-)}) \le 0$	*IF* $\bar{\phi}_{M,n+1}^{d,trial}(M, \bar{q}_M^{d,(-)}) \le 0$
$M_{n+1}^{p} = M_{n+1}^{trial}$	$M_{n+1}^{d} = M_{n+1}^{trial}$
$K_{n+1}^{p} = K_n^{p}$	$D_{n+1} = D_n$
$\xi_{n+1}^{p} = \xi_n^{p}$	$\xi_{n+1}^{d} = \xi_n^{d}$
ELSEIF $\bar{\phi}_{M,n+1}^{p,trial}(M, \bar{q}_M^{p,(-)}) > 0$	*ELSEIF* $\bar{\phi}_{M,n+1}^{d,trial}(M, \bar{q}_M^{d,(+)}) > 0$
solve $\bar{\phi}_{M,n+1}^{p}(M, \bar{q}_M^{p,(-)}) = 0$ *with*	*solve* $\bar{\phi}_{M,n+1}^{d}(M, \bar{q}_M^{d,(+)}) = 0$ *with*
$M_{n+1} = M_{n+1}^{trial} - \gamma_{n+1}^{p} EI \frac{\partial \bar{\phi}_{M,n+1}^{p}}{\partial M}$	$M_{n+1}^{d} = M_{n+1}^{trial} - \gamma_{n+1}^{d} D_n^{-1} \frac{\partial \phi_{M,n+1}^{d}}{\partial M}$
$K_{n+1}^{p,(-)} = K_n^{p,(-)} + \gamma_{n+1}^{p} \frac{\partial \bar{\phi}_{M,n+1}^{p}}{\partial M}$	$D_{n+1}^{(-)} = D_n^{(-)} + \gamma_{n+1}^{d} \frac{1}{\left\|M_{n+1}^{d}\right\|}$
$\xi_{n+1}^{p,(-)} = \xi_n^{p,(-)} + \gamma_{n+1}^{p}$	$\left(\delta^{(-)} =\right) \xi_{n+1}^{d,(-)} = \xi_n^{d,(-)} + \gamma_{n+1}^{d}$

ELSEIF($\frac{M_{n+1}^{trial}}{M_n} < 0$ and $K_{n+1}^{(i)} < \left|\delta^{(-)}\right|$) or *ELSEIF*($M_n > 0$ and 'damage=true')

Elastic step with reduced stiffness

$$M_{n+1}^{trial} = M_n + D_n^{-1,(-)} I\left(\Delta K_{n+1}^{(i)} - K_n^{p,(-)}\right)$$

$$M_{n+1} = M_{n+1}^{trial}$$

$$K_{n+1}^{p,(-)} = K_n^{p,(-)}$$

$$\xi_{n+1}^{p,(-)} = \xi_n^{p,(-)}$$

damage=true

6.4. Identification of the constitutive model parameters

The identification of the constitutive model parameters is an extension of the identification procedure presented in the previous chapter, where we have presented the theoretical background and the implementation of the proposed methodology. In this section, we practically use the same objective function and all other steps previously proposed in the identification procedure. The loading program is changed with the cyclic loading instead of the monotonic loading. The load is applied in terms of imposed displacements.

The structural connection A_{cyclic} and B_{cyclic} are in the focus of our interest, and they are completely the same as structural connections A1 and B1, which are presented in the previous chapter. At the beginning of the identification process, we match the experimentally measured responses of structural connections with the numerically obtained responses. The numerical computations for the case of the monotonic loading, are performed with the beam model proposed in this chapter with the constitutive parameters of the beam identified in the previous chapter, see Figure 6.10.

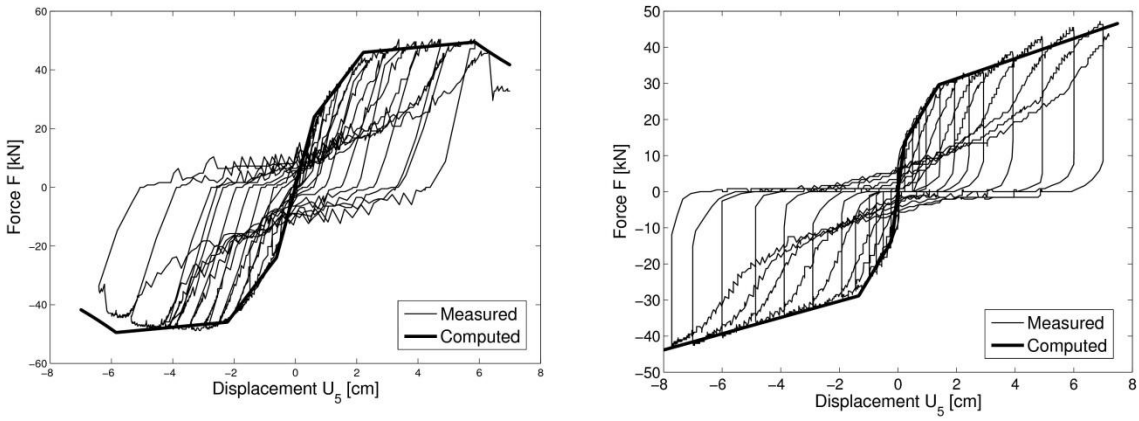

a) A_{cyclic} connection *b) B_{cyclic} connection*

Figure 6.10 Computed vs. experimental responses of the connections: A_{cyclic} and B_{cyclic}

From the results shown in Figure 6.10 we can conclude that good matching between the computed response and the contour of the hysteresis is obtained. This validates previously identified constitutive parameters. The experimental observation has inspired assumption that the damage is beginning at the same moment as the plasticity. This assumption reduces identification problem to only one unknown per each connection.

The identification procedure can be performed in one phase, with the objective function defined in the previous chapter:

$$J\left(\mathbf{d}_p\right)=\sum_1^3 a\left(F_{Pi}^{com}-F_{Pi}^{\exp}\right)^2+\sum_1^3 b\left(U_{Pi}^{com}-U_{Pi}^{\exp}\right)^2+\sum_1^3 b\left(U_{S,Pi}^{com}-U_{S,Pi}^{\exp}\right)^2+\sum_1^3 c\left(\psi_{Pi}^{com}-\psi_{Pi}^{\exp}\right)^2+$$
$$+\sum_1^2 d\left(\Delta\psi_{Pi}^{com}-\Delta\psi_{Pi}^{\exp}\right)^2+\sum_1^3 e\left(\kappa_{Pi}^{com}-\kappa_{Pi}^{\exp}\right)^2+\sum_1^3 g\left(\Delta\kappa_{Pi}^{com}-\Delta\kappa_{Pi}^{\exp}\right)^2 \tag{6.21}$$

where: $F_{Pi}^{com}, F_{Pi}^{\exp}$ are forces for different load level (P_i); $U_{Pi}^{com}, U_{Pi}^{\exp}$ are the corresponding displacements (P_i) ; $U_{S,Pi}^{com}, U_{S,Pi}^{\exp}$ are shear displacements (P_i); $\psi_{Pi}^{com}, \psi_{Pi}^{\exp}$ are rotations of the connection (P_i); $\Delta\psi_{Pi}^{com}=\psi_{Pi+1}^{com}-\psi_{Pi}^{com}$ and $\Delta\psi_{Pi}^{\exp}=\psi_{Pi+1}^{\exp}-\psi_{Pi}^{\exp}$ are gradients of rotation between two different load (P_i) ; $\kappa_{Pi}^{com}, \kappa_{Pi}^{\exp}$ are curvatures of the section (P_i); $\Delta\kappa_{Pi}^{com}=\kappa_{Pi+1}^{com}-\kappa_{Pi}^{com}$ and

$\Delta\kappa_{Pi}^{\exp} = \kappa_{Pi+1}^{\exp} - \kappa_{Pi}^{\exp}$ are gradients of the curvature between two different load (Pi); while *a, b, c, d, e, g* are constants.

6.4.1. Experimental structure A_{cyclic}

The measured response of the experimental structure A_{cyclic} is shown in Figure 6.3. The structure A_{cyclic} is completely the same as the experimental structure A1, which is presented in the previous chapter. The previously identified constitutive parameters are used for obtaining the numerical response of the structural connection under monotonic loading. The comparison of the computed and the measured response is shown Figure 6.10a, where a good matching between the results is observed. This reduces the number of unknowns to one parameter.

Figure 6.11 shows a shape of the objective function (6.21). The shape of the objective function is convex which thus has a minimum. By using the identification procedure presented in previous chapters, we are able to determine the unknown parameter.

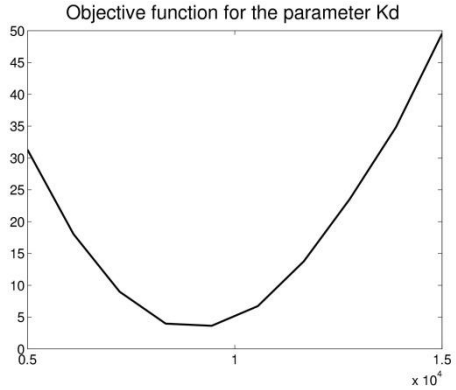

Figure 6.11 The shape of the objective function

Using the identified parameter, we have performed the numerical simulation of the experimental test A_{cyclic}. The comparison of the computed and the measured response is shown in Figure 6.12. In Figure 6.12a the computed and the measured hysteresis are shown. One extracted cycle is shown in Figure 6.12b. Both of them indicate that proposed model is capable of representing the connection behavior, including many phenomena characteristic for this structural connection type.

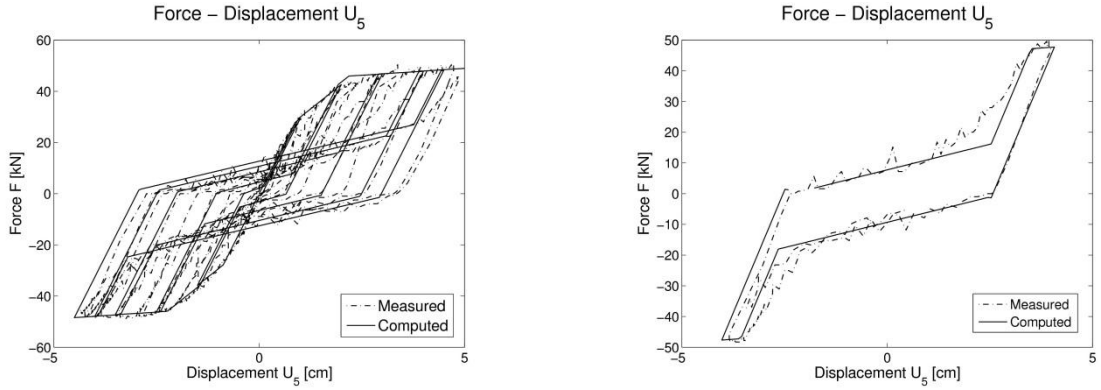

a) Hysteresis *b) One cycle of the hysteresis*

Figure 6.12 Computed vs. measured response of the experimental structure A_{cyclic}

6.4.2. Experimental structure B_{cyclic}

In Figure 6.6 the measured response of the experimental structure B_{cyclic} is shown. This structure is completely the same as the experimental structure B1, which is presented in the previous chapter. The constitutive parameters obtained for the experimental structure B1 have been used in the numerical simulation of the test B_{cyclic}. The computation has been performed for the monotonic loading. The computed and measured responses of the experimental structure B_{cyclic} are shown in Figure 6.10b. A good matching between the responses is obtained which allows us to reduce the number of the unknown parameters to only one.

In the identification procedure the objective function (6.21) has been used. Figure 6.13 shows the convex shape of the objective function for the unknown parameter which thus can be minimized.

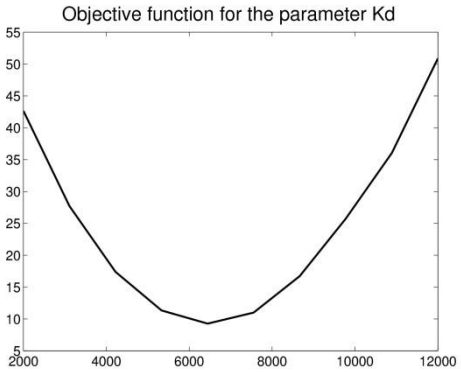

Figure 6.13 The shape of the objective function for the unknown parameter (B_{cyclic})

The numerical simulation of the cyclic experimental test B_{cyclic}, has been performed with the proposed beam element and identified parameters. Figure 6.14 shows a comparison of computed and measured responses of the experimental structure B_{cyclic}, under cyclic loading. The difference between responses is visible, but we can conclude that proposed beam model significantly improves the response prediction in comparison with the model of the plasticity or the damage.

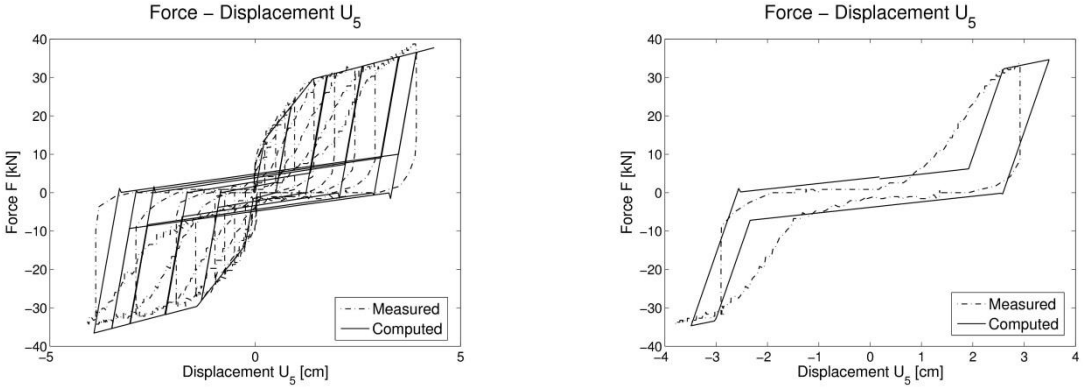

c) Hysteresis *d) One cycle of the hysteresis*

Figure 6.14 Computed vs. measured response of the experimental structure B_{cyclic}

6.5. Concluding remarks

In this chapter, we have presented an experimental and numerical study of the moment-resistant structural connection behavior under cyclic loading. A total of two experimental tests have been performed for two different types of the structural connection. The experimental observations have shown that the behavior of the structural connection is affected by the load type. During the tests with the change in the direction of the applied load, we have measured the less stiff response of structural connections. With the intention to include this phenomenon in a numerical prediction, we have proposed a modification of the beam model. The proposed beam model is geometrically exact beam with hardening and softening part of the response included. The hardening part of the response is described by coupled plasticity-damage model. The ability of the proposed beam model to represent the connection behavior is confirmed through several numerical simulations where good matching between measured and computed responses is observed. The computed response is obtained by using the set of parameters which were identified from experimental measurements. The identification procedure is briefly presented.

Chapter 7

Conclusions and perspectives

7.1. Conclusions

In this thesis we have presented the methodology for the ultimate limit load analysis of a steel frame structure with included structural connections behavior. The main idea is that the behavior of the connection can be included in the global response of the whole structure by placing beam elements in the corners of the steel frame structure. Other elements members of the steel frame structure can be modeled with nonlinear beam elements.

The research has two parts with the same goal. The first part deals with the behavior of structural connections, including many phenomena, which characterize them. The second proposes beam model, which is able to represent the behavior of steel elements, beams and columns.

In the first part, we have done the research on the connection behavior and the possibility of representing it with the beam element. We have assumed that the connection response could be captured with the coupled plasticity-damage model in the pre-peak part of the response, and the nonlinear softening law with different mechanisms of the failure in the post-peak part of the response. The hardening behavior is split to the bending and the shearing, but all combinations are included. This model is capable of describing a wide range of problems. We have proposed a methodology for constitutive parameters identification procedure of the connection and the material. The most important conclusions can be stated as follows:

- The proposed methodology is able to identify all unknown parameters (eighteen) when these parameters are split into three phases: elasticity, hardening and softening. In every phase, we use local and global measurements.
- Successful identification is conditioned with sufficient experimental measurements during the test and adequate loading program. In this part we have presented requirements for measurements and loading program. The loading program contains cycles of loading-unloading. In the hardening we need to have minimum three cycles for every case.
- The focus was on the behavior of the constitutive models and on the choice of the objective function. We have showed that using loading and unloading cycles we can obtain all unknown constitutive parameters. These cycles are needed to make a difference between plasticity and damage model. Both models can describe the same behavior in the loading regime, and only in unloading we can see the difference between them.
- All cases of identification were presented. For an illustration of the complete procedure, we first used the academic example of the inverse analysis and all experimental results were obtained from FEM model. This example has been used as a preparation for the experimental tests, which were performed later. Then, two practical examples were shown, but only for partial measurements that correspond to bending of the connection. These are the only results found in the scientific papers.

At the same time, we were working on the development of the beam model, which is able to represent response of a steel frame structure without connection behavior. The presented geometrically non-linear planar beam model provides the main novelty with its ability to account for both bending and shear failure. The proposed constitutive model contains both coupled plasticity with isotropic hardening and nonlinear law for softening with three different failure mechanisms. The hardening response, providing the interaction between bending moment, shear force, and axial force can be calibrated against damage of beams or columns in a steel frame. The softening response can be activated to model different failure mechanisms. Which of mechanisms will be activated depends on interplay and stress redistribution during the limit load analysis.

By using the proposed beam element, we can perform ultimate limit analysis of any frame planar steel structure, including the second order effects as well as different failure mechanisms. The geometrically nonlinear analysis allows the ultimate limit analysis with large displacement, without any need for correction of the proposed property. This advantage is very important in a steel frame structure because of a large ductility of steel.

The results for all numerical examples illustrate an excellent performance of the proposed beam element.

In the continuation of the research on the connection behavior, we have presented an experimental and numerical study of the moment-resistant connection behavior. A total of three connection types have been analyzed and eight experimental tests have been performed. The connection behavior in structural response is included where we model every joint with beam element. In this part of the research, we have proposed two beam models appropriate for representation of connection behavior in a framework of the large displacement. We have firstly proposed beam element suitable for monotonic loading, while the second proposed beam model is appropriate for the cyclic loading. The proposed beam elements have seventeen and eighteen unknown constitutive parameters. The identification methodology, which was presented in first part of the thesis, has been used. The unknown parameters, based on the results of the experimental tests, have been identified. We found that the proposed beam model with identified constitutive parameters can successfully represent connection behavior. The capability of the proposed beam models for representing connection behavior is confirmed with a good matching between experimental and computed results. The set of the constitutive parameters of the firstly proposed beam model can be obtained by using the EC3 procedure, which provides a good prediction of elastic response and bending, while the plastic response prediction is overly conservative, sometimes up to 40%. EC3 procedure for the prediction of a connection behavior does not provide prediction of the behavior of the structural steel connection under cyclic load.
The influence of the connection behavior on the steel frame response is shown in two numerical simulations. The numerical results demonstrate the importance of the joints behavior in the steel frame structure response, where we can see a difference in results to up to 30%.

By using proposed beam models and identification procedure, we are able to perform ultimate load limit analysis of a steel frame structure with included connection behavior, which provides real stress distribution. The proposed beam models also provide the capability to perform complete collapse analysis, where we can follow the development of the failure mechanism.

7.2. Perspectives

The presented research on connections behavior and novel numerical beam models have the potential for enhancements. The enhancements of the research could be realized through few stages:

- The connection response strongly depends on human work during the building process, where errors can be expected. The probability studies of connections behavior in a frame steel structure have a great potential.
- The proposed identification procedure and numerical beam models can also be used in studies on the behavior of other connection types.
- The presented numerical model of the geometrically exact planar beam could be extended to the 3D beam model.
- The enhancement of the proposed beam model could be realized as an extension to dynamic response framework, which is crucial for the real-time analysis of a steel frame structure under the seismic load.

Bibliography

(Abidelah et al., 2014) Abidelah, , Bouchaïr, A. & Kerdal, D.E., 2014. Influence of the flexural rigidity of the bolt on the behavior of the T-stub steel connection. *Engineering Structures*, 81, pp.181-94.

(Ayhan et al., 2013) Ayhan, B., Jehel, P., Brancherie, D. & Ibrahimbegovic, A., 2013. Coupled damage-plasticity model for cyclic loading: Theoretical formulation and numerical implementation. *Engineering Structures*, 50, pp.30-42.

(Bui et al., 2014) Bui, N.N. et al., 2014. Enriched Timoshenko beam finite element for modeling bending and shear failure of reinforced concrete frames. *Computers and Structures*, 143, pp.9-18.

(Drucker, 1956) Drucker, D.C., 1956. Effect of shear on the plastic bending of beams. 23.

(Dujc et al., 2010) Dujc, J., Brank, B. & Ibrahimbegovic, A., 2010. Multi-scale computational model for failure analysis of metal frames that includes softening and local buckling. *Computer Methods Applied Mechanics Engineering*, 199 (1371-1385).

(EC3, 2005) EC3, 2005. *EN 1993-1-8: Eurocode 3: Design of steel structures - Part 1-8: Design of joint*. Bruxelles: European Commitee.

(Faella et al., 2000) Faella, C., Piluso, V. & Rizzano, G., 2000. *Structural Steel Semirigid Connections: Theory, Design, and Software*. CRC Press LLC.

(Gang Shi et al., 2007) Gang Shi, Y.S.Y.W., 2007. Behaviour of end-plate moment connections under earthquake loading. *Engineering Structures*, 29, pp.703–16.

(Hill, 1950) Hill, R., 1950. *The Mathematical Theory of Plasticity*. Oxford: Clarendon Press.

(Hu et al., 2012) Hu, , Leon, R. & Taehyo , P., 2012. Mechanical models for the analysis of bolted T-stub connections under cyclic loads. *Journal of Constructional Steel Research*, 78, pp.45-57.

(Ibrahimbegovic , 2009) Ibrahimbegovic, A., 2009. *Nonlinear Solid Mechanics*. Springer.

(Ibrahimbegovic et al., 1993a) Ibrahimbegovic, A. & Frey, F., 1993a. Finite element analysis of linear and non-linear planar deformations of elastic initially curved beam. *International Journal for Numerical Methods in Engineering*, 36, 3239-3258, pp.3239-58.

(Ibrahimbegovic et al., 1993b) Ibrahimbegovic, A. & Frey, F., 1993b. Geometrically non-linear method of incompatible modes in application to finite eleasticity with indepedent rotations. 36, (4185-4200).

(Ibrahimbegovic et al., 2013) Ibrahimbegovic, A., Hajdo, E. & Dolarevic, S., 2013. Linear instability or buckling problems for mechanical and coupled thermomechanical extreme conditions. *Coupled Systems Mechanics*, 4, pp.349-74.

(Ibrahimbegovic et al., 2008) Ibrahimbegovic, A., Jehel, P. & Davenne, L., 2008. Coupled damage-plasticity constitutive model and direct stress interpolation. *Computational Mechanics*, 42, pp.1–11.

(Ibrahimbegovic et al., 2004) Ibrahimbegovic, A., Knopf-Lenoir, C., Kučerova, A. & Villon, P., 2004. Optimal design and optimal control of structures undergoing finite rotations and elastic deformations. *International Journal for Numerical Methods in Engineering*, 61, pp.2428-60.

(Ibrahimbegovic et al., 1991) Ibrahimbegovic, A. & Wilson, E., 1991. A modified method of incompatible modes. *Communication in Numerical Methods in Engineering*, 7, pp.187-94.

(Imamovic et al., 2015) Imamovic, I., Ibrahimbegovic, A., Knopf-Lenoir, C. & Mesic, E., 2015. Plasticity-Damage Model Parameters Identification for Structural Connections. *Coupled Systems Mechanics*, 4(4(337-364)).

(Imamovic et al., 2017) Imamovic, I., Ibrahimbegovic, A. & Mesic, E., 2017. Nonlinear kinematics Reissner's beam with combined hardening/softening elastoplasticity. *Computers and Structures*, In press.

(Imamovic et al., 2010) Imamovic, I. & Mesic, E., 2014. Non-linear analysis of end plate connections with four bolts in a row and their effects on the global behaviorof a frame. *EUROSTEEL 2014*. Naples, Italy, 2014.

(Jehel et al., 2010) Jehel, P., Davenne, L., Ibrahimbegovic, A. & Léger, P., 2010. Towards robust viscoelastic-plastic-damage material model with different hardenings/softenings capable of representing salient phenomena in seismic loading applications. *Computers and Concrete*, 7(4), pp.365-86.

(Kozar et al., 2017) Kozar, I., Rukavina, T. & Ibrahimbegovic, A., 2017. Material model for load rate sensitivity. In Ibrahimbegovic, A., Brank , B. & Kozar, I., eds. *ECCOMAS MSF 2017 Thematic conference*. Ljubljana, Slovenia, 2017.

(Kucerova et al., 2009) Kucerova, A. et al., 2009. Novel anisotropic continuum-discrete damage model capable of represenetnig localized failure of massive structures; Part II: Identification from test under heterogeneous stress field. *Engineering Computations: International Journal for Computer-Aided Engineering and Software*, 26, pp.128-44.

(Latour et al., 2014) Latour, M., Rizzano, G., Santiago, A. & Simões , L.d.S., 2014. Experimental analysis and mechanical modeling of T-stubs with four bolts per row. *Journal of Constructional Steel Research*, 101, pp.158-74.

(Medic et al., 2013) Medic, S., Dolarevic, S. & Ibrahimbegovic, A., 2013. Beam model refinement and reduction. 50 (158-169).

(Mesic, 2003) Mesic, E., 2003. Analysis of timber frames with localized nonlinearities. *Facta Universitatis, Series: Architecture and Civil Engineering*, 2(5), pp.307 - 320.

(Neal, 1961) Neal, B.G., 1961. Effect of shear and Nnormal forces on the fully plastic moment of a beam of rectangular cross-section. 23(2).

(Nikolic et al., 2015) Nikolic, M. & Ibrahimbegovic, A., 2015. Rock mechanics model capable of representing initial heterogeneities and full set of 3D failure mechanisms. *Computer Methods in Applied Mechanics and Engineering*, 290, pp.209-27.

(Nikolic et al., 2015) Nikolic, M., Ibrahimbegovic, A. & Miscevic, P., 2015. Brittle and ductile failure of rocks: Embedded discontinuity approach for representing mode i and mode ii failure mechanisms. *International Journal for Numerical Methods in Engineering*, 8(102).

(Pirmanšek et al., 2017) Pirmanšek, K., Češarek, , Zupan, & Saje, , 2017. Material softening and strain localization in spatial geometrically exact beam finite element method with embedded discontinuity. *Computers & Structures*, 182, pp.267–83.

(Reissner, 1972) Reissner, E., 1972. On One-Dimensional Finite-Strain Beam Theory: the Plane Problem. 23.

(Ribeiro et al., 2015) Ribeiro, , Santiago, A., Constança, R. & Simões da Silva, d.S., 2015. Analytical model for the response of T-stub joint component under impact loading. *Journal of Constructional Steel Research*, 106, pp.23-34.

(Simo et al., 1984) Simo, J.C., Hjelmstad, K.D. & Taylor, R.L., 1984. Numerical formulations of elasto-viscoplastic response of beams accounting for the effect of shear. 42.

(Taylor, 2008) Taylor, R.L., 2008. *FEAP - A Finite Element Analysis Program*. Berkeley.

(Wagner et al., 2002) Wagner, & Gruttmann, F., 2002. Modeling of Shell–Beam Transitions in the Presence of Finite Rotations. *Computer Assisted Mechanics and Engineering Sciences*, 9, pp.405-18.